# THE EFFECTS OF CEREBRAL ARTERY VARIATIONS ON THE OCCURRENCE OF INTRACRANIAL ATHEROSCLEROSIS: SERIAL HOSPITAL-BASED CLINICAL RESEARCH

LI JIA

PhD

The Hong Kong Polytechnic University

2021

The Hong Kong Polytechnic University

Department of Health Technology and Informatics

# The Effects of Cerebral Artery Variations on the Occurrence of Intracranial Atherosclerosis: Serial Hospital-based Clinical Research

**Li Jia**

A thesis submitted in partial fulfilment of the requirements for the degree of Doctor of Philosophy

**May 2021**

# CERTIFICATE OF ORIGINALITY

I hereby declare that this thesis is my own work and that, to the best of my knowledge and belief, it reproduces no material previously published or written, nor material that has been accepted for the award of any other degree or diploma, except where due acknowledgement has been made in the text.

_____(Signed)

LI Jia (Name of Student)

# Abstract

## Background

Ischemic stroke (IS) is a major cause of adult disability and death all over the world. Intracranial atherosclerosis (ICAS) is the most common etiology of IS among Chinese stroke patients, and involves the major cerebral large arteries growing atherosclerotic plaques. The current advances in imaging technology have greatly facilitated the detection of the cerebral artery anatomical variations and the intracranial atherosclerotic plaques among the general populations. Nonetheless, few studies investigated the underlying influence of the cerebral artery variations on ICAS, including the common variability in the circle of Willis (COW) structure and in the vertebrobasilar junction (VBJ) angle magnitude.

## Purpose

Our research aimed to explore the effects of the cerebral vascular variations, namely the COW structural anomaly and the varying VBJ-angle degrees, on the occurrence and progression of ICAS among stroke patients, via using high-resolution magnetic resonance imaging (HR-MRI).

## Methods and materials

This hospital-based research consecutively recruited adult patients with acute IS or transient ischemic attack, who were scanned by both routine cerebral MRI and intracranial vessel-wall 3.0-Tesla MRI sequences. Magnetic resonance angiography was used to assess the anatomical completeness of the COW and the degrees of the VBJ angle. The COW consists of the anterior COW (A-COW) and the posterior COW (P-COW). The VBJ angle was stratified into the angle above 90° or the angle below 90°. HR-MRI was utilized to evaluate the plaque imaging features quantitatively and qualitatively. The intracranial

atherosclerotic lesions were categorized as asymptomatic or symptomatic, based on acute cerebral infarction on diffusion-weighted imaging and/or acute stroke symptoms.

**Results**

This research enrolled a total of 125 acute stroke patients with intracranial large artery atherosclerosis between 2014 and 2020, among whom 96 patients had the complete imaging scan covering the intracranial vertebral artery segments. Besides, 107 patients had the atherosclerotic lesions in the middle cerebral artery (MCA) detected by HR-MRI, and 68 patients with vertebrobasilar atherosclerotic lesions were included in the subsequent analyses.

Firstly, among 96 patients with intracranial large artery atherosclerosis (mean age = 63.41 ± 10.31 years old; 60 were male), the incomplete COW subtypes were prevalent (the incomplete A-COW, 44.8%; the incomplete P-COW, 83.3%). Two hundred and ninety-two intracranial atherosclerotic plaques were detected in patients with intracranial large artery atherosclerosis (224 were asymptomatic and 68 were symptomatic). The prevalence of the symptomatic plaques in the first segment of the MCA was observed to be 82.8% in the incomplete A-COW subtype, and significantly higher than 48.7% in the complete A-COW subtype ($P = 0.005$). Yet, no significant difference in the location of the symptomatic plaques within the second segment of the MCA, the basilar artery, or the vertebral artery was found between the complete and incomplete A-COW subtypes (all P values > 0.05/4 times of the repeated comparisons).

Secondly, among 107 patients with MCA atherosclerosis (mean age = 62.50 ± 11.69 years old; 67 were male), the prevalence of the incomplete A-COW subtype was 43.0%, while that of the incomplete P-COW subtype went up to 85.0%. One hundred and fifty-eight MCA plaques were detected in patients with MCA atherosclerosis (96 were asymptomatic and 62 were symptomatic). Compared to the complete A-COW, the incomplete A-COW had more

inferior-wall plaques, but fewer ventral-wall plaques in the MCAs, regardless of whether the MCA plaques were symptomatic or not (P values < 0.05). Besides, the dysplasia or absence of the posterior communicating artery (80.4%) was the most prevalent among patients with MCA atherosclerosis, followed by the dysplasia or absence of the anterior cerebral artery (34.6%), the anterior communicating artery (ACoA) (29.9%), and the posterior cerebral artery (27.1%). The dysplasia or absence of ACoA, as a typical incomplete A-COW pattern, was then found in independent association with symptomatic MCA atherosclerosis (odds ratio, 3.132, [95%CI, 1.412-6.946]; P = 0.005) after controlling the potential confounders.

Thirdly, among 68 patients with vertebrobasilar artery atherosclerosis (mean age = 63.53 ± 9.42 years old; 63.2% were male), the VBJ angles ranged in magnitude between 29.45° and 124.20°. 48.5% of patients with vertebrobasilar atherosclerosis had the VBJ angles ≥ 90°, while 51.5% possessed the VBJ angles < 90°. One hundred and thirty-one vertebrobasilar plaques were detected in patients with vertebrobasilar artery atherosclerosis. The VBJ angles ≥ 90° had more vertebrobasilar plaques on the ventral walls (50.14% versus 25.49%, P = 0.003), but fewer vertebrobasilar plaques on the dorsal walls (7.32% versus 40.34%, P < 0.001) than the VBJ angles < 90°. Additionally, the values of wall thickness, luminal stenosis and plaque burden in vertebrobasilar artery atherosclerosis were significantly increased in the VBJ angles ≥ 90°, rather than the VBJ angles < 90° (all P values < 0.05). The VBJ angles ≥ 90° also possessed more vertebrobasilar plaques with hypointensity signal, intraplaque hemorrhage, and symptomatic status (all P values < 0.05).

**Conclusion**

In our research, 1) the incomplete A-COW subtype was significantly associated with the occurrence of the symptomatic atherosclerotic lesions in the MCA-M1 segment among patients with intracranial large artery atherosclerosis. 2) The incomplete A-COW structure

might strongly influence the MCA plaque location on the vessel walls in patients with MCA atherosclerosis. 3) The ACoA dysplasia or absence might serve as an independent risk factor for developing symptomatic MCA atherosclerotic lesions in patients with MCA atherosclerosis. 4) The structure of the VBJ angles ≥ 90° might robustly affect the vertebrobasilar plaque location on the vessel walls among patients with vertebrobasilar artery atherosclerosis. 5) The VBJ angles ≥ 90° were significantly related to the progressive vertebrobasilar atherosclerotic lesions in patients with vertebrobasilar artery atherosclerosis. Accordingly, our findings highlight the important roles of the cerebral artery variations in the occurrence and progression of ICAS among stroke patients.

# Publications and Presentations

## Publications

### *Research Articles*

1. **Li J**, Zheng L, Yang WJ, Sze-To CY, Leung TW, Chen XY. Plaque Wall Distribution Pattern of the Atherosclerotic Middle Cerebral Artery Associates With the Circle of Willis Completeness. Front Neurol. 2021 Jan 11;11:599459. doi: 10.3389/fneur.2020.599459.

2. Yang WJ, Wasserman BA, Zheng L, Huang ZQ, **Li J**, Abrigo J, Wong SM, Ying TC, Chu CW, Wong KS, Leung TW, Chen XY. Understanding the Clinical Implications of Intracranial Arterial Calcification Using Brain CT and Vessel Wall Imaging. (Accepted, 2021)

3. Chen D, Sun W, **Li J (co-first author)**, Wei B, Liu W, Wang X, Song F, Chen L, Yang J, Yu L. Serum Cystatin C and Coronavirus Disease 2019: A Potential Inflammatory Biomarker in Predicting Critical Illness and Mortality for Adult Patients. Mediators Inflamm. 2020 Oct 8;2020:3764515. doi: 10.1155/2020/3764515.

4. **Li J**, Long D, Wu S, Wu X, Wei B, Chen D, Shao Y, Wang H, Cui L, Chen X, Yu L. Association of CFH polymorphism with susceptibility to sepsis caused by Pseudomonas aeruginosa in Chinese Han populations: A multi-center study. Gene. 2020 Jan 5;722:144127. doi: 10.1016/j.gene.2019.144127.

5. Chen F, Wang Y, Zhang W, Cai Y, Zhao T, Mai H, Tao S, Wei W, **Li J**, Chen X, Li X, Tang P, Fan W, Yang J, Ou M, Lu F, Lai Z, Chen H, Zou T, Sun F, Shao Y, Cui L. A Functional Polymorphism-Mediated Disruption of EGR1/ADAM10 Pathway Confers the

Risk of Sepsis Progression. mBio. 2019 Aug 6;10(4):e01663-19. doi: 10.1128/mBio.01663-19.

***Review Article***

1. **Li J**, Li K, Chen X. Inflammation-regulatory microRNAs: Valuable targets for intracranial atherosclerosis. J Neurosci Res. 2019 Oct;97(10):1242-1252. doi: 10.1002/jnr.24487.

***Manuscripts Submitted***

1. Zheng L, **Li J (co-first author)**, Yang WJ, Lam HC, Wong KS, Leung TW, Chen XY. Patterns and implications of intracranial atherosclerosis in anterior and posterior circulation identified by high-resolution magnetic resonance imaging among acute stroke patients. (Under review)

**Conference Abstracts**

1. **Li J**, Zheng L, Yang WJ, Sze-To CY, Leung TW, Chen XY. Relevance of the circle of Willis integrity to the plaque distributions in symptomatic intracranial atherosclerosis. Joint European Stroke Organization and World Stroke Organization Conference (ESO-WSO 2020), Virtual Conference. (7 - 9 November, 2020) (included in the International Journal of Stroke)

2. **Li J**, Yang WJ, Zheng L, Du H, Huang CM, Leung TW, Chen XY. Clinical implication and significance of the vertebrobasilar junction angle over 90° in vertebrobasilar artery atherosclerosis: An intracranial high-resolution MRI study. The 89$^{th}$ European Atherosclerosis Society Congress, Virtual Congress. (30 May - 2 June, 2021) (included in the EAS Atherosclerosis Journal)

# Acknowledgements

May it be your journey on

To light the day

~ *May It Be - Enya*

When I worked as a clinician in the Department of Critical Care Medicine, I always considered it as a higher priority to do scientific research. Only then did I realized that I did not have enough knowledge about clinical research. A first step was needed to get myself trained for Ph.D. position, I thought. Now I am looking back on this journey, even not knowing where I got the courage and determination to set foot on the road. It was generally reckoned enthusiasm, or a bit of luck indeed.

I still remember how I met my current supervisor, Dr. Xiangyan Chen. She gave me this precious opportunity at that moment, so that I could further my study as a research student in the Hong Kong Polytechnic University. I cannot forget the help and the encouragement from my supervisor as well, when the local social riots seriously affected our work and study, and when I was extremely worried about my parents back home due to the outbreak of the epidemic of COVID-19. She said, at that time, if you could not concentrate on analyzing the imaging data, you could try to start writing the literature review section of your thesis. I followed her advice. She also gave me plenty of space, when we settled the academic issues. Under her guidance over the past three years, I could independently reflect on and deal with the research issues. I am much obliged in all sincerity to my supervisor for helping me on this journey.

The current thesis not only represents the results of my doctoral study and scientific work in the past three years, but also incorporates the help from my teachers, friends and

colleagues from many parts of the world to whom I would like to express my deep sense of gratitude here.

First of all, sincere thanks to Prof. Keshen Li in the Clinical Neuroscience Institute, Jinan University, Guangzhou. Because of his encouragement and referral, I got this chance to pursue a Ph.D. degree in Hong Kong. Whenever I encountered any academic difficulties, moreover, he was always here and able to give me correct and timely guidance.

Many especial thanks to Dr. Wenjie Yang in the Russell H. Morgan Department of Radiology and Radiological Sciences, the Johns Hopkins Hospital, and to Dr. Lu Zheng in the Department of Neurology, the Third Affiliated Hospital of Sun Yat-sen University. They are my academic collaborators and mentors in the neuro-imaging field. I could have never finished the present thesis without their lavish support and help.

Also many thanks to Dr. Thomas Waihong Leung in the Prince of Wales Hospital for the study coordination and the patient recruitment, and to Mr. Cheukyin Szeto in the Hong Kong Sanatorium & Hospital for the data preparation. Besides, I greatly appreciate Mr. Yao Song in the Hong Kong Polytechnic University and Ms. Jinghong Xu in the Sun Yat-sen University guiding me in the statistical analyses.

I would like to show my full appreciation and thanks to Prof. Michael T.C. Ying, Prof. Jing Cai, Dr. Lawrence W.C. Chan, and Dr. Chiming Wong in the Department of Health Technology and Informatics for the professional advice on my research, and to Ms. Alison W.H. Sin, Ms. Pamela Y.N. Mui, Mr. David W.L. Lau, and all HTI stuff for offering me practical assistance with my campus life.

Moreover, I would like to appreciate my two roommates, Mr. Haonan Xiao and Mr. Jiang Zhang, and my two desk mates in the HTI office, Ms. Nonhlanhla Chambara and Ms. Adenike E. Adesanya. They are all Ph.D. students in the Department of HTI. Many thanks to

Mr. Heng Du and all my PolyU friends as well. Every moment with them was much unforgettable and enjoyable.

Last but not the least, my deepest gratitude to my parents and other family members. Owing to their unconditional love, whenever and wherever, I can carry on my journey. Believe and I find the way. A promise lives within me now.

# Table of Contents

# List of Tables

# List of Figures

# List of Abbreviations

| | |
|---|---|
| ACA | anterior cerebral artery |
| ACoA | anterior communicating artery |
| A-COW | anterior circle of Willis |
| AIS | acute ischemic stroke |
| BA | basilar artery |
| BFR | blood flow rate |
| BOD | branch occlusive disease |
| CBF | cerebral blood flow |
| CI | confidence interval |
| COW | circle of Willis |
| CTA | computed tomographic angiography |
| DSA | digital subtraction angiography |
| DWI | diffusion-weighted imaging |
| ECA | extracranial carotid artery |
| FOV | field-of-view |
| HR-MRI | high-resolution magnetic resonance imaging |
| HST1 | high signal intensity on T1-weighted |
| ICA | internal carotid artery |
| ICAS | intracranial atherosclerosis |
| IPH | intra-plaque hemorrhage |
| IQR | interquartile range |
| IS | ischemic stroke |
| LA | lumen area |

| | |
|---|---|
| MCA | middle cerebral artery |
| MES | micro-embolic signal |
| MRA | magnetic resonance angiography |
| MRI | magnetic resonance imaging |
| NR | negative remodeling |
| PCA | posterior cerebral artery |
| PCoA | posterior communicating artery |
| P-COW | posterior circle of Willis |
| PR | positive remodeling |
| RI | remodeling index |
| RNF213 | ring finger protein 213 |
| SD | standard deviation |
| SI | signal intensity |
| SMC | smooth muscle cell |
| T1w | T1-weighted |
| TE | time-of-echo |
| TIA | transient ischemic attack |
| TOF | Time-Of-Flight |
| TR | time-of-repetition |
| VA | vertebral artery |
| VA | vessel area |
| VBJ | vertebrobasilar junction |
| VISTA | Volumetric ISotropically Turbo spin echo Acquisition |
| VSMC | vascular smooth muscle cell |

| | |
|---|---|
| VV | vasa vasorum |
| WA | wall area |
| WASID | Warfarin versus Aspirin for Symptomatic Intracranial Disease |
| WSS | wall shear stress |

# PART ONE

# Chapter 1. Introduction of the thesis

## 1.1 Background

Ischemic stroke (IS) still remains one of the major threats to the public health and the global economy, despite the continuous improvement of current diagnostic and therapeutic technology and the increasing awareness of disease prevention [1-4]. According to the literature, the causes of IS include atherosclerosis in the intracranial large arteries, cardioembolic origin, occlusion in the cerebral small vessels, stroke of other known causes, and stroke of unknown causes [5]. There are nearly 40% of patients suffering from IS caused by intracranial atherosclerosis (ICAS) among Asians, which are higher than those among Caucasians (15%) or African-Americans (29%); even worse, patients with IS attributed to ICAS are at ascending risk of stroke recurrence [6-8]. In this thesis, therefore, we confine our attention to ICAS.

In general, the structure and function of the intracranial vasculature impact directly upon the cerebral hemodynamic stress, which may be linked to one of important mechanisms of developing ICAS [9]. The circle of Willis (COW), especially the communicating arteries in the anterior COW (A-COW) and the posterior COW (P-COW), has been found protective of the intracranial arteries from blood flow stress [10]. Apparently, the anatomical anomaly in the A-COW or the P-COW may produce a significant change in the cerebral hemodynamic force [11, 12], hence the need for an exploration of the underlying role of the COW variations in the pathogenesis of ICAS. Meanwhile, a series of numerical and experimental studies suggested earlier that the larger vertebrobasilar junction (VBJ) angles might be associated with higher risks of occurring atherosclerosis, which was achieved primarily via the effect on the cerebral hemodynamic patterns [13-15]. Accordingly, further investigation into the influence of the

varying VBJ-angle degrees on the progression of vertebrobasilar atherosclerosis is also vital for understanding ICAS in patients with IS.

Currently, the clinical routine angiographic examinations only give limited information on intracranial artery stenosis, which may underestimate the severity of ICAS [16]. Yet, high-resolution intracranial magnetic resonance imaging (MRI) succeeds in fulfilling a promise to visualize the intracranial vessel-wall changes caused by ICAS [17-19]. Several imaging biomarkers indicating the atherosclerotic changes in the intracranial arterial walls were previously validated by the corresponding histological findings in our serial autopsy studies [20-22]. Consistent with our observations, some imaging biomarkers, such as plaque contrast enhancement, positive remodeling pattern, and T1-weighted hyperintensity signal, were found to be strongly correlated with the subsequent cerebral ischemic events in other studies [23]. High-resolution intracranial MRI provides clinicians and researchers with a great convenience to investigate the underlying pathogenesis of ICAS in patients with IS.

### 1.2 Objectives and organization of this thesis

From 2014 to 2020, this hospital-based prospective research included 125 consecutive adult patients with acute IS or transient ischemic attack (TIA) owing to ICAS in total, who were admitted to the Prince of Wales Hospital. Via a three-dimensional T1-weighted Volumetric ISotropically Turbo spin echo Acquisition sequence, 3.0-Tesla MRI was used for scanning the intracranial vessel-wall changes. Based on our research experience between 2014 and 2015, the scanning protocol of high-resolution intracranial MRI was modified to include the intracranial segments of the bilateral vertebral arteries (VAs) from 2016 to 2020. **Figure 1-1** illuminates the subject inclusion for each research chapter. Our research aimed at describing two major cerebral vascular variations (the COW structural anomaly and the VBJ confluence angle magnitude) among Chinese stroke patients. Then, the potential clinical

impacts of the two cerebral arterial variations on the formation and progression of intracranial large artery atherosclerosis were explored, respectively.

**Objectives:**

1. To explore the relationship between the COW anatomical completeness and the vascular locations of the intracranial large-artery atherosclerotic lesions among patients with ICAS;
2. To investigate the correlation of the incomplete COW geometry with the essential feature of the plaque wall orientation in the middle cerebral arteries (MCAs) among patients with MCA atherosclerosis;
3. To describe the anatomical patterns of the incomplete A-COW and the incomplete P-COW in patients with MCA atherosclerosis, and to examine the underlying influence of each incomplete COW pattern on the progression of symptomatic MCA atherosclerosis;
4. To explore the morphological characteristics of the vertebrobasilar plaque wall orientation affected by the VBJ angle exceeding 90° among patients with vertebrobasilar artery atherosclerosis;
5. To depict the imaging characters of the vertebrobasilar plaques quantitatively and qualitatively in patients with vertebrobasilar artery atherosclerosis, and to investigate the association of the VBJ angle over 90° with vertebrobasilar artery atherosclerosis.

**Organization of the thesis:**

The current thesis consists of four parts, including eight chapters in total.

**Part One** introduces the general information about this thesis through two chapters. **Chapter 1** gives a brief overview of the thesis. **Chapter 2** is the literature review entitled

‘Patterns of intracranial large artery atherosclerosis determine precision medicine for symptomatic stroke patients: Anatomy, hemodynamics, and histopathology’.

**Part Two** (**Chapter 3** to **5**) demonstrates the potential influences of the COW structural anomaly on intracranial large artery atherosclerosis, particularly MCA atherosclerosis. **Chapter 3** discusses the issue of the association between the anatomical integrity of the COW and the vascular locations of the intracranial atherosclerotic plaques in acute stroke patients due to ICAS (accepted as a Conference Abstract in the ESO-WSO 2020). **Chapter 4** includes patients with MCA atherosclerosis, which is entitled ‘The pattern of plaque wall distribution in middle cerebral artery atherosclerosis is correlated with the incomplete circle of Willis’ (published in the Frontiers in Neurology, 2021). **Chapter 5** also focuses on the patients with MCA atherosclerosis, discussing the topic of the clinical impact of the COW anomaly patterns on the development of symptomatic MCA atherosclerosis.

**Part Three** (**Chapter 6** and **7**) shows the underlying roles of the VBJ angle exceeding 90° in the occurrence of vertebrobasilar artery atherosclerosis. In **Chapter 6**, we are chiefly concerned with the relationship between the VBJ angle over 90° and the pattern of the vertebrobasilar plaque wall location in patients with vertebrobasilar artery atherosclerosis. In **Chapter 7**, we take an interest in the observation about the involvement of the VBJ angle more than 90° in the progression of the vertebrobasilar plaques among patients with vertebrobasilar artery atherosclerosis (accepted as a Conference Abstract in the 89$^{th}$ EAS Congress, 2021).

**Part Four** (**Chapter 8**) summarizes the findings of our research, and briefly introduces the future study directions in the areas of stroke, particularly intracranial large artery atherosclerosis.

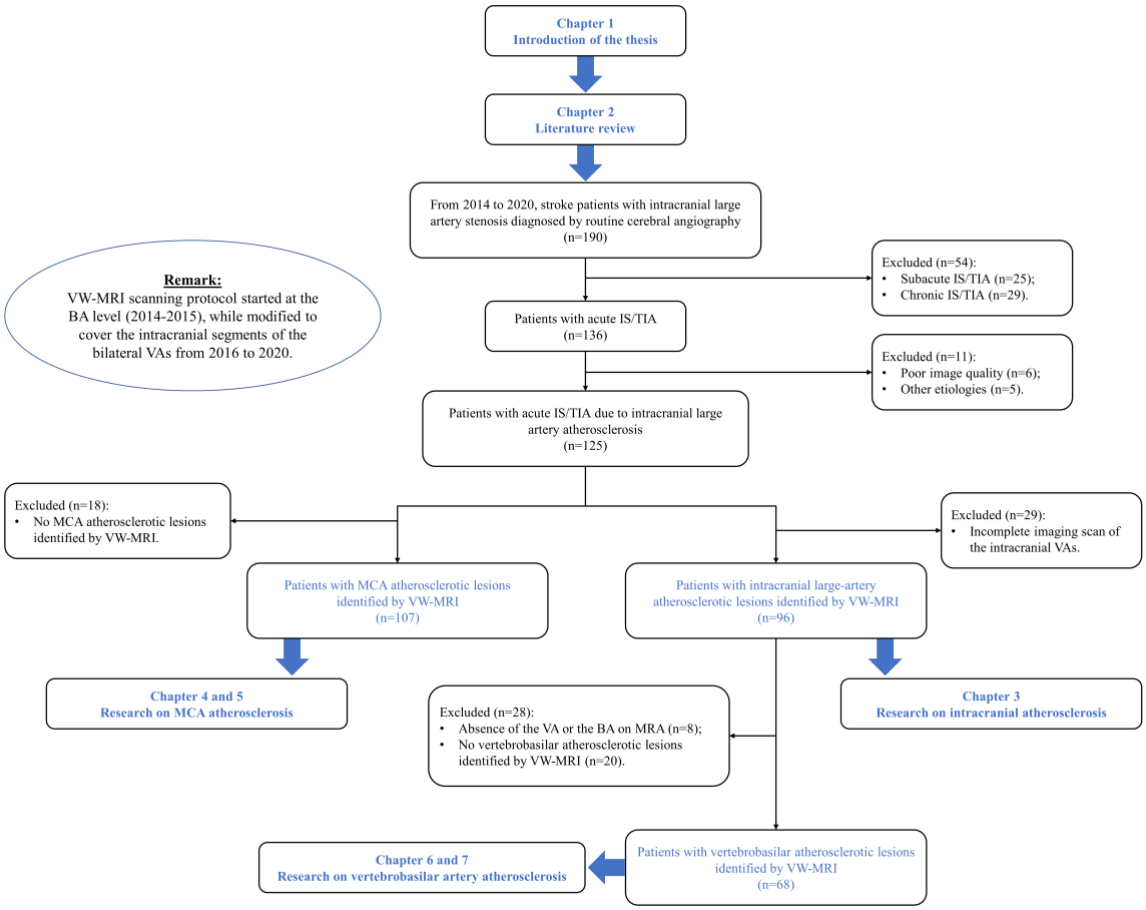


**Figure 1-1. The flow chart shows the patient selection for each research chapter. BA**, basilar artery; **IS**, ischemic stroke; **MCA**, middle cerebral artery; **MRA**, magnetic resonance angiography; **TIA**, transient ischemic attack; **VA**, vertebral artery; **VW-MRI**, vessel-wall magnetic resonance imaging.

## References


1. Diseases GBD, Injuries C. Global burden of 369 diseases and injuries in 204 countries and territories, 1990-2019: A systematic analysis for the global burden of disease study 2019. *Lancet*. 2020;396:1204-1222
2. Kim J, Thayabaranathan T, Donnan GA, Howard G, Howard VJ, Rothwell PM, et al. Global stroke statistics 2019. *Int J Stroke*. 2020;15:819-838
3. Wang YJ, Li ZX, Gu HQ, Zhai Y, Jiang Y, Zhao XQ, et al. China stroke statistics 2019: A report from the national center for healthcare quality management in neurological diseases, china national clinical research center for neurological diseases, the chinese stroke association, national center for chronic and non-communicable disease control and prevention, chinese center for disease control and prevention and institute for global neuroscience and stroke collaborations. *Stroke Vasc Neurol*. 2020;5:211-239
4. Rajsic S, Gothe H, Borba HH, Sroczynski G, Vujicic J, Toell T, et al. Economic burden of stroke: A systematic review on post-stroke care. *Eur J Health Econ*. 2019;20:107-134
5. Adams HP, Jr., Bendixen BH, Kappelle LJ, Biller J, Love BB, Gordon DL, et al. Classification of subtype of acute ischemic stroke. Definitions for use in a multicenter clinical trial. Toast. Trial of org 10172 in acute stroke treatment. *Stroke*. 1993;24:35-41
6. Lange MC, Ribas G, Scavasine V, Ducci RD, Mendes DC, Zetola VHF, et al. Stroke recurrence in the different subtypes of ischemic stroke. The importance of the intracranial disease. *Arq Neuropsiquiatr*. 2018;76:649-653

7. Saber H, Thrift AG, Kapral MK, Shoamanesh A, Amiri A, Farzadfard MT, et al. Incidence, recurrence, and long-term survival of ischemic stroke subtypes: A population-based study in the middle east. *Int J Stroke*. 2017;12:835-843

8. Holmstedt CA, Turan TN, Chimowitz MI. Atherosclerotic intracranial arterial stenosis: Risk factors, diagnosis, and treatment. *Lancet Neurol*. 2013;12:1106-1114

9. Ritz K, Denswil NP, Stam OC, van Lieshout JJ, Daemen MJ. Cause and mechanisms of intracranial atherosclerosis. *Circulation*. 2014;130:1407-1414

10. Vrselja Z, Brkic H, Mrdenovic S, Radic R, Curic G. Function of circle of willis. *J Cereb Blood Flow Metab*. 2014;34:578-584

11. Routsonis KG, Stamboulis E, Christodoulaki M. Anomalies of the circle of willis and atherosclerosis. *Vasc Surg*. 1973;7:141-145

12. Hartkamp MJ, van Der Grond J, van Everdingen KJ, Hillen B, Mali WP. Circle of willis collateral flow investigated by magnetic resonance angiography. *Stroke*. 1999;30:2671-2678

13. Ravensbergen J, Krijger JK, Hillen B, Hoogstraten HW. The influence of the angle of confluence on the flow in a vertebro-basilar junction model. *J Biomech*. 1996;29:281-299

14. Ravensbergen J, Ravensbergen JW, Krijger JK, Hillen B, Hoogstraten HW. Localizing role of hemodynamics in atherosclerosis in several human vertebrobasilar junction geometries. *Arterioscler Thromb Vasc Biol*. 1998;18:708-716

15. Zhang Y, Menon NV, Li C, Chan V, Kang Y. The role of bifurcation angles on collective smooth muscle cell biomechanics and the implication in atherosclerosis development. *Biomater Sci*. 2016;4:430-438

16. Leng X, Wong KS, Liebeskind DS. Evaluating intracranial atherosclerosis rather than intracranial stenosis. *Stroke*. 2014;45:645-651

17. Xu W. High-resolution mri of intracranial large artery diseases: How to use it in clinical practice? *Stroke Vasc Neurol*. 2019;4:102-104

18. Arenillas JF, Dieleman N, Bos D. Intracranial arterial wall imaging: Techniques, clinical applicability, and future perspectives. *Int J Stroke*. 2019;14:564-573

19. Song JW, Wasserman BA. Vessel wall mr imaging of intracranial atherosclerosis. *Cardiovasc Diagn Ther*. 2020;10:982-993

20. Yang WJ, Chen XY, Zhao HL, Niu CB, Zhang B, Xu Y, et al. Postmortem study of validation of low signal on fat-suppressed t1-weighted magnetic resonance imaging as marker of lipid core in middle cerebral artery atherosclerosis. *Stroke*. 2016;47:2299-2304

21. Yang WJ, Chen XY, Zhao HL, Niu CB, Xu Y, Wong KS, et al. In vitro assessment of histology verified intracranial atherosclerotic disease by 1.5t magnetic resonance imaging: Concentric or eccentric? *Stroke*. 2016;47:527-530

22. Chen XY, Wong KS, Lam WW, Ng HK. High signal on t1 sequence of magnetic resonance imaging confirmed to be intraplaque haemorrhage by histology in middle cerebral artery. *Int J Stroke*. 2014;9:E19

23. Song JW, Pavlou A, Xiao J, Kasner SE, Fan Z, Messe SR. Vessel wall magnetic resonance imaging biomarkers of symptomatic intracranial atherosclerosis: A meta-analysis. *Stroke*. 2021;52:193-202

# Chapter 2. Literature review

# Patterns of intracranial large artery atherosclerosis determine precision medicine for symptomatic stroke patients: Anatomy, hemodynamics, and histopathology

## 2.1 Background

Ischemic stroke is a primary cause of stroke-related death and long-term disability, which remains a serious challenge to the global public health [1, 2]. Despite recent advances in the medical management and prevention of IS, a rise in the quantities of incident first strokes, stroke-related deaths and disability-adjusted life-years lost has been revealed in direct relevance to IS for the past decades [3, 4]. The situation becomes much worse in the developing countries, where the incidence rate of IS continues to ascend [3, 4]. Of note, ICAS leads to a higher level of IS prevalent among Asians than that among African-Americans or Caucasians [5, 6]. As major etiology of IS, ICAS even increases the likelihood of stroke recurrence [7, 8].

Symptomatic ICAS occurs within any intracranial large artery where the atherosclerotic lesions dynamically and unstably grow, and causes clinical signs or symptoms of neurological dysfunction related to the downstream ischemia in the corresponding arterial territory [9]. The development of symptomatic ICAS is independently correlated with the non-modifiable risk factors, such as age, race and male sex [10, 11]. The paramount modifiable risk factors for symptomatic ICAS includes hypertension, diabetes, dyslipidemia, metabolic syndrome and unhealthy lifestyle [10, 11]. Besides, the structural variations in the COW are regarded as potential risk factors for symptomatic ICAS [10, 12]. Specific polymorphisms for ICAS are also identified in the genome wide association analyses [13, 14].

The progress of symptomatic ICAS has two basic features: First, the prominent function of cerebrovascular anatomy on altering intracranial artery hemodynamics, thereby worsening the vessel wall conditions to develop atherosclerosis [10]. Second, the histopathology of intracranial atherosclerotic plaque itself characterizes the atherogenesis in the cerebral vascular system [10]. Investigating the main patterns in symptomatic ICAS regarding anatomy, hemodynamics and histopathology may conduce more to our understanding of this disease, and in turn guide precise diagnostic and therapeutic strategies for stroke patients, which is still much to discuss. This review, therefore, aims to cover the anatomical, hemodynamic and histopathological aspects of ICAS via summarizing available and relevant literature.

### 2.2 Cerebrovascular anatomical variations and ICAS

The COW refers to the basic arterial linkage of cerebral blood supply from the bilateral internal carotid arteries (ICAs) and the vertebrobasilar circulation (**Figure 2-1**). This arterial anastomotic system is divided into two parts, including the anterior COW and the posterior COW. The A-COW is comprised of the anterior communicating artery (ACoA) and the first segments of both left and right anterior cerebral arteries (ACA-A1). The P-COW is formed by the bilateral posterior communicating arteries (PCoAs) and the first segments of both left and right posterior cerebral arteries (PCA-P1).

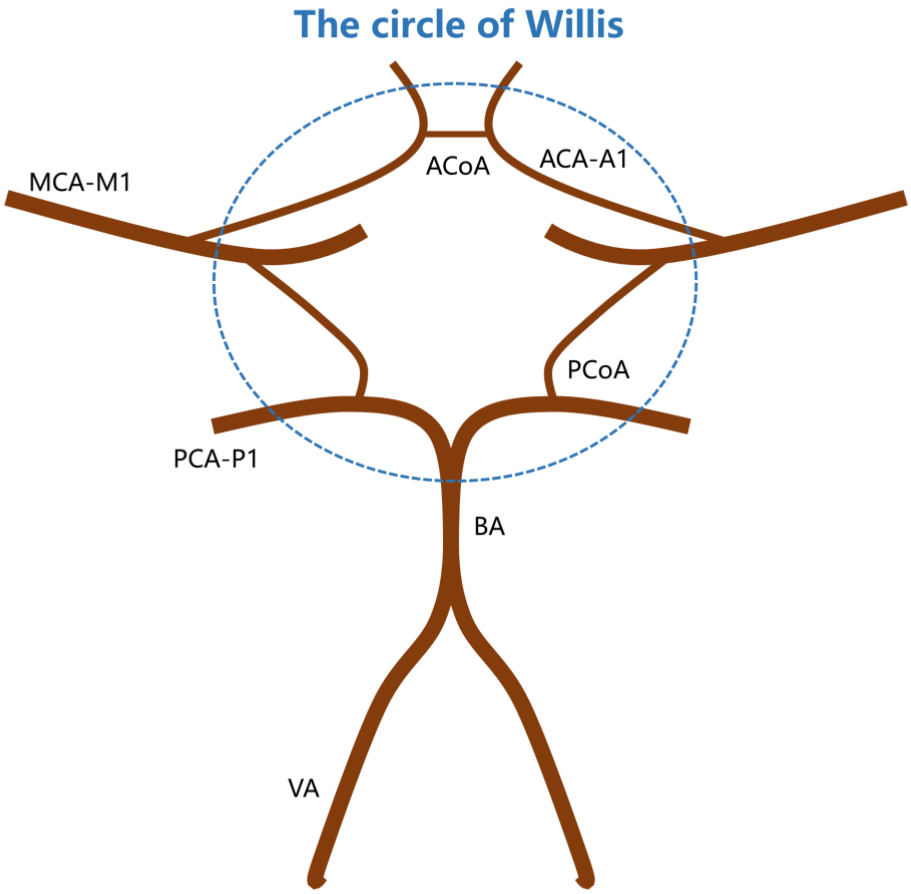


**Figure 2-1. The typical structure of the circle of Willis (in the blue dashed outline). ACA**, anterior cerebral artery; **ACoA**, anterior communicating artery; **BA**, basilar artery; **MCA**, middle cerebral artery; **PCA**, posterior cerebral artery; **PCoA**, posterior communicating artery; **VA**, vertebral artery.

The level of anatomical integrity in the COW varies substantially in different populations [15-17]. One recent autopsy study of 73 human brain specimens showed that only 6.8% had a complete COW [18]. The anatomical abnormalities were identified in one hundred and nineteen arteries of the COW, 44.5% of which were found in the PCoAs [18]. The other research with a larger scale via using computed tomographic angiography (CTA) suggested that 37.1% of all 834 cases had a complete COW, which was more prevalent among female individuals [19]. Similarly, the absence of the bilateral PCoAs was the most common variation in the COW, followed by the absence of the right PCoA and the left PCoA [19]. Generally, the variation of the COW completeness is a universal phenomenon, although the differences of the study cohorts or the detection methods may lead to the fluctuation in the prevalence of each COW subtype. A total of 2,246 healthy Chinese male individuals were scanned by magnetic resonance angiography (MRA) to analyze the COW variations, of whom 12.2% possessed a complete COW, 21.4% had an incomplete A-COW, and 83.9% showed an incomplete P-COW [20]. Another MRA study, besides, detected a complete COW in 12.7% of all 482 subjects with symptomatic carotid artery atherosclerosis, an incomplete A-COW in 40.7%, and an incomplete P-COW in 79.7% [21].

The arterial dimension in the cerebral vascular system differs greatly among normal individuals as well [22, 23]. In one research of measuring ex vivo human COW samples, high-resolution magnetic resonance imaging (HR-MRI) precisely revealed the considerable variability in the vessel wall thickness throughout the whole arteries of the COW [24]. On average, patients with cerebrovascular disease had thicker vessel walls in the COW, compared to those without cerebrovascular disease [24]. In another MRA study of Kosovo's population, a larger diameter of the PCoA and a longer dimension of the ACoA were observed in female, whereas male subjects possessed significantly larger sizes of other arteries in the COW [25]. Differences in the arterial diameters of the COW were also significant

between the subjects less than and more than 40 years old [25]. Evidence is now mounting to present the anatomical variability of the intracranial arterial segments. The mean luminal diameter of the basilar arteries (BAs) was reported in inverse association with the COW completeness [26]. The luminal sizes of the ICAs and the VAs were significantly different between sub-groups on sexes, or between left and right sides [27]. Notably, various types of anatomical variations in the MCAs, like the curve orientation or the branching pattern in the MCA-M1 segment, were recognized in the recent clinical studies [28, 29].

These anatomical variations in the intracranial vasculature were of potential importance in the clinical practice for stroke patients. An incomplete COW might serve as an independent risk factor for developing unstable carotid atherosclerotic plaques with intra-plaque hemorrhage (IPH) [21]. On the other hand, a complete structure of the COW might be a protective factor against white matter hyperintensities in patients with severe unilateral ICA atherosclerotic stenosis [30]. Importantly, the assessment on the COW completeness with a scoring system (0-2: poor integrity; 3-6: good integrity) further suggested that a low integrity score (0-2) of symptomatic patients with severe ICAS was shown in significant correlation with a high stroke recurrence risk [31, 32]. A study on the distinct geometry of the MCA, in addition, found that a curved M1 segment with an inferior orientation was independently related to a decreased risk of stroke occurrence [28]. These clinical results demonstrated that the anatomical variability in the intracranial vascular system might help with the risk stratification for patients with symptomatic ICAS. Interestingly, some current case reports observed a possible relationship between the COW anomaly and the entity of deadly or rare cerebral infarction [33, 34], which might provide insight into the underlying stroke pathogenesis in terms of the intracranial artery variations. Future clinical research is needed to elucidate this phenomenon.

### 2.3 Hemodynamics in ICAS

Intracranial artery hemodynamics should be continually reappraised, as the occurrence and development of atherosclerotic lesions are largely influenced by the significant changes to the hemodynamics within the intracranial atherosclerotic arteries [10, 35, 36]. This process involves multi-factors, namely post-ischemic hypo-perfusion, collateral compensation from the COW, as well as cerebral micro-emboli (**Table 2-1)**, which may have a further impact on the therapeutic options and overall outcomes for symptomatic patients with ICAS [37-39].

**Table 2-1. A summary of the potential methods of monitoring hemodynamic factors in intracranial atherosclerosis.**

| Hemodynamic factors | Potential monitoring methods | Arteries investigated in the studies | Authors |
|---|---|---|---|
| Post-ischemic hypo-perfusion | Fluid-attenuated inversion recovery vascular hyperintensity | MCA-M2 | Nomura T, et al [46] |
| | Delta waves | MCA | Sakamoto S, et al [47] |
| | Upper extremity somatosensory evoked potentials | Carotid artery | Khattar NK, et al [48] |
| | Eight-channel electroencephalography | Carotid artery | Khattar NK, et al [48] |
| The COW collateral compensation | Total cerebral blood flow | ICA | Zarrinkoob L, et al [59] |
| | Cerebral blood flow velocity | MCA | Wei W, et al [60] |
| | Blood flow rate | Carotid artery / MCA / ACA-A2 | Zarrinkoob L, et al [61] |
| Cerebral micro-emboli | Cerebral micro-embolic signal | MCA | Sun DJ, et al [75] |
| | Cerebral micro-embolic signal | ICA | Farina F, et al [76] |
| | Cerebral micro-embolic signal | Carotid artery | Spence JD [77] |

ACA, anterior cerebral artery; COW, circle of Willis; ICA, internal carotid artery; MCA, middle cerebral artery.

### 2.3.1 Cerebral hypo-perfusion and ICAS

Early cerebral hemisphere hypo-perfusion caused by the blocked intracranial artery may result in relevant clinical symptoms of neurological dysfunction in patients with IS or TIA [40-42]. Consequently, the treatment strategy for intracranial artery steno-occlusion is designed to address a real issue of recanalization for this obstructive cerebral vessel. During post-ischemic reperfusion, yet, cerebral hypo-perfusion may still progress in either peripheral or central ischemic territories, which thus may induce lower availability of oxygen and even aggravate tissue impairment in the brain [43]. Under such circumstances, therapeutic management should aim at ensuring the maintenance of cerebral blood flow (CBF) and avoiding persistent post-ischemic hypo-perfusion in the impaired brain region [44, 45]. This pathophysiologic perception of ICAS stresses the importance of monitoring hemodynamic process, which may be beneficial to guiding therapy choice for these patients.

A growing number of research demonstrated that cerebral hypo-perfusion status could be quantitatively analyzed in patients with ICAS. For example, higher signal intensity of fluid-attenuated inversion recovery vascular hyperintensity within the MCA-M2 segment might reflect severer hypo-perfused territory of the occlusive MCA-M1 segment [46]. An interesting clinical case of a patient with MCA occlusion undergoing extracranial-intracranial bypass surgery also indicated that the cerebral hypo-perfusion areas were distributed with delta waves before surgery, whereas these waves could not be detected after operation when the CBF was improved [47]. Besides, a large study cohort of 584 subjects with carotid artery stenosis evaluated the perioperative conditions of stroke after carotid endarterectomy treatment [48]. One of the results showed that the cerebral hypo-perfusion in these patients could be monitored during intraoperative management by upper extremity somatosensory evoked potentials and eight-channel electroencephalography [48]. These results may imply the further utilization in ICAS.

Monitoring cerebral hypo-perfusion is of clinical importance in ICAS. In the impaired hemisphere of patients with acute IS, the hypo-perfusion region where the steno-occlusive cerebral arteries could not be compensated was associated with the pathologically increased levels of oxygen extraction fraction, a marker suggestive of the brain area at risk [49]. In another study of 787 consecutive patients with acute IS in anterior circulation, the cerebral hypo-perfusion was reported the most common in the unilateral occlusive ICAs, rather than in the unilateral occlusive MCAs [50]. This finding implied that cerebral hypo-perfusion might differentiate high-risk arterial territories in anterior circulation. As also revealed in patients with acute IS, the area of moderately hypo-perfused lesion was independently related to the occurrence of brain parenchymal hematoma after treated with intra-arterial tissue-type plasminogen activator [51]. Moreover, cerebral hypo-perfusion in an arterial territory owing to severe intracranial atherosclerotic steno-occlusion might suggest endovascular revascularization therapy as a priority to these stroke patients [52].

### 2.3.2 The COW collateral compensation and ICAS

Cerebral collateral circulation may, as needed, supplement an encephalic arterial lesion with additional perfusion of nutrients, if the cerebrovascular disease has decreased or obstructed the main cerebral blood supply to that region. It should be emphasized that the COW functions as the most pivotal compensatory pathway in the collateral circulation, especially when intracranial artery steno-occlusion occurs [53, 54]. Fundamentally, the size, the existence or the absence of the major arterial components in the COW may determine its capacity for compensating collateral blood supply for intracranial steno-occlusive lesions [55-57]. Better collateral compensation from the COW is supposed to indicate higher possibility of successful reperfusion in the symptomatic intracranial atherosclerotic lesions, which may even help to improve stroke outcomes with thrombolytic or endovascular therapy [53, 54, 58].

It is also obvious from the basic features of symptomatic ICAS process that intracranial artery hemodynamics may be mostly affected by the COW structure and its collateral compensation, which ultimately decides the progress and outcome of the patients. One HR phase-contrast MRI study demonstrated that the distribution of the total CBF in the contralateral ICA was higher than that in the ipsilateral ICA, when the ACA-A1 segment was found absent or hypoplastic in the healthy adult individuals [59]. In stroke patients, moreover, the severe unilateral ICA stenosis itself could significantly diminish the CBF velocity of the ipsilateral MCA [60]. Yet, this CBF velocity was significantly elevated, when the ACoA was the only collateral pathway, rather than the PCoA [60]. This observation indicated that the damaged cerebral perfusion of severe unilateral ICA stenosis might be better compensated through the ACoA collaterals [60]. Another recent research on patients with carotid steno-occlusion further showed that an increase in blood flow rate (BFR) was detected in the contralateral carotid artery, compared to that in the ipsilateral carotid artery [61]. The contralateral ICA via the ACA-A1 segment served as main collaterals to equalize the BFR and to supply the bilateral territories of the ACAs [61]. The collaterals could compensate the BFR of the ipsilateral MCA and the ipsilateral ACA-A2 segment [61]. Clearly, the role of the COW collateral compensation in altering cerebral artery hemodynamics draws our attention to the importance of evaluating the COW collateral status based on the entire intracranial vasculature, and this strategy will put ICAS patients in a favorable position to predict their prognosis [62-64].

### 2.3.3 Cerebral micro-emboli and ICAS

The pathology of ICAS regarding intracranial artery hemodynamics includes micro-embolic injury in the brain as well. Hypo-perfusion or inadequate collateral flows after intracranial artery steno-occlusion may not wash out perilous cerebral micro-emboli, which potentially contributes to subsequent thromboembolic events or recurrent stroke [65-68]. Our

prior study indicated that cerebral micro-emboli in symptomatic MCA stenosis were more commonly detectable in the high degree of intracranial ICA calcification on the ipsilateral side [69]. This finding widened the scope of knowledge on underlying mechanisms of ICAS that the hemodynamic clearance of cerebral micro-emboli might be damaged in the downstream arterial territory, when the upstream intracranial artery was highly calcified [69].

Sources of active cerebral micro-emboli are heterogeneous, but those micro-emboli from cardiovascular origin are beyond our discussion in ICAS. Atherosclerosis or platelet-rich fibrin may generate cerebral micro-emboli causing micro-infarcts, which were reported in strong relevance to ICAS by an autopsy study [70]. For instance, the micro-emboli of the ipsilateral MCA were mainly derived from the ulcerated plaques and the intraluminal thrombus in severe ICA atherosclerotic stenosis [71]. Notably, numerous cerebral micro-emboli may even originate from vulnerable carotid plaques after mechanically therapeutic procedures [72].

Despite various origins of cerebral micro-emboli that possibly lead to a highly variable course, detecting the occurrence or development of cerebral micro-embolic signals (MES) via transcranial ultrasound may give valuable clues to assessing ICAS conditions in symptomatic stroke patients [73, 74]. The presence of cerebral MES was significantly correlated with plaque vulnerability and neurological function decline [75]. Besides, the prevalence of cerebral MES was higher in symptomatic patients with ICAS than that in asymptomatic patients [75]. More importantly, higher MES in ICAS patients after endovascular therapy was found in significant association with severer ipsilateral ICA steno-occlusion, lower collateral status, and insufficient arterial recanalization [76]. On the contrary, a reduction in the cerebral MES might be related to the stabilization of carotid plaques after intensive medical treatment [77]. These investigations, along with other evidence that cerebral micro-emboli might largely result in silent stroke and impaired cognition, all highlighted the functional role of MES in

prognosticating ICAS after interventions [78-82]. However, some observation with a large study sample size also revealed low sensitivity of investigating the incidence of cerebral MES among unselected patients with IS [83]. For this reason, the clinical routine implement of monitoring cerebral MES should still be critically evaluated with more convincing research on whether cerebral MES could serve as a reliable parameter in ICAS patients [74].

## 2.4 Histopathology of ICAS

### 2.4.1 Luminal stenosis in ICAS

Modern medical assessment of ICAS is mainly dependent on the angiographic measurement of luminal stenosis expressed as a percentage score of the complete vascular lumen [84]. It is clear that grading the severity of luminal stenosis in the intracranial arteries can act as a rough guide to the medical management. In this regard, evaluating evolutionary growth of luminal stenosis after medical or endovascular therapy may help with stratifying the risks of stroke recurrence over the long term [85]. In a Warfarin versus Aspirin for Symptomatic Intracranial Disease (WASID) trial, 70-99% atherosclerotic stenosis in an intracranial artery was defined as ‘severe’, and proved to be an independent risk factor for stroke recurrence [86]. Nevertheless, the reality of clinical practice was always more complicated. 50-69% stenosis was regarded as ‘moderate’ in ICAS, but did not catch as much attention as severe stenosis [86]. In ICAS patients with moderate narrowing, the incidence rate of recurrent stroke was still up to ten percent within a year, also as shown in the WASID study [86]. Even worse, the significant association of less than 50% luminal stenosis with a risk of stroke recurrence was reported in patients with advanced ICAS [87].

There are overwhelming evidence showing that the anatomical stenosis estimated by angiography may not entirely reflect all the conditions of ICAS [84]. For instance, the luminal stenosis might not represent the functional status of distal flow limitation in the intracranial

atherosclerotic arteries [88]. A recent Chinese ICAS cohort study further clarified that a worse hemodynamic state in moderate-to-severe MCA-M1 stenosis, rather than a higher luminal stenosis degree, significantly elevated the possibility of developing severer white matter changes in the ipsilateral cerebral hemisphere [89]. Another case also proved the limitation of sole reliance on grading luminal stenosis. The occurrence of acute cerebral infarction caused by symptomatic MCA stenosis was found to be correlated with plaque enhancement and downstream perfusion damage, but not with arterial stenosis percentage [90]. In the future, consequently, patients with symptomatic ICAS may better benefit from the practical combination of measuring arterial lumen stenosis with other clinical information, like the hemodynamic parameters quantified by computational fluid dynamics or the features of plaque stability [91, 92].

### 2.4.2 Plaque components and morphology in ICAS

Based on a revised system of the American Heart Association Classification [93], atherosclerotic plaques have distinct histopathological characteristics at each stage. Non-diseased vascular segments are free from the intimal thickening or the inflammatory infiltration. In the early stage of atherosclerotic plaques, intimal thickening is identified as accumulative smooth muscle cells (SMCs), fatty streak as an accumulation of foamy macrophages, and pathological intimal thickening as amassed SMCs and proteoglycans. In the advanced stage of plaques, fibrosis is shown as collagen rich, fibro-calcification as calcified, and fibro-lipid as lipid-rich tissue covered by a fibrous cap with a lipid core or calcification (over 40% of the lipid area). Atherosclerotic plaques are regarded as complicated advanced in virtue of IPH, a rupturing fibrous cap, a chronic complete steno-occlusion and an eroded luminal surface (**Figure 2-2**).

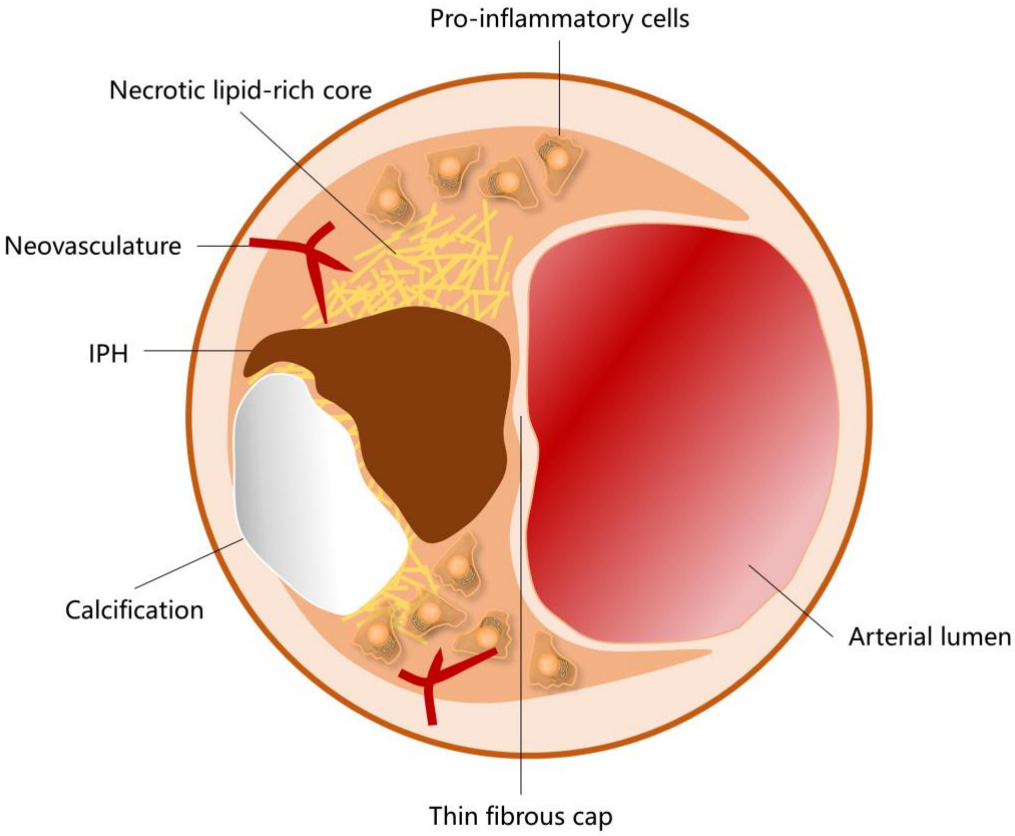


**Figure 2-2. Representative components of a vulnerable atherosclerotic plaque.** IPH, intra-plaque hemorrhage.

This categorization system of plaque components is widely utilized in the clinical field, and is beneficial for the risk stratification in ICAS. Our previous study demonstrated that the plaques with lipid area more than 40%, IPH, neovasculature or thrombus were more prevalent in the symptomatic MCA atherosclerotic lesions related to cerebral infarcts [94]. The infiltration of macrophages and T lymphocytes within the MCA lesions was also reported in correlation with cerebral infarcts [94]. Lipid area and intra-plaque neovasculature, together with luminal stenosis, were independently associated with the risks of occurring ischemic events in the MCA territory [94]. As another typical alteration in the morphology, the patterns of plaque wall thickening can be categorized into eccentric and concentric. We found that the differences of plaque burden and cerebral infarctions were not significant between eccentric and concentric patterns of the MCA plaques, implying no relevance of both geometric patterns to the elevated risks in the MCA lesions [95]. On the other hand, the simultaneous occurrence of eccentric and concentric plaque wall thickening within the BA lesions was suggested as the advanced stage of ICAS along with an increased risk of developing IS [96].

Other ICAS research further indicated that the development and progression of intracranial atherosclerotic lesions might have their own rules. The atherosclerotic plaques were systematically explored in both large and small arteries along the entire COW [97]. The intracranial large arteries, including the ICA, the MCA, the BA and the VA, were more vulnerable to developing the early and advanced atherosclerotic plaques [97]. Interestingly, the VA was the most likely to grow external elastic lamina, high-density elastin fibrous media and calcification [97]. Another histopathological evidence was the difference of the adventitial vasa vasorum (VV) among the intracranial atherosclerotic large arteries from our postmortem research [98]. The VV may function as a determinant in the formation, development and destabilization of atherosclerotic plaques [99]. Compared with the BA and the MCA, the VA had a higher occurrence of the adventitial VV [98]. The adventitial VV in the VA was

significantly related to the progressive atherosclerotic lesions with heavier plaque burden, severer luminal narrowing, as well as more plaques of concentricity and calcification [98]. Moreover, the VA with the adventitial VV was characterized by larger luminal diameter, thicker vessel wall, and wider intima-media than the VV-free VA [98].

More examples could be given that the histopathological characters of atherosclerotic lesions were robustly associated with the spatial distributions of plaques throughout the intracranial arterial tree. Our prior autopsy study revealed that the MCA atherosclerotic lesions possessed severer degree of luminal stenosis and more plaques of eccentricity than the BA lesions and the VA lesions, while the BA lesions had more luminal thrombi, and the VA lesions were more possible to grow calcified [100]. It was reasonable to assume that the respective risk factors and stroke mechanisms of ICAS in anterior and posterior circulation led to the individual histopathology of atherosclerotic lesions within the intracranial vasculature [101-103]. Apparently, future research is eagerly required to explain thoroughly why the histomorphological changes in the atherosclerotic lesions may differ among various segments of the intracranial arterial tree.

### 2.4.3 Plaque vulnerability in ICAS

The occurrence of ICAS runs through the whole life of human beings, but the largest part of atherosclerotic plaques in the COW stay in an early and stable condition, without inducing any downstream infarct in the vascular territory [99]. Those complicated advanced plaques, which are also described as “vulnerable”, may often cause life-threatening cerebral thrombosis during the exacerbation of ICAS [99]. Accordingly, discriminating vulnerable plaques in patients with ICAS has a certain value from the perspectives of both researchers and clinicians. The plaque vulnerability, for example, was shown to be correlated with arterial embolization in the multiple lesions of MCA infarction [104]. This finding demonstrated

that the unstable or ruptured atherosclerotic plaques generated many arterial emboli, and might further lead to ischemia in the several downstream regions of the MCA [104]. These vulnerable atherosclerotic plaques not only predicted artery-to-artery embolism as an intracranial artery infarction pattern, but also independently indicated the increased likelihood of occurring recurrent stroke in symptomatic ICAS [105-107]. Current studies validated in more detail that the prominent features of plaque vulnerability, such as IPH, fibrous cap rupture and lipid-rich core necrosis (**Table 2-2)**, might be conducive to the characterization of symptomatic ICAS and the identification of stroke patients at greater risks [108-110].

**Table 2-2. A summary of the potential clinical value of the vulnerable plaque components in intracranial atherosclerosis.**

| Plaque features | Potential clinical value | Arteries investigated in the studies | Authors |
|---|---|---|---|
| Intra-plaque hemorrhage | Independently related to cortical cerebral micro-infarcts and impaired cognition | Carotid artery | Takasugi J, et al [112] |
| | Independent risk factor for severe intracranial atherosclerotic stenosis | Carotid artery | Xu Y, et al [113] |
| | Related to a high rate of acute ischemic events | BA | Yu JH, et al [115] |
| | Positively related to the infarction volume and the maximum region of deep subcortical infarction | MCA | Shen M, et al [116] |
| Fibrous cap rupture | Moderate-to-severe carotid stenosis | Carotid artery | Gao T, et al [117] |
| | Symptomatic carotid atherosclerotic lesions | Carotid artery | Millon A, et al [105] |
| Lipid-rich core necrosis | Positively related to the carotid plaque intima-media thickness | Intracranial atherosclerotic arteries | Iwakiri T, et al [123] |
| | Independently predicted cerebrovascular events within a year | Carotid artery | Li J, et al [124] |
| | Coexisting carotid plaque necrotic core with intracranial atherosclerotic stenosis independently predicted cerebral artery infarcts in a year | Carotid artery | Li J, et al [125] |
| | A potential indicator for a heavy plaque burden | BA | Lee YK, et al [126] |
| | A potential therapeutic target for plaque stabilization | Intracranial atherosclerotic arteries | Rollo M, et al [120] |

BA, basilar artery; MCA, middle cerebral artery.

IPH is an essential marker for identifying the extra-intracranial vulnerable plaques and stratifying the risks among patients with ICAS [111]. The existence of IPH in the carotid plaques was independently correlated with the elevated possibility of developing cortical cerebral micro-infarcts and impaired cognition in patients with carotid artery atherosclerosis [112]. Interestingly, the carotid plaque IPH might also act as an independent risk factor for severe atherosclerotic stenosis in the intracranial arteries [113]. Compared with the extracranial carotid arteries (ECAs) evolving into atherosclerosis, however, the intracranial atherosclerotic arteries were observed to have higher incidence rates of IPH (25% and 13.5%) and severe stenotic narrowing (26.9% and 9.6%) among Asian patients with symptomatic IS [114]. Detecting IPH is particularly useful in ICAS. IPH within the BA plaques was significantly more common in the symptomatic BA lesions, as well as in the severer stenotic BAs, which was related to a high rate of acute ischemic events [115]. Moreover, the MCA plaque IPH was revealed in positive correlation with the infarction volume and the maximum region of deep subcortical infarction, which provided insight into investigating the etiology of MCA atherosclerosis for patients with acute IS [116].

Fibrous cap rupture is another obvious target for defining plaque vulnerability. The change in status of fibrous cap is determined by the development of atherosclerotic plaques, which means the more advanced a plaque, the less intact a fibrous cap [105]. The fibrous cap thinning or rupture was more prevalently detected in patients with moderate-to-severe carotid artery atherosclerosis [117], while a higher frequency of the ruptured fibrous cap was also found in the symptomatic carotid atherosclerotic lesions than that in the asymptomatic lesions [105]. Various studies showed that the process of fibrous cap rupture might be multifactorial. The fibrous cap rupture of carotid artery plaques was stimulated by the inflammatory cytokines and proteinase secreted from the infiltrating macrophages and T cells, which then led to

symptomatic carotid artery atherosclerosis [118]. Another plausible explanation might be offered that the rupture of plaque fibrous cap might result from the pulsatile pressure on the vessel wall owning to blood flow, and subsequently cause thrombotic events [67]. It was also suggested in ICAS that the plaque with fibrous cap eroded in the severest atherosclerotic narrowing of the MCA-M1 segment was formed under the high wall shear stress (WSS) during the systolic phase of cardiac cycle [119]. As yet little was known about fibrous cap rupture and ICAS, hence an in-depth investigation into testifying to their relationship.

Assessing the state of a lipid-rich core in the vulnerable plaques may help with a sound understanding of ICAS [120-122]. An earlier autopsy study reported that the presence of a lipid-rich necrotic core in the intracranial atherosclerotic arteries was positively correlated with the carotid plaque intima-media thickness, implying the advanced alteration in the atherosclerotic vessel walls [123]. Similarly, the lipid-rich core necrosis was shown in significant relevance to the carotid plaque surface irregularity, which independently suggested cerebrovascular events within a year [124]. Besides, the coexistence of a carotid plaque necrotic core with intracranial atherosclerotic stenosis also independently predicted cerebral artery infarcts in one year of follow-up [125]. More importantly, recent research valued a necrotic core as a potential indicator for a heavy plaque burden in BA atherosclerosis [126]. Among ICAS patients with instable or ruptured plaques, above all, lipid-rich core necrosis may be considered as a diagnostic biomarker for plaque vulnerability, or even a therapeutic target for plaque stabilization [120].

Apart from the above discussion of vulnerable plaque components, the relationship between plaque vulnerability and other systemic factors was further explored in symptomatic stroke patients. The independent association of systolic blood pressure with IPH was concluded, after adjustment for the conventional cardiovascular risk factors [127]. In addition, the incomplete structure of the COW was independently related to the development of carotid

plaque IPH, indicating the impact of the COW completeness upon the carotid plaque vulnerability [21]. Considering the compensatory role of the COW in maintaining cerebral blood supply, the cerebrovascular hemodynamics and the progression of plaque vulnerability may be linked in ICAS patients. In other words, a direct connection between anatomical-hemodynamic and histopathological patterns may be established in symptomatic ICAS, which should be elucidated specifically in future studies.

### 2.5 Arterial remodeling in ICAS

As an autoregulation pattern responding to atherosclerotic narrowing, arterial remodeling plays a critical role in the pathogenesis of ICAS, including positive remodeling (PR) and negative remodeling (NR) [128-130]. In general, the PR pattern may enlarge the luminal area in compensation, hold the actual use of vascular lumen in reserve, and ease the stenotic condition [131]. Contrariwise, the NR pattern may paradoxically constrict the blood vessel in the atherosclerotic lesion [131]. Growing evidence have suggested the involvement of genetic, cellular, humoral and hemodynamic factors with arterial remodeling in ICAS. Single nucleotide polymorphisms, like ring finger protein 213 (RNF213) gene variants, were considered in correlation with NR of the atherosclerotic MCAs [132]. Besides, increased levels of antithyroid peroxidase-antibody might affect arterial remodeling in ICAS through directly activating the media-to-intima migration of vascular smooth muscle cells [133]. The chronic stimulation of high WSS might outward remodel the intracranial atherosclerotic arteries and destabilize the vulnerable plaques as well [134].

Confirming the arterial remodeling patterns is meaningful in ICAS. First, the PR pattern was significantly correlated with MESs and multiple infarcts in patients with MCA atherosclerosis [135, 136], which implied the potential role of determining the arterial remodeling patterns in illuminating stroke mechanisms of ICAS. Second, ICAS patients may benefit

from differentiating the arterial remodeling patterns, when stratified risks for acute ischemia. For instance, the PR pattern of the atherosclerotic MCAs was revealed in significant relevance to the symptomatic lesions, a larger plaque area, as well as a higher score of National Institute of Health stroke scale [137, 138]. Additionally, recent evidence in a Meta-analysis further demonstrated that PR of the intracranial atherosclerotic lesions was significantly related to the acute occurrence of vascular infarction in the downstream territory [139]. An explanation in this study was given that PR was suggestive of higher plaque vulnerability, compared to NR in the same stenotic state [139]. Third, evaluating the arterial remodeling patterns may also be helpful in the prognosis of ICAS patients. Another systemic review reported the significant association of the PR pattern detected in the non-stenotic intracranial arteries with several risk factors for IS and overall outcomes of neurological dysfunction [111]. However, a higher prevalence of perforator ostia occlusion after BA endovascular therapy was observed in the NR pattern (27.3%) than that in the PR pattern (0%) among symptomatic patients with BA atherosclerosis [140]. This research speculated that the luminal area that could be dilated might be smaller in the NR site, where more pressure might act on the plaque during mechanical procedures [140]. Micro-emboli generated from the plaque might then spread more widely, thereby more likely causing perforator stroke [140].

Of note, the arterial walls in various intracranial segments may display different vascular remodeling patterns [141]. Among patients with ICAS, the posterior-circulation arteries showed the PR pattern more frequently and carried a heavier plaque burden than the anterior-circulation arteries, which suggested that the intracranial arteries in posterior circulation might be more capable of PR in reaction to the formation of atherosclerotic plaques [142]. Nevertheless, the underlying mechanism is still unclear. Given the mentioned multi-factors involved in arterial remodeling of ICAS, further studies that are investigating the arterial

remodeling process need to consider the characteristics of the intracranial atherosclerotic lesions concerning anatomy, hemodynamics, and histopathology [143].

### 2.6 Precise evaluation of ICAS

A first challenge to assess ICAS has to be faced at the early stage when the symptomatic lesion is fresh and routine brain imaging is normal [3]. Cerebral angiographic tools can determine the severity of stenosis in the arterial lumen, but cannot provide more details about the pathological characters of the intracranial atherosclerotic lesions in relation to subsequent thrombotic events [144]. Obviously, grading the stenotic conditions alone may lead to the sole focus on advanced ICAS, and ignore the early risks of atherosclerotic lesions [87]. More studies then put emphasis on evaluating intracranial atherosclerotic plaque itself, instead of only measuring the maximal narrowing degree in the arterial lumen [145-147]. As an emerging noninvasive diagnostic technique, HR-MRI can describe valuable morphological changes in the intracranial atherosclerotic lesions in vivo, and differentiate ICAS from other stroke etiology [145, 148-150]. HR-MRI favors the accurate assessment of ICAS via localizing the high-risk plaques in the intracranial arteries from various aspects [151].

HR-MRI could characterize the plaque components in MCA atherosclerosis, including IPH and fibrous cap [152]. High signal intensity on T1-weighted fat-suppressed images (HST1) of the MCA atherosclerotic plaques were measured by HR-MRI, and was highly implicit in an existence of fresh IPH [153]. The occurrence of HST1 was higher in the symptomatic MCA atherosclerotic lesion than that in the asymptomatic lesion, and was implied in association with ipsilateral stroke [153]. HR-MRI could also identify the plaque wall distribution in MCA atherosclerosis [154]. The MCA atherosclerotic plaques mainly lay on the ventral and inferior vessel walls [154]. Compared with the asymptomatic plaques, the symptomatic MCA plaques were located in more superior but fewer inferior walls [154]. Similarly, the plaques in

penetrating artery infarctions were positively correlated with the superior wall, but negatively with the ventral and inferior walls [154]. HR-MRI could be applied to calculating remodeling index (RI) in advanced BA atherosclerosis [128]. Compared to the NR (RI < 1.05) lesions, the PR (RI ≥ 1.05) lesions were more often detected in advanced BA atherosclerosis, with bigger plaque size and larger percent of plaque burden [128]. The PR pattern was indicated in significant relevance to plaque instability and cerebral thrombosis [128].

HR-MRI could precisely classify the pathologies of different entities in intracranial artery stenosis [155-157], and even elucidate stroke mechanisms of ICAS [150, 158, 159]. For example, the wall imaging enhancement pattern might be shown as 'eccentric' in the intracranial atherosclerotic lesions, but 'concentric' in the cerebral inflammatory vessels [155]. Based on the vascular remodeling patterns and the plaque features, the distinction between branch occlusive disease (BOD) and non-BOD in ICAS could be drawn as well [158]. However, current research pointed out the inadequacy of HR-MRI, like severely overestimating the measurements of the vessel wall thickness [160]. The early vessel wall thickening caused by ICAS was hardly distinguishable from the normal vessel walls in such circumstance [160]. Further evidence is still required, and new insight into the accurate evaluation of ICAS should be given by well-designed HR-MRI research.

### 2.7 Treatment perspectives and conclusions

The current approach to preventing recurrent stroke in patients with symptomatic ICAS generally includes the aggressive control of the cerebrovascular risk factors, the medical therapy to stabilize vulnerable plaques, and the endovascular intervention to improve cerebral perfusion [161-164]. It is clear from numerous studies that the evolutionary change in the atherosclerotic lesions may be associated with the individual condition and the therapeutic option for these ICAS patients [165-167]. The regressive course of asymptomatic ICAS was

independently correlated with the low levels of fasting glucose and the angiotensin-receptor blocker treatment, whereas the symptomatic ICAS regression were found in independent relevance to the high levels of high-density lipoprotein cholesterol and the cilostazol therapy [168]. Although high-dose statin could stabilize the symptomatic plaques, the ICAS patients using high-dose statin still suffered from ischemic events in the cerebrovascular territory, particularly among those with BOD etiology [169, 170].

Selecting high-risk patients with symptomatic ICAS for precision medicine depends on a thorough knowledge of the underlying pathogenesis of ICAS regarding the anatomical, hemodynamic and histopathological patterns. Modern medical treatment for plaque stabilization and risk factor modification may mainly target the vulnerable atherosclerotic plaques causing artery-to-artery embolism, while endovascular revascularization may be the most advantageous to the cerebral hypo-perfused regions in ICAS [11, 52]. Of note, even succeeded by the endovascular thrombectomy, the symptomatic ICAS patients might derive an early benefit from the personalized hemodynamic control [171]. A joint reflection on the unique anatomical structure of the intracranial vasculature, the significant changes to the cerebrovascular hemodynamics and the pivotal histopathological characteristics of the atherosclerotic lesions is essential throughout the development of a therapeutic strategy for these ICAS patients.

Furthermore, precision medicine also provides a wider perspective on the medical management of symptomatic ICAS, bringing other dominant factors and potential drugs to our notice. The genetic variation of RNF213 in ICAS patients was identified to have a pivotal effect on the intracranial artery diameter and hemodynamics [172]. A three-month therapy with catechin might maintain endothelial function and protect the intracranial vessel walls from severe dyslipidemia, thereby resulting in the preservation of CBF [173]. Considering the exact

functions of the RNF213 variants and catechin in regulating ICAS conditions, the use of polymorphisms and medicines with high specificity will be feasible in the clinical field.

In conclusion, symptomatic ICAS confers an increased risk of stroke recurrence, especially among Asians. The progression of symptomatic ICAS involves multiple factors with regard to the intracranial artery anatomy, hemodynamics and histopathology. In addition to the degree of luminal stenosis, the anatomical, hemodynamic and histopathological characters of the targeted intracranial atherosclerotic lesions need to be taken into consideration, when we evaluate the conditions of symptomatic ICAS for these stroke patients. HR-MRI may serve as a favorable cerebral imaging modality of selecting the high-risk patients for precision medicine. In the near future, the customized diagnostic and therapeutic strategies are believed to yield a reduced rate of recurrent stroke in patients with symptomatic ICAS.

## References


1. Yanez N, Useche JN, Bayona H, Porras A, Carrasquilla G. Analyses of mortality and prevalence of cerebrovascular disease in colombia, south america (2014-2016): A cross-sectional and ecological study. *J Stroke Cerebrovasc Dis*. 2020:104699
2. Li S, Cui LY, Anderson C, Zhu S, Xu P, Wei T, et al. Public awareness of stroke and the appropriate responses in china: A cross-sectional community-based study (fast-right). *Stroke*. 2019;50:455-462
3. Balla SR, Cyr DD, Lokhnygina Y, Becker RC, Berkowitz SD, Breithardt G, et al. Relation of risk of stroke in patients with atrial fibrillation to body mass index (from patients treated with rivaroxaban and warfarin in the rivaroxaban once daily oral direct factor xa inhibition compared with vitamin k antagonism for prevention of stroke and embolism trial in atrial fibrillation trial). *Am J Cardiol*. 2017;119:1989-1996
4. Feigin VL, Forouzanfar MH, Krishnamurthi R, Mensah GA, Connor M, Bennett DA, et al. Global and regional burden of stroke during 1990-2010: Findings from the global burden of disease study 2010. *Lancet*. 2014;383:245-254
5. Holmstedt CA, Turan TN, Chimowitz MI. Atherosclerotic intracranial arterial stenosis: Risk factors, diagnosis, and treatment. *Lancet Neurol*. 2013;12:1106-1114
6. Suri MF, Johnston SC. Epidemiology of intracranial stenosis. *J Neuroimaging*. 2009;19 Suppl 1:11S-16S
7. Wang Y, Zhao X, Liu L, Soo YO, Pu Y, Pan Y, et al. Prevalence and outcomes of symptomatic intracranial large artery stenoses and occlusions in china: The chinese intracranial atherosclerosis (cicas) study. *Stroke*. 2014;45:663-669

8. Lange MC, Ribas G, Scavasine V, Ducci RD, Mendes DC, Zetola VHF, et al. Stroke recurrence in the different subtypes of ischemic stroke. The importance of the intracranial disease. *Arq Neuropsiquiatr*. 2018;76:649-653

9. Randolph SA. Ischemic stroke. *Workplace Health Saf*. 2016;64:444

10. Ritz K, Denswil NP, Stam OC, van Lieshout JJ, Daemen MJ. Cause and mechanisms of intracranial atherosclerosis. *Circulation*. 2014;130:1407-1414

11. Banerjee C, Chimowitz MI. Stroke caused by atherosclerosis of the major intracranial arteries. *Circ Res*. 2017;120:502-513

12. Pascalau R, Padurean VA, Bartos D, Bartos A, Szabo BA. The geometry of the circle of willis anatomical variants as a potential cerebrovascular risk factor. *Turk Neurosurg*. 2019;29:151-158

13. Hindy G, Engstrom G, Larsson SC, Traylor M, Markus HS, Melander O, et al. Role of blood lipids in the development of ischemic stroke and its subtypes: A mendelian randomization study. *Stroke*. 2018;49:820-827

14. Chong M, Sjaarda J, Pigeyre M, Mohammadi-Shemirani P, Lali R, Shoamanesh A, et al. Novel drug targets for ischemic stroke identified through mendelian randomization analysis of the blood proteome. *Circulation*. 2019;140:819-830

15. Fattahian R, Gorji RA, Sadeghi M, Bagheri SR. Assessment of the prevalence of vascular anomalies of the circle of willis based on the autopsy of cadavers in kurdish race between 2016 and 2017. *Mater Sociomed*. 2018;30:189-192

16. Hamming AM, van Walderveen MAA, Mulder IA, van der Schaaf IC, Kappelle LJ, Velthuis BK, et al. Circle of willis variations in migraine patients with ischemic stroke. *Brain Behav*. 2019;9:e01223

17. Eaton RG, Shah VS, Dornbos D, 3rd, Zaninovich OA, Wenger N, Dumont TM, et al. Demographic age-related variation in circle of willis completeness assessed by digital subtraction angiography. *Brain Circ*. 2020;6:31-37

18. Wijesinghe P, Steinbusch HWM, Shankar SK, Yasha TC, De Silva KRD. Circle of willis abnormalities and their clinical importance in ageing brains: A cadaveric anatomical and pathological study. *J Chem Neuroanat*. 2020;106:101772

19. Zaninovich OA, Ramey WL, Walter CM, Dumont TM. Completion of the circle of willis varies by gender, age, and indication for computed tomography angiography. *World Neurosurg*. 2017;106:953-963

20. Qiu C, Zhang Y, Xue C, Jiang S, Zhang W. Mra study on variation of the circle of willis in healthy chinese male adults. *Biomed Res Int*. 2015;2015:976340

21. Zhou C, Yuan C, Li R, Wang W, Li C, Zhao X, et al. Association between incomplete circle of willis and carotid vulnerable atherosclerotic plaques. *Arterioscler Thromb Vasc Biol*. 2018;38:2744-2749

22. Yeniceri IO, Cullu N, Deveer M, Yeniceri EN. Circle of willis variations and artery diameter measurements in the turkish population. *Folia Morphol (Warsz)*. 2017;76:420-425

23. Shatri J, Cerkezi S, Ademi V, Reci V, Bexheti S. Anatomical variations and dimensions of arteries in the anterior part of the circle of willis. *Folia Morphol (Warsz)*. 2019;78:259-266

24. Harteveld AA, Denswil NP, Van Hecke W, Kuijf HJ, Vink A, Spliet WGM, et al. Ex vivo vessel wall thickness measurements of the human circle of willis using 7t mri. *Atherosclerosis*. 2018;273:106-114

25. Shatri J, Bexheti D, Bexheti S, Kabashi S, Krasniqi S, Ahmetgjekaj I, et al. Influence of gender and age on average dimensions of arteries forming the circle of willis study

by magnetic resonance angiography on kosovo's population. *Open Access Maced J Med Sci*. 2017;5:714-719

26. Del Brutto OH, Mera RM, Costa AF, Del Brutto VJ. Basilar artery diameter is inversely associated with fetal type circle of willis. *Eur Neurol*. 2017;78:217-220

27. Spasojevic G, Vujmilovic S, Vujkovic Z, Gajanin R, Malobabic S, Ponorac N, et al. Internal carotid and vertebral arteries diameters and their interrelationships to sex and left/right side. *Folia Morphol (Warsz)*. 2019

28. Yu YN, Li ML, Xu YY, Meng Y, Trieu H, Villablanca JP, et al. Middle cerebral artery geometric features are associated with plaque distribution and stroke. *Neurology*. 2018;91:e1760-e1769

29. Gunnal SA, Farooqui MS, Wabale RN. Study of middle cerebral artery in human cadaveric brain. *Ann Indian Acad Neurol*. 2019;22:187-194

30. Ye H, Wu X, Yan J, Wang J, Qiu J, Wang Y. Completeness of circle of willis and white matter hyperintensities in patients with severe internal carotid artery stenosis. *Neurol Sci*. 2019;40:509-514

31. Kim KM, Kang HS, Lee WJ, Cho YD, Kim JE, Han MH. Clinical significance of the circle of willis in intracranial atherosclerotic stenosis. *J Neurointerv Surg*. 2016;8:251-255

32. Park BJ, Kim KM, Lee WJ, Chun IK, Kim I, Lee SJ, et al. Clinical significance of the circle of willis in patients with symptomatic internal carotid artery occlusion. *World Neurosurg*. 2018;115:e585-e591

33. Anello MG, Miao TL, Pandey SK, Mandzia JL. Rare bilateral caudate infarction in a patient with a common circle of willis variant. *Can J Neurol Sci*. 2019;46:593-594

34. Sonobe A, Kato H, Mathis BJ, Hiramatsu Y. Catastrophic cerebral infarction during extracorporeal life support due to a rare anomaly in the circle of willis. *Interact Cardiovasc Thorac Surg*. 2019;29:816-817

35. Nixon AM, Gunel M, Sumpio BE. The critical role of hemodynamics in the development of cerebral vascular disease. *J Neurosurg*. 2010;112:1240-1253

36. Chien A, Vinuela F. Analyzing circle of willis blood flow in ischemic stroke patients through 3d stroke arterial flow estimation. *Interv Neuroradiol*. 2017;23:427-432

37. Klijn CJ, Kappelle LJ. Haemodynamic stroke: Clinical features, prognosis, and management. *Lancet Neurol*. 2010;9:1008-1017

38. Lyu J, Ma N, Tian C, Xu F, Shao H, Zhou X, et al. Perfusion and plaque evaluation to predict recurrent stroke in symptomatic middle cerebral artery stenosis. *Stroke Vasc Neurol*. 2019;4:129-134

39. Guenego A, Fahed R, Albers GW, Kuraitis G, Sussman ES, Martin BW, et al. Hypoperfusion intensity ratio correlates with angiographic collaterals in acute ischaemic stroke with m1 occlusion. *Eur J Neurol*. 2020

40. Fukui T, Hasegawa Y, Seriyama S, Takeuchi T, Sugita K, Tsukagoshi H. Hemiballism-hemichorea induced by subcortical ischemia. *Can J Neurol Sci*. 1993;20:324-328

41. Wang Y, Xiao J, Luo Y, Wang S, Liang H, Jin L. Risk factors of perfusion and diffusion abnormalities on mri in hemispheric tia: A case-control study. *Ann Transl Med*. 2019;7:808

42. Okamoto K, Shiga H, Nakamura H, Matsui M, Miwa T. Relationship between olfactory disturbance after acute ischemic stroke and latent thalamic hypoperfusion. *Chem Senses*. 2020;45:111-118

43. Traupe H, Kruse E, Heiss WD. Reperfusion of focal ischemia of varying duration: Postischemic hyper- and hypo-perfusion. *Stroke*. 1982;13:615-622

44. Takagi K, Zhao W, Busto R, Ginsberg MD. Local hemodynamic changes during transient middle cerebral artery occlusion and recirculation in the rat: A [14c]iodoantipyrine autoradiographic study. *Brain Res*. 1995;691:160-168

45. Semenenko AI, Khrebtii HI, Malyk SL, Dmytriiev DV, Bodnar RY, Zheliba LM, et al. Influence of different qualitative composition of infusion solutions on cerebral hemodynamics in patients with acute ischemic stroke. *Wiad Lek*. 2020;73:272-277

46. Nomura T, Okamoto K, Igarashi H, Watanabe M, Hasegawa H, Oishi M, et al. Vascular hyperintensity on fluid-attenuated inversion recovery indicates the severity of hypoperfusion in acute stroke. *J Stroke Cerebrovasc Dis*. 2020;29:104467

47. Sakamoto S, Ide W, Hashimoto I, Kamada H, Tanaka H, Sekihara K. Recovery of spontaneous neuromagnetic activity after extracranial-intracranial bypass in a patient with middle cerebral artery occlusion. *Acta Neurochir (Wien)*. 2008;150:1285-1290; discussion 1290

48. Khattar NK, Friedlander RM, Chaer RA, Avgerinos ED, Kretz ES, Balzer JR, et al. Perioperative stroke after carotid endarterectomy: Etiology and implications. *Acta Neurochir (Wien)*. 2016;158:2377-2383

49. Fan AP, Khalil AA, Fiebach JB, Zaharchuk G, Villringer A, Villringer K, et al. Elevated brain oxygen extraction fraction measured by mri susceptibility relates to perfusion status in acute ischemic stroke. *J Cereb Blood Flow Metab*. 2020;40:539-551

50. Zhang K, Li T, Tian J, Li P, Fu B, Yang X, et al. Subtypes of anterior circulation large artery occlusions with acute brain ischemic stroke. *Sci Rep*. 2020;10:3442

51. Wu B, Liu N, Wintermark M, Parsons MW, Chen H, Lin L, et al. Optimal delay time of ct perfusion for predicting cerebral parenchymal hematoma after intra-arterial tpa treatment. *Front Neurol*. 2018;9:680

52. Leung TW, Wabnitz AM, Miao Z, Chimowitz MI. Angioplasty and stenting. *Front Neurol Neurosci*. 2016;40:152-163

53. Ginsberg MD. The cerebral collateral circulation: Relevance to pathophysiology and treatment of stroke. *Neuropharmacology*. 2018;134:280-292

54. Jung S, Wiest R, Gralla J, McKinley R, Mattle H, Liebeskind D. Relevance of the cerebral collateral circulation in ischaemic stroke: Time is brain, but collaterals set the pace. *Swiss Med Wkly*. 2017;147:w14538

55. van Raamt AF, Mali WP, van Laar PJ, van der Graaf Y. The fetal variant of the circle of willis and its influence on the cerebral collateral circulation. *Cerebrovasc Dis*. 2006;22:217-224

56. Huang GP, Yu H, Yang Z, Schwieterman R, Ludwig B. 1d simulation of blood flow characteristics in the circle of willis using thinks. *Comput Methods Biomech Biomed Engin*. 2018;21:389-397

57. Millesi K, Mutzenbach JS, Killer-Oberpfalzer M, Hecker C, Machegger L, Bubel N, et al. Influence of the circle of willis on leptomeningeal collateral flow in anterior circulation occlusive stroke: Friend or foe? *J Neurol Sci*. 2019;396:69-75

58. Bonnin P, Pansiot J, Paven E, Eloi M, Renolleau S, Baud O, et al. Controlled arterial reflow after ischemia induces better outcomes in the juvenile rat brain. *J Cereb Blood Flow Metab*. 2017;37:3091-3096

59. Zarrinkoob L, Ambarki K, Wahlin A, Birgander R, Eklund A, Malm J. Blood flow distribution in cerebral arteries. *J Cereb Blood Flow Metab*. 2015;35:648-654

60. Wei W, Yi X, Ruan J, Duan X, Luo H, Lv Z. Influence of collateral circulation on cerebral blood flow and frontal lobe cognitive function in patients with severe internal carotid artery stenosis. *BMC Neurol*. 2019;19:151

61. Zarrinkoob L, Wahlin A, Ambarki K, Birgander R, Eklund A, Malm J. Blood flow lateralization and collateral compensatory mechanisms in patients with carotid artery stenosis. *Stroke*. 2019;50:1081-1088

62. Hoksbergen AW, Legemate DA, Csiba L, Csati G, Siro P, Fulesdi B. Absent collateral function of the circle of willis as risk factor for ischemic stroke. *Cerebrovasc Dis*. 2003;16:191-198

63. Kennedy McConnell F, Payne S. The dual role of cerebral autoregulation and collateral flow in the circle of willis after major vessel occlusion. *IEEE Trans Biomed Eng*. 2017;64:1793-1802

64. Zhao H, Wang B, Xu G, Dong Y, Dong Q, Cao W. Collateral grade of the willis' circle predicts outcomes of acute intracranial internal carotid artery occlusion before thrombectomy. *Brain Behav*. 2019;9:e01452

65. Torvik A, Skullerud K. Watershed infarcts in the brain caused by microemboli. *Clin Neuropathol*. 1982;1:99-105

66. Spence JD, Tamayo A, Lownie SP, Ng WP, Ferguson GG. Absence of microemboli on transcranial doppler identifies low-risk patients with asymptomatic carotid stenosis. *Stroke*. 2005;36:2373-2378

67. Dempsey RJ, Vemuganti R, Varghese T, Hermann BP. A review of carotid atherosclerosis and vascular cognitive decline: A new understanding of the keys to symptomology. *Neurosurgery*. 2010;67:484-493; discussion 493-484

68. Brown WR, Thore CR. Review: Cerebral microvascular pathology in ageing and neurodegeneration. *Neuropathol Appl Neurobiol*. 2011;37:56-74

69. Wu XH, Chen XY, Fan YH, Leung TW, Wong KS. High extent of intracranial carotid artery calcification is associated with downstream microemboli in stroke patients. *J Stroke Cerebrovasc Dis*. 2017;26:442-447

70. Zheng L, Vinters HV, Mack WJ, Zarow C, Ellis WG, Chui HC. Cerebral atherosclerosis is associated with cystic infarcts and microinfarcts but not alzheimer pathologic changes. *Stroke*. 2013;44:2835-2841

71. Sitzer M, Muller W, Siebler M, Hort W, Kniemeyer HW, Jancke L, et al. Plaque ulceration and lumen thrombus are the main sources of cerebral microemboli in high-grade internal carotid artery stenosis. *Stroke*. 1995;26:1231-1233

72. Rapp JH, Pan XM, Yu B, Swanson RA, Higashida RT, Simpson P, et al. Cerebral ischemia and infarction from atheroemboli <100 microm in size. *Stroke*. 2003;34:1976-1980

73. Azarpazhooh MR, Chambers BR. Clinical application of transcranial doppler monitoring for embolic signals. *J Clin Neurosci*. 2006;13:799-810

74. Best LM, Webb AC, Gurusamy KS, Cheng SF, Richards T. Transcranial doppler ultrasound detection of microemboli as a predictor of cerebral events in patients with symptomatic and asymptomatic carotid disease: A systematic review and meta-analysis. *Eur J Vasc Endovasc Surg*. 2016;52:565-580

75. Sun DJ, Zhuang AX, Zeng QH, Jiang YL, Jiang JD, Feng SQ, et al. A study of microemboli monitoring of atherosclerotic thrombotic cerebral infarction and artery stenosis. *Genet Mol Res*. 2014;13:6734-6745

76. Farina F, Palmieri A, Favaretto S, Viaro F, Cester G, Causin F, et al. Prognostic role of microembolic signals after endovascular treatment in anterior circulation ischemic stroke patients. *World Neurosurg*. 2018;110:e882-e889

77. Spence JD. Transcranial doppler monitoring for microemboli: A marker of a high-risk carotid plaque. *Semin Vasc Surg*. 2017;30:62-66

78. Russell D. Cerebral microemboli and cognitive impairment. *J Neurol Sci*. 2002;203-204:211-214

79. Rapp JH, Pan XM, Neumann M, Hong M, Hollenbeck K, Liu J. Microemboli composed of cholesterol crystals disrupt the blood-brain barrier and reduce cognition. *Stroke*. 2008;39:2354-2361

80. Komotar RJ, Kellner CP, Raper DM, Strozyk D, Higashida RT, Meyers PM. Update on the natural history of intracranial atherosclerotic disease: A critical review. *World J Radiol*. 2010;2:166-171

81. Lam TD, Lammers S, Munoz C, Tamayo A, Spence JD. Diabetes, intracranial stenosis and microemboli in asymptomatic carotid stenosis. *Can J Neurol Sci*. 2013;40:177-181

82. Spence JD. Transcranial doppler emboli identifies asymptomatic carotid patients at high stroke risk: Why this technique should be used more widely. *Angiology*. 2017;68:657-660

83. Poppert H, Sadikovic S, Sander K, Wolf O, Sander D. Embolic signals in unselected stroke patients: Prevalence and diagnostic benefit. *Stroke*. 2006;37:2039-2043

84. van den Wijngaard IR, Holswilder G, van Walderveen MA, Algra A, Wermer MJ, Zaidat OO, et al. Treatment and imaging of intracranial atherosclerotic stenosis: Current perspectives and future directions. *Brain Behav*. 2016;6:e00536

85. Yu SCH, Lau TWW, Wong SSM, Lee KT, Wong LKS, Leung TWH. Long-term evolutionary change in the lumen of intracranial atherosclerotic stenosis following angioplasty and stenting. *Oper Neurosurg (Hagerstown)*. 2018;14:128-138

86. Kasner SE, Chimowitz MI, Lynn MJ, Howlett-Smith H, Stern BJ, Hertzberg VS, et al. Predictors of ischemic stroke in the territory of a symptomatic intracranial arterial stenosis. *Circulation*. 2006;113:555-563

87. Arenillas JF. Intracranial atherosclerosis: Current concepts. *Stroke*. 2011;42:S20-23

88. Zanaty M, Rossen JD, Roa JA, Nakagawa D, Hudson JS, Kasab SA, et al. Intracranial atherosclerosis: A disease of functional, not anatomic stenosis? How trans-stenotic pressure gradients can help guide treatment. *Oper Neurosurg (Hagerstown)*. 2019

89. Fang H, Leng X, Pu Y, Zou X, Pan Y, Song B, et al. Hemodynamic significance of middle cerebral artery stenosis associated with the severity of ipsilateral white matter changes. *Front Neurol*. 2020;11:214

90. Lu SS, Ge S, Su CQ, Xie J, Mao J, Shi HB, et al. Mri of plaque characteristics and relationship with downstream perfusion and cerebral infarction in patients with symptomatic middle cerebral artery stenosis. *J Magn Reson Imaging*. 2018;48:66-73

91. Leng X, Scalzo F, Ip HL, Johnson M, Fong AK, Fan FS, et al. Computational fluid dynamics modeling of symptomatic intracranial atherosclerosis may predict risk of stroke recurrence. *PLoS One*. 2014;9:e97531

92. Alexander MD, Cooke DL, Meyers PM, Amans MR, Dowd CF, Halbach VV, et al. Lesion stability characteristics outperform degree of stenosis in predicting outcomes following stenting for symptomatic intracranial atherosclerosis. *J Neurointerv Surg*. 2016;8:19-23

93. Virmani R, Kolodgie FD, Burke AP, Farb A, Schwartz SM. Lessons from sudden coronary death: A comprehensive morphological classification scheme for atherosclerotic lesions. *Arterioscler Thromb Vasc Biol*. 2000;20:1262-1275

94. Chen XY, Wong KS, Lam WW, Zhao HL, Ng HK. Middle cerebral artery atherosclerosis: Histological comparison between plaques associated with and not associated with infarct in a postmortem study. *Cerebrovasc Dis*. 2008;25:74-80

95. Yang WJ, Chen XY, Zhao HL, Niu CB, Xu Y, Wong KS, et al. In vitro assessment of histology verified intracranial atherosclerotic disease by 1.5t magnetic resonance imaging: Concentric or eccentric? *Stroke*. 2016;47:527-530

96. Zhu X, Liu L, He X, Zhang X, Hu L, Du B, et al. Wall thickening pattern in atherosclerotic basilar artery stenosis. *Neurol Sci*. 2016;37:269-276

97. Denswil NP, van der Wal AC, Ritz K, de Boer OJ, Aronica E, Troost D, et al. Atherosclerosis in the circle of willis: Spatial differences in composition and in distribution of plaques. *Atherosclerosis*. 2016;251:78-84

98. Zheng L, Yang WJ, Niu CB, Zhao HL, Wong KS, Leung TWH, et al. Correlation of adventitial vasa vasorum with intracranial atherosclerosis: A postmortem study. *J Stroke*. 2018;20:342-349

99. Yang WJ, Wong KS, Chen XY. Intracranial atherosclerosis: From microscopy to high-resolution magnetic resonance imaging. *J Stroke*. 2017;19:249-260

100. Yang WJ, Fisher M, Zheng L, Niu CB, Paganini-Hill A, Zhao HL, et al. Histological characteristics of intracranial atherosclerosis in a chinese population: A postmortem study. *Front Neurol*. 2017;8:488

101. Kim JS, Nah HW, Park SM, Kim SK, Cho KH, Lee J, et al. Risk factors and stroke mechanisms in atherosclerotic stroke: Intracranial compared with extracranial and anterior compared with posterior circulation disease. *Stroke*. 2012;43:3313-3318

102. Lopez-Cancio E, Matheus MG, Romano JG, Liebeskind DS, Prabhakaran S, Turan TN, et al. Infarct patterns, collaterals and likely causative mechanisms of stroke in symptomatic intracranial atherosclerosis. *Cerebrovasc Dis*. 2014;37:417-422

103. Xu Z, Li M, Lyu J, Hou Z, He J, Mo D, et al. Different risk factors in identical features of intracranial atherosclerosis plaques in the posterior and anterior circulation in high-resolution mri. *Ther Adv Neurol Disord*. 2020;13:1756286420909991

104. Kim JM, Jung KH, Sohn CH, Moon J, Han MH, Roh JK. Middle cerebral artery plaque and prediction of the infarction pattern. *Arch Neurol*. 2012;69:1470-1475

105. Millon A, Boussel L, Brevet M, Mathevet JL, Canet-Soulas E, Mory C, et al. Clinical and histological significance of gadolinium enhancement in carotid atherosclerotic plaque. *Stroke*. 2012;43:3023-3028

106. Kim JM, Jung KH, Sohn CH, Moon J, Shin JH, Park J, et al. Intracranial plaque enhancement from high resolution vessel wall magnetic resonance imaging predicts stroke recurrence. *Int J Stroke*. 2016;11:171-179

107. Wu F, Song H, Ma Q, Xiao J, Jiang T, Huang X, et al. Hyperintense plaque on intracranial vessel wall magnetic resonance imaging as a predictor of artery-to-artery embolic infarction. *Stroke*. 2018;49:905-911

108. Saam T, Yuan C, Chu B, Takaya N, Underhill H, Cai J, et al. Predictors of carotid atherosclerotic plaque progression as measured by noninvasive magnetic resonance imaging. *Atherosclerosis*. 2007;194:e34-42

109. Shi ZS, Feng L, He X, Ishii A, Goldstine J, Vinters HV, et al. Vulnerable plaque in a swine model of carotid atherosclerosis. *AJNR Am J Neuroradiol*. 2009;30:469-472

110. Watanabe Y, Nagayama M. Mr plaque imaging of the carotid artery. *Neuroradiology*. 2010;52:253-274

111. Wang Y, Liu X, Wu X, Degnan AJ, Malhotra A, Zhu C. Culprit intracranial plaque without substantial stenosis in acute ischemic stroke on vessel wall mri: A systematic review. *Atherosclerosis*. 2019;287:112-121

112. Takasugi J, Miwa K, Watanabe Y, Okazaki S, Todo K, Sasaki T, et al. Cortical cerebral microinfarcts on 3t magnetic resonance imaging in patients with carotid artery stenosis. *Stroke*. 2019;50:639-644

113. Xu Y, Li D, Yuan C, Zhou Z, He L, Li R, et al. Association of severity between carotid and intracranial artery atherosclerosis. *Ann Clin Transl Neurol*. 2018;5:843-849

114. Li D, Dai W, Cai Y, Han Y, Yao G, Chen H, et al. Atherosclerosis in stroke-related vascular beds and stroke risk: A 3-d mr vessel wall imaging study. *Ann Clin Transl Neurol*. 2018;5:1599-1610

115. Yu JH, Kwak HS, Chung GH, Hwang SB, Park MS, Park SH. Association of intraplaque hemorrhage and acute infarction in patients with basilar artery plaque. *Stroke*. 2015;46:2768-2772

116. Shen M, Gao P, Zhang Q, Jing L, Yan H, Li H. Middle cerebral artery atherosclerosis and deep subcortical infarction: A 3t magnetic resonance vessel wall imaging study. *J Stroke Cerebrovasc Dis*. 2018;27:3387-3392

117. Gao T, Zhang Z, Yu W, Zhang Z, Wang Y. Atherosclerotic carotid vulnerable plaque and subsequent stroke: A high-resolution mri study. *Cerebrovasc Dis*. 2009;27:345-352

118. Golledge J, Greenhalgh RM, Davies AH. The symptomatic carotid plaque. *Stroke*. 2000;31:774-781

119. Suh DC, Park ST, Oh TS, Park SO, Lim OK, Park S, et al. High shear stress at the surface of enhancing plaque in the systolic phase is related to the symptom presentation of severe m1 stenosis. *Korean J Radiol*. 2011;12:515-518

120. Rollo M, Tartaglione T, Pedicelli A, Settecasi C. Atherosclerosis of carotid and intracranial arteries. *Rays*. 2001;26:247-268

121. Labadzhyan A, Csiba L, Narula N, Zhou J, Narula J, Fisher M. Histopathologic evaluation of basilar artery atherosclerosis. *J Neurol Sci*. 2011;307:97-99

122. Chung GH, Kwak HS, Hwang SB, Noh SJ. Magnetic resonance imaging of intracranial atherosclerosis: Comparison of ex vivo 3t mri and histologic findings. *Eur J Radiol*. 2017;97:110-114

123. Iwakiri T, Yano Y, Sato Y, Hatakeyama K, Marutsuka K, Fujimoto S, et al. Usefulness of carotid intima-media thickness measurement as an indicator of generalized atherosclerosis: Findings from autopsy analysis. *Atherosclerosis*. 2012;225:359-362

124. Li J, Li D, Yang D, Hang H, Wu Y, Yao R, et al. Irregularity of carotid plaque surface predicts subsequent vascular event: A mri study. *J Magn Reson Imaging*. 2020

125. Li J, Li D, Yang D, Huo R, Chen X, Xu Y, et al. Co-existing cerebrovascular atherosclerosis predicts subsequent vascular event: A multi-contrast cardiovascular magnetic resonance imaging study. *J Cardiovasc Magn Reson*. 2020;22:4

126. Lee YK, Kwak HS, Chung GH, Hwang SB. Lipid-rich necrotic core of basilar artery atherosclerotic plaque: Contrast-enhanced black blood imaging on vessel wall imaging. *Diagnostics (Basel)*. 2019;9

127. Song X, Zhao X, Liebeskind DS, Xu W, Zhang J, Wei C, et al. Associations between systemic blood pressure parameters and intraplaque hemorrhage in symptomatic intracranial atherosclerosis: A high-resolution mri-based study. *Hypertens Res*. 2020

128. Ma N, Jiang WJ, Lou X, Ma L, Du B, Cai JF, et al. Arterial remodeling of advanced basilar atherosclerosis: A 3-tesla mri study. *Neurology*. 2010;75:253-258

129. Gutierrez J, Goldman J, Honig LS, Elkind MS, Morgello S, Marshall RS. Determinants of cerebrovascular remodeling: Do large brain arteries accommodate stenosis? *Atherosclerosis*. 2014;235:371-379

130. Lee WJ, Choi HS, Jang J, Sung J, Kim TW, Koo J, et al. Non-stenotic intracranial arteries have atherosclerotic changes in acute ischemic stroke patients: A 3t mri study. *Neuroradiology*. 2015;57:1007-1013

131. Burke AP, Kolodgie FD, Farb A, Weber D, Virmani R. Morphological predictors of arterial remodeling in coronary atherosclerosis. *Circulation*. 2002;105:297-303

132. Hongo H, Miyawaki S, Imai H, Shinya Y, Ono H, Mori H, et al. Smaller outer diameter of atherosclerotic middle cerebral artery associated with rnf213 c.14576g>a variant (rs112735431). *Surg Neurol Int*. 2017;8:104

133. Zhang X, Zhou Y, Ding W, Zhang R, Yan S, Deng Y, et al. Tpo-ab plays a role in arterial remodeling in patients with intracranial stenosis. *Atherosclerosis*. 2019;280:140-146

134. Dolan JM, Kolega J, Meng H. High wall shear stress and spatial gradients in vascular pathology: A review. *Ann Biomed Eng*. 2013;41:1411-1427

135. Shi MC, Wang SC, Zhou HW, Xing YQ, Cheng YH, Feng JC, et al. Compensatory remodeling in symptomatic middle cerebral artery atherosclerotic stenosis: A high-resolution mri and microemboli monitoring study. *Neurol Res*. 2012;34:153-158

136. Zhao DL, Deng G, Xie B, Gao B, Peng CY, Nie F, et al. Wall characteristics and mechanisms of ischaemic stroke in patients with atherosclerotic middle cerebral artery stenosis: A high-resolution mri study. *Neurol Res*. 2016;38:606-613

137. Zhao DL, Deng G, Xie B, Ju S, Yang M, Chen XH, et al. High-resolution mri of the vessel wall in patients with symptomatic atherosclerotic stenosis of the middle cerebral artery. *J Clin Neurosci*. 2015;22:700-704

138. Zhang DF, Chen YC, Chen H, Zhang WD, Sun J, Mao CN, et al. A high-resolution mri study of relationship between remodeling patterns and ischemic stroke in patients

with atherosclerotic middle cerebral artery stenosis. *Front Aging Neurosci*. 2017;9:140

139. Lee HN, Ryu CW, Yun SJ. Vessel-wall magnetic resonance imaging of intracranial atherosclerotic plaque and ischemic stroke: A systematic review and meta-analysis. *Front Neurol*. 2018;9:1032

140. Ma N, Xu Z, Lyu J, Li M, Hou Z, Liu Y, et al. Association of perforator stroke after basilar artery stenting with negative remodeling. *Stroke*. 2019;50:745-749

141. Ward MR, Pasterkamp G, Yeung AC, Borst C. Arterial remodeling. Mechanisms and clinical implications. *Circulation*. 2000;102:1186-1191

142. Qiao Y, Anwar Z, Intrapiromkul J, Liu L, Zeiler SR, Leigh R, et al. Patterns and implications of intracranial arterial remodeling in stroke patients. *Stroke*. 2016;47:434-440

143. Pasterkamp G, de Kleijn DP, Borst C. Arterial remodeling in atherosclerosis, restenosis and after alteration of blood flow: Potential mechanisms and clinical implications. *Cardiovasc Res*. 2000;45:843-852

144. Cai B, Peng B. Intracranial artery stenosis: Current status of evaluation and treatment in china. *Chronic Dis Transl Med*. 2017;3:197-206

145. Leng X, Wong KS, Liebeskind DS. Evaluating intracranial atherosclerosis rather than intracranial stenosis. *Stroke*. 2014;45:645-651

146. Brinjikji W, Huston J, 3rd, Rabinstein AA, Kim GM, Lerman A, Lanzino G. Contemporary carotid imaging: From degree of stenosis to plaque vulnerability. *J Neurosurg*. 2016;124:27-42

147. Dempsey RJ, Varghese T, Jackson DC, Wang X, Meshram NH, Mitchell CC, et al. Carotid atherosclerotic plaque instability and cognition determined by ultrasound-

measured plaque strain in asymptomatic patients with significant stenosis. *J Neurosurg*. 2018;128:111-119

148. Bodle JD, Feldmann E, Swartz RH, Rumboldt Z, Brown T, Turan TN. High-resolution magnetic resonance imaging: An emerging tool for evaluating intracranial arterial disease. *Stroke*. 2013;44:287-292

149. Dieleman N, van der Kolk AG, Zwanenburg JJ, Harteveld AA, Biessels GJ, Luijten PR, et al. Imaging intracranial vessel wall pathology with magnetic resonance imaging: Current prospects and future directions. *Circulation*. 2014;130:192-201

150. Gao T, Yu W, Liu C. Mechanisms of ischemic stroke in patients with intracranial atherosclerosis: A high-resolution magnetic resonance imaging study. *Exp Ther Med*. 2014;7:1415-1419

151. de Havenon A, Mossa-Basha M, Shah L, Kim SE, Park M, Parker D, et al. High-resolution vessel wall mri for the evaluation of intracranial atherosclerotic disease. *Neuroradiology*. 2017;59:1193-1202

152. Yang WQ, Huang B, Liu XT, Liu HJ, Li PJ, Zhu WZ. Reproducibility of high-resolution mri for the middle cerebral artery plaque at 3t. *Eur J Radiol*. 2014;83:e49-55

153. Xu WH, Li ML, Gao S, Ni J, Yao M, Zhou LX, et al. Middle cerebral artery intraplaque hemorrhage: Prevalence and clinical relevance. *Ann Neurol*. 2012;71:195-198

154. Xu WH, Li ML, Gao S, Ni J, Zhou LX, Yao M, et al. Plaque distribution of stenotic middle cerebral artery and its clinical relevance. *Stroke*. 2011;42:2957-2959

155. Swartz RH, Bhuta SS, Farb RI, Agid R, Willinsky RA, Terbrugge KG, et al. Intracranial arterial wall imaging using high-resolution 3-tesla contrast-enhanced mri. *Neurology*. 2009;72:627-634

156. Mandell DM, Matouk CC, Farb RI, Krings T, Agid R, terBrugge K, et al. Vessel wall mri to differentiate between reversible cerebral vasoconstriction syndrome and central nervous system vasculitis: Preliminary results. *Stroke*. 2012;43:860-862

157. Ryoo S, Cha J, Kim SJ, Choi JW, Ki CS, Kim KH, et al. High-resolution magnetic resonance wall imaging findings of moyamoya disease. *Stroke*. 2014;45:2457-2460

158. Ryoo S, Lee MJ, Cha J, Jeon P, Bang OY. Differential vascular pathophysiologic types of intracranial atherosclerotic stroke: A high-resolution wall magnetic resonance imaging study. *Stroke*. 2015;46:2815-2821

159. Kim BJ, Lee DH, Kang DW, Kwon SU, Kim JS. Branching patterns determine the size of single subcortical infarctions. *Stroke*. 2014;45:1485-1487

160. van Hespen KM, Zwanenburg JJM, Harteveld AA, Luijten PR, Hendrikse J, Kuijf HJ. Intracranial vessel wall magnetic resonance imaging does not allow for accurate and precise wall thickness measurements: An ex vivo study. *Stroke*. 2019;50:e283-e284

161. Teleb MS, Asif K, Castonguay AC, Zaidat OO. Endovascular management of intracranial atherosclerosis. *Neurosurg Clin N Am*. 2014;25:593-605

162. Esenwa C, Gutierrez J. Secondary stroke prevention: Challenges and solutions. *Vasc Health Risk Manag*. 2015;11:437-450

163. Aznaouridis K, Masoura C, Vlachopoulos C, Tousoulis D. Statins in stroke. *Curr Med Chem*. 2019;26:6174-6185

164. Shitara S, Fujiyoshi A, Hisamatsu T, Torii S, Suzuki S, Ito T, et al. Intracranial artery stenosis and its association with conventional risk factors in a general population of japanese men. *Stroke*. 2019;50:2967-2969

165. Derdeyn CP, Chimowitz MI, Lynn MJ, Fiorella D, Turan TN, Janis LS, et al. Aggressive medical treatment with or without stenting in high-risk patients with

intracranial artery stenosis (sammpris): The final results of a randomised trial. *Lancet*. 2014;383:333-341

166. Leung TW, Wang L, Soo YO, Ip VH, Chan AY, Au LW, et al. Evolution of intracranial atherosclerotic disease under modern medical therapy. *Ann Neurol*. 2015;77:478-486

167. Hoshino T, Sissani L, Labreuche J, Ducrocq G, Lavallee PC, Meseguer E, et al. Prevalence of systemic atherosclerosis burdens and overlapping stroke etiologies and their associations with long-term vascular prognosis in stroke with intracranial atherosclerotic disease. *JAMA Neurol*. 2018;75:203-211

168. Kim BJ, Hong KS, Cho YJ, Lee JH, Koo JS, Park JM, et al. Predictors of symptomatic and asymptomatic intracranial atherosclerosis: What is different and why? *J Atheroscler Thromb*. 2014;21:605-617

169. Chung JW, Hwang J, Lee MJ, Cha J, Bang OY. Previous statin use and high-resolution magnetic resonance imaging characteristics of intracranial atherosclerotic plaque: The intensive statin treatment in acute ischemic stroke patients with intracranial atherosclerosis study. *Stroke*. 2016;47:1789-1796

170. Chung JW, Cha J, Lee MJ, Yu IW, Park MS, Seo WK, et al. Intensive statin treatment in acute ischaemic stroke patients with intracranial atherosclerosis: A high-resolution magnetic resonance imaging study (stamina-mri study). *J Neurol Neurosurg Psychiatry*. 2020;91:204-211

171. Petersen NH, Silverman A, Strander SM, Kodali S, Wang A, Sansing LH, et al. Fixed compared with autoregulation-oriented blood pressure thresholds after mechanical thrombectomy for ischemic stroke. *Stroke*. 2020;51:914-921

172. Choi EH, Lee H, Chung JW, Seo WK, Kim GM, Ki CS, et al. Ring finger protein 213 variant and plaque characteristics, vascular remodeling, and hemodynamics in patients

with intracranial atherosclerotic stroke: A high-resolution magnetic resonance imaging and hemodynamic study. *J Am Heart Assoc*. 2019;8:e011996

173. Bolduc V, Baraghis E, Duquette N, Thorin-Trescases N, Lambert J, Lesage F, et al. Catechin prevents severe dyslipidemia-associated changes in wall biomechanics of cerebral arteries in ldlr-/-:Hapob+/+ mice and improves cerebral blood flow. *Am J Physiol Heart Circ Physiol*. 2012;302:H1330-1339

# PART TWO

# Chapter 3. Association of the circle of Willis integrity with the vascular location of intracranial atherosclerosis in acute patients with ischemic stroke

## 3.1 Background

ICAS is the most common cause of ischemic stroke, and has the highest rate of stroke recurrence among Asians [1-3]. This disease involves the intracranial large arteries in growing atherosclerotic plaques that may cause subsequent ischemia in the corresponding arterial territory [4, 5]. Generally, the formation and development of intracranial atherosclerotic plaques may be affected by the hemodynamic function depending on the anatomical structure in the cerebrovascular system [6-8]. Of note, the structural variants of the COW are considerable among the normal individuals, and may play a pivotal role in regulating the hemodynamic state of the intracranial large arteries [9-11]. However, little is discussed the underlying influence of the COW structural variability on the occurrence and progression of atherosclerosis along the intracranial vasculature.

This study aimed at investigating the correlation of the anatomical completeness of the COW with the vascular distribution of atherosclerosis within the major intracranial large arteries among acute stroke patients due to ICAS. We hypothesized that the structural integrity of the COW differs among patients with ICAS, and may have a great effect on the nonrandom vascular location of intracranial atherosclerotic lesions [12]. Our observation may further the understanding of the underlying role of the COW variations in the progression of intracranial large artery atherosclerosis among patients with acute IS.

## 3.2 Methods

### 3.2.1 Study subjects

A hospital-based prospective database was analyzed in the current study. Consecutive adult patients were recruited between 2014 and 2020, when admitted to the Prince of Wales Hospital. Subjects with the following conditions were included in this study: first-ever acute IS or TIA in seven days; at least one intracranial large artery stenosis verified by MRA or digital subtraction angiography (DSA); complete imaging scan covering the intracranial segments of the bilateral VAs. Subjects were excluded, if suffering from non-atherosclerotic stenosis (vasculitis, dissection, or moyamoya disease), cardio-embolism (atrial fibrillation or valvular heart diseases), coexistence of more than 50% stenosis of the ICA and/or the ECA, any known brain tumor or vascular malformation, history of cerebral artery surgical/interventional procedure or recurrent stroke, or contraindications to MRI. The patient clinical information at admission (age, sex, hypertension, hyperlipidemia, diabetes and smoking status) were collected during hospitalization. This study was approved by an institutional review board, and followed the Declaration of Helsinki. Each participant signed the written informed consent before recruitment.

### 3.2.2 Imaging protocol

A 3.0-Tesla Achieva magnetic resonance system with a standardized eight-channel head coil (Philips Healthcare, Cleveland, OH, USA) was utilized to scan all the subjects. The imaging protocol comprised a Time-Of-Flight (TOF) MRA sequence and a transverse three-dimensional T1-weighted (T1w) Volumetric ISotropically Turbo spin echo Acquisition (VISTA) sequence before and after administrating a contrast agent containing gadolinium with 0.1 mL/kg to every patient (Dotarem, Gadoteric acid 0.5 mmol/mL, Guerbet, Roissy CdG Cedex, France). The TOF MRA sequence parameters included field-of-view (FOV) 200*200*56mm$^3$, acquired resolution 0.4*0.6*0.7mm$^3$, time-of-repetition (TR)/time-of-echo (TE) 23/3.5ms, and scan duration 3:07min. The imaging parameters for the T1w VISTA sequence were as follows: FOV 200*167*45mm$^3$, acquired resolution 0.6*0.6*1.0mm$^3$,

reconstructed resolution 0.5*0.5*0.5 $mm^3$ with zero filling, TR 1500ms, TE 36ms, turbo-spin-echo + startup echoes 56+6, echo spacing 4.0ms, SENSE factor 1.5 with phase-encode direction, and scan duration 6:51min.

### 3.2.3 Imaging evaluation

Visual image assessment was conducted on the source images with axial orientation, as well as on the three-dimensional reconstructed images. Image quality evaluation was based on a three-point scale (3: excellent, 2: adequate, and 1: poor). Images graded over two were used for the subsequent imaging analyses.

Two observers were blind to the clinical information of all the study subjects, and assessed the intra- and inter-observer agreement. Thirty subjects were randomly selected. One observer analyzed the images two times over a three-month period between the first and the second analysis. Another observer independently analyzed the images of the same thirty subjects once.

### 3.2.4 Imaging analysis

The plaques were visually inspected among all the included subjects, if identified as focal vessel wall thickening on the three-dimensional T1w VISTA images, regardless of the luminal stenosis degree shown on MRA [13]. The presence of intracranial atherosclerotic plaques was detected along the first and the second segments of the bilateral MCAs (MCA-M1 and MCA-M2), the BA, and the fourth segments of the bilateral VAs (**Figure 3-1**, **Figure 3-2** and **Figure 3-3**). The classification of each plaque into the asymptomatic or symptomatic lesion was based on the possibility if the plaque could contribute to the downstream ischemic events in the corresponding cerebral arteries, such as the findings of acute infarction on diffusion-weighted imaging (DWI) and/or acute symptom of neurological dysfunction [14]. A symptomatic lesion was described as the situation where the only or the

most stenotic/enhanced plaque was within the ipsilateral vascular territory of IS or TIA. If a plaque was not located in the IS/TIA vascular territory, or it was within the ischemic territory but not the most stenotic/enhanced, this lesion was regarded as asymptomatic. This assessment was performed independently of the analysis of the COW integrity.

The completeness of the COW was then evaluated, according to the anatomical structure of the COW detected by MRA imaging [15]. The COW contained two parts: the A-COW and the P-COW. An incomplete A-COW or P-COW referred to the dysplasia or absence of any arterial component in the A-COW or P-COW, respectively (**Figure 3-4**). A dysplastic or absent vessel within the A-COW or P-COW was defined as the threshold arterial diameter less than 0.8mm [16].

### 3.2.5 Statistical analysis

All statistical data were analyzed by the SPSS version 26.0 (IBM, NY, USA). Continuous variables were summarized as means ± standard deviation (SD), and categorical variables were described as frequency percentages. Chi-squared test or Fisher's exact test with Bonferroni method for adjusting P values was performed to compare the plaque locations between asymptomatic and symptomatic intracranial atherosclerotic lesions, and to determine the relationship between the COW integrity and the vascular distribution of intracranial atherosclerotic plaques. The statistically significant level of P value was set as 0.05/times of the repeated comparisons. For other analyses, P value < 0.05 was regarded as statistical significance. Intra- and inter-observer agreement was examined by Cohen κ or intraclass correlation coefficient with 95% confidence intervals (CIs). A coefficient more than 0.81 was considered as excellence.

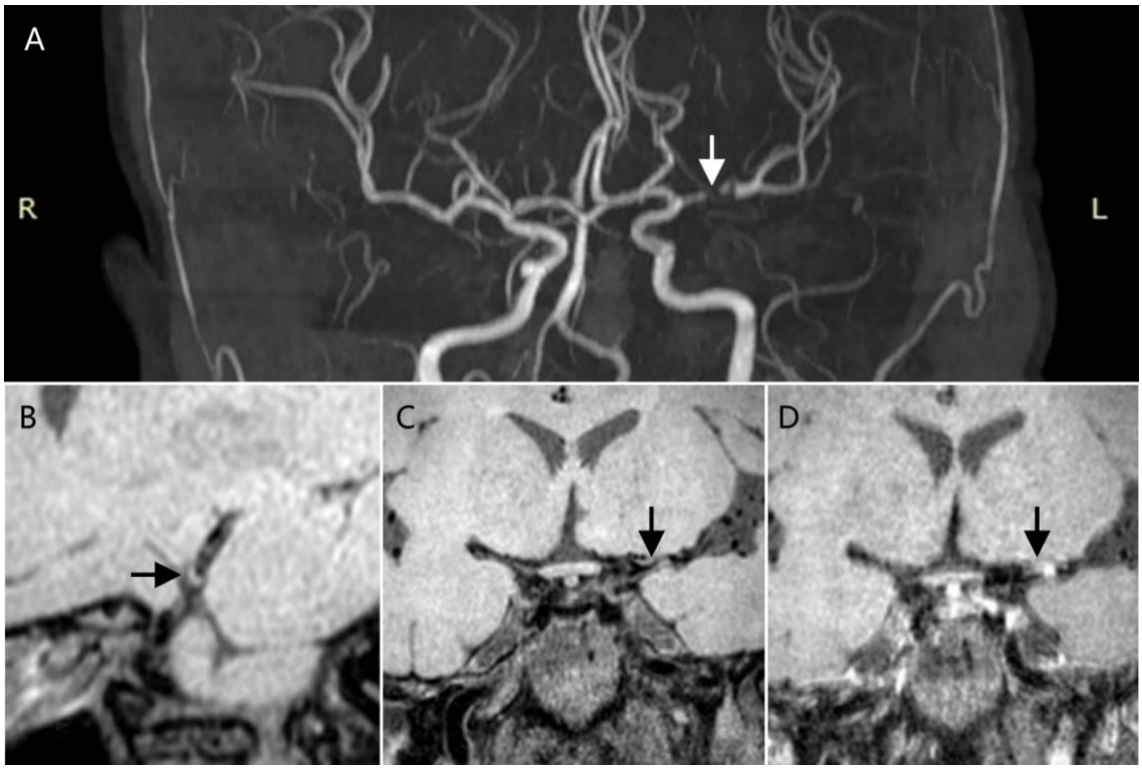


**Figure 3-1. A 59-year-old female patient with acute ischemic stroke caused by a left MCA atherosclerotic stenosis. A**, a symptomatic atherosclerotic stenosis of the left MCA-M1 segment on the MRA image (white arrow). **B**, an eccentric, focal plaque in the left MCA-M1 segment on the T1w image (black arrow). **C** and **D**, the plaque in the left MCA-M1 segment before and after administrating contrast on the T1w images, respectively (black arrows). MCA, middle cerebral artery; MRA, magnetic resonance angiography; T1w, T1-weighted.


**Figure 3-2. A 63-year-old male patient with acute infarction due to atherosclerotic stenosis of the left MCA-M1 segment. A**, a symptomatic atherosclerotic stenosis of the left MCA-M1 segment on the MRA image (white arrow). **B**, an eccentric, focal plaque in the BA as an asymptomatic atherosclerotic lesion on the T1w image (white arrow). **C**, an eccentric, focal plaque in the MCA-M2 segment as an asymptomatic atherosclerotic lesion on the T1w image (white arrow). BA, basilar artery; MCA, middle cerebral artery; MRA, magnetic resonance angiography; T1w, T1-weighted.

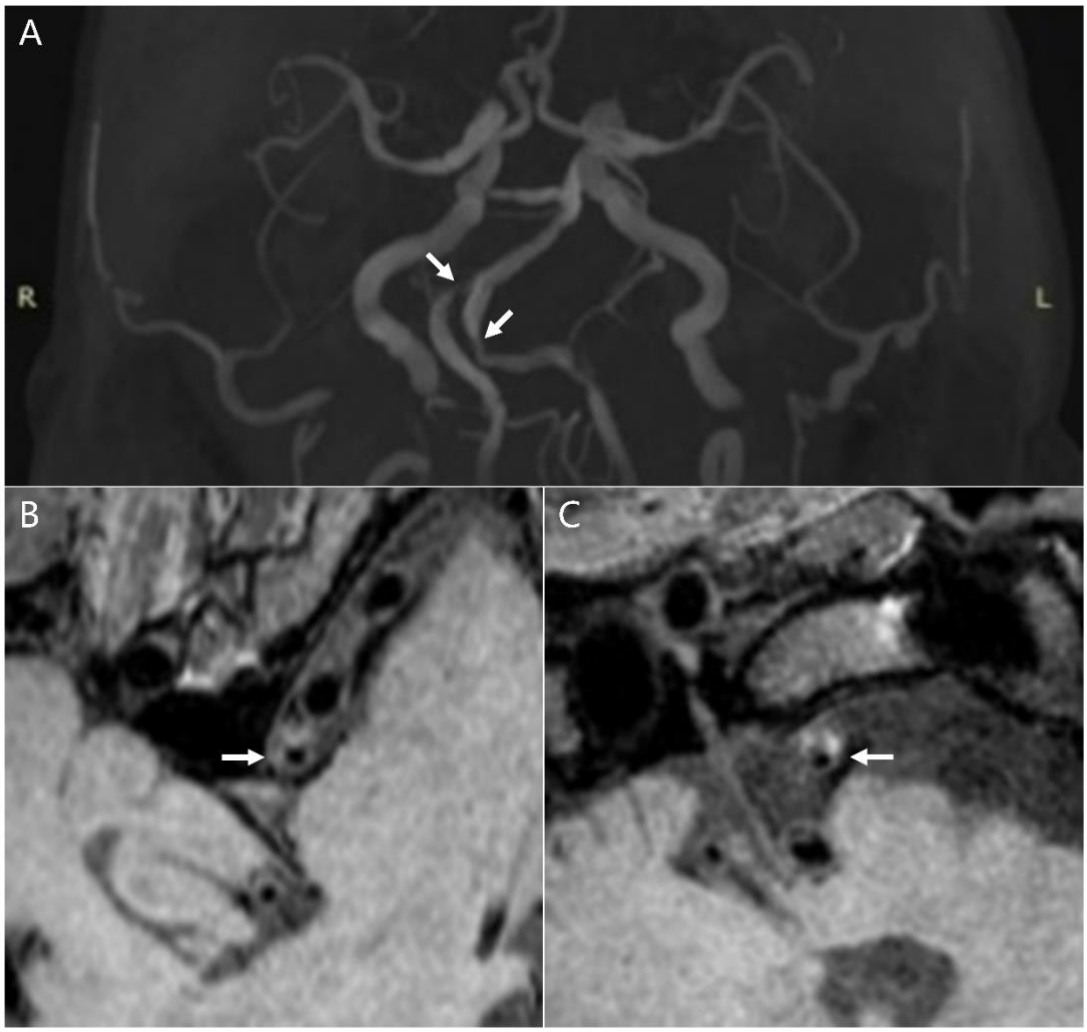


**Figure 3-3. A 62-year-old male patient with acute posterior-circulation infarction. A**, an asymptomatic atherosclerotic stenosis of the right VA and a symptomatic atherosclerotic stenosis of the left VA on the MRA image (white arrows). **B** and **C**, the eccentric, focal plaques in the right and left VAs on the T1w images, respectively (white arrows). MRA, magnetic resonance angiography; T1w, T1-weighted; VA, vertebral artery.

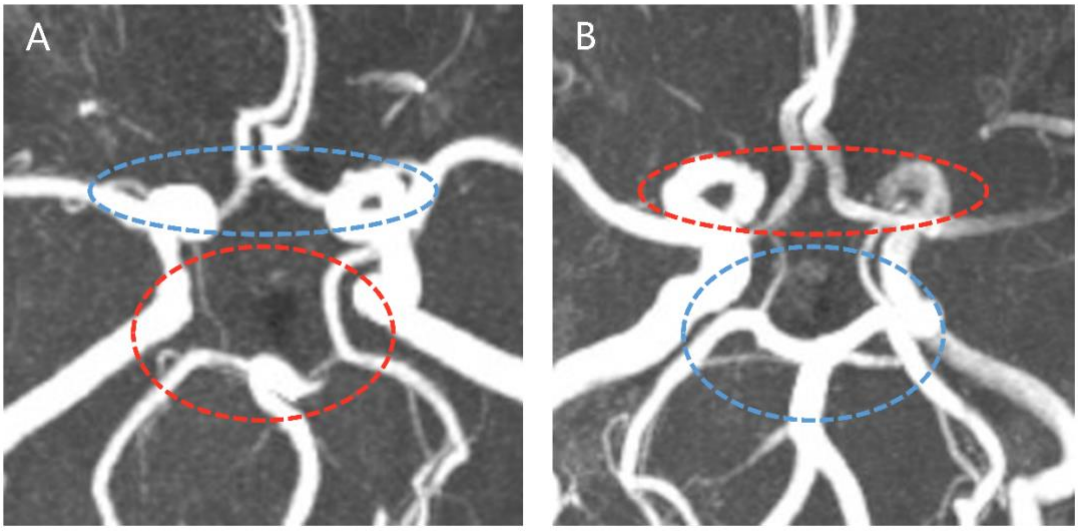


**Figure 3-4. Different structural types of the A-COW and the P-COW shown on the MRA images. A**, a complete A-COW in the blue dashed outline and an incomplete P-COW in the red dashed outline; **B**, an incomplete A-COW in the red dashed outline and a complete P-COW in the blue dashed outline. COW, circle of Willis; A-COW, anterior COW; P-COW, posterior COW; MRA, magnetic resonance angiography.

## 3.3 Results

### 3.3.1 Patient clinical features

Ninety-six subjects with ICAS were included in the present study. The patient baseline demographic and clinical characters were summarized in **Table 3-1**. The mean age of all the ICAS subjects was 63.41 ± 10.31 years old. Sixty subjects were male. The prevalence of hypertension was up to 77.1% among all the subjects, while that of current smoking status was only 28.1%. The occurrence of IS as an index event was higher than that of TIA (88.5% versus 11.5%). Besides, the incomplete P-COW subtype was more prevalent than the incomplete A-COW subtype among subjects with ICAS (83.3% versus 44.8%).

**Table 3-1. Demographic and clinical characteristics of patients with ICAS.**

| Parameters | Subjects with ICAS (n=96) |
|---|---|
| Age, years, mean ± SD | 63.41 ± 10.31 |
| Male/Female, n | 60/36 |
| Hypertension, n (%) | 74 (77.1%) |
| Hyperlipidemia, n (%) | 54 (56.3%) |
| Diabetes, n (%) | 30 (31.3%) |
| Smoking, n (%) | 27 (28.1%) |
| Index event | |
| Stroke, n (%) | 85 (88.5%) |
| TIA, n (%) | 11 (11.5%) |
| COW integrity | |
| Incomplete A-COW, n (%) | 43 (44.8%) |
| Incomplete P-COW, n (%) | 80 (83.3%) |

COW, circle of Willis; A-COW, anterior COW; P-COW, posterior COW; ICAS, intracranial atherosclerosis; TIA, transient ischemic attack.

### 3.3.2 Vascular distribution of the intracranial atherosclerotic plaques among the asymptomatic and symptomatic lesions

In total, 292 intracranial atherosclerotic plaques were identified in patients with ICAS, of which 224 were asymptomatic and 68 were symptomatic. **Table 3-2** displayed the plaque locations within the major intracranial arteries among the asymptomatic and symptomatic intracranial atherosclerotic lesions.

Among the symptomatic intracranial atherosclerotic lesions, the MCA-M1 segment was the most common site (63.2%), followed by the VA (19.1%), the MCA-M2 segment (11.8%), and the BA (5.9%). However, the VA was the most commonly detected among the asymptomatic intracranial atherosclerotic lesions (40.6%), while the MCA-M2 segment was the least (11.6%). In addition, the incidence of the symptomatic atherosclerotic lesions in the MCA-M1 segment was significantly higher than that of the asymptomatic lesions (63.2% versus 33.9%, $P < 0.001$). The prevalence of the asymptomatic VA atherosclerotic lesions was significantly higher than that of the symptomatic lesions (40.6% versus 19.1%, $P = 0.001$).

**Table 3-2. Vascular locations of the plaques between asymptomatic and symptomatic intracranial atherosclerotic lesions.**

| Distribution | Asymptomatic lesions (n=224) | Symptomatic lesions (n=68) | P value |
|---|---|---|---|
| Middle cerebral artery | | | |
| M1 segment, n (%) | 76 (33.9%) | 43 (63.2%) | **0.000** |
| M2 segment, n (%) | 26 (11.6%) | 8 (11.8%) | 0.972 |
| Basilar artery, n (%) | 31 (13.8%) | 4 (5.9%) | 0.077 |
| Vertebral artery, n (%) | 91 (40.6%) | 13 (19.1%) | **0.001** |

### 3.3.3 Relationship between the COW completeness and the vascular distribution of intracranial atherosclerotic plaques

The plaque locations in the four intracranial arteries between the complete and incomplete COW subtypes were described in all lesions (**Table 3-3**), and in the asymptomatic and symptomatic lesions (**Table 3-4**), respectively. As shown in **Table 3-3**, no statistical significance was observed in the difference of the vascular locations of all the plaques between the complete and incomplete A-COW groups, as well as between the complete and incomplete P-COW groups (all P values > 0.0125). Similarly, there were no significant differences in the arterial locations of the asymptomatic plaques between the complete and incomplete COW subtypes (all P values > 0.0125, **Table 3-4**).

On the other hand, the cerebrovascular locations of the symptomatic atherosclerotic plaques were significantly different between the complete and incomplete A-COW groups (P = 0.012, **Table 3-4**). The incident rate of the symptomatic plaques in the MCA-M1 segment was observed to be 82.8% in the incomplete A-COW subtype, and significantly higher than 48.7% in the complete A-COW subtype (P = 0.005, **Table 3-4**). Yet, the locations of the symptomatic plaques in other intracranial arteries (the MCA-M2, the BA, or the VA) were not significantly different between the complete and incomplete A-COW subtypes (all P values > 0.0125, **Table 3-4**). Besides, the vascular locations of the symptomatic plaques in the four intracranial arteries were not different between the complete and incomplete P-COW subtypes as well (all P values > 0.0125, **Table 3-4**).

**Table 3-3. Association between the COW integrity and the plaque locations in all intracranial atherosclerotic lesions.**

| | Plaques within complete A-COW (n=172) | Plaques within incomplete A-COW (n=120) | $P_1$ value | Plaques within complete P-COW (n=50) | Plaques within incomplete P-COW (n=242) | $P_2$ value |
|---|---|---|---|---|---|---|
| Distribution | | | 0.254 | | | 1 |
| M1 segment, n (%) | 64 (37.2%) | 55 (45.8%) | 0.148 | 20 (40.0%) | 99 (40.9%) | 1 |
| M2 segment, n (%) | 24 (14.0%) | 10 (8.3%) | 0.194 | 6 (12.0%) | 28 (11.6%) | 1 |
| Basilar artery, n (%) | 19 (11.0%) | 16 (13.3%) | 0.586 | 6 (12.0%) | 29 (12.0%) | 1 |
| Vertebral artery, n (%) | 65 (37.8%) | 39 (32.5%) | 0.386 | 18 (36.0%) | 86 (35.5%) | 1 |

COW, circle of Willis; A-COW, anterior COW; P-COW, posterior COW.

$P_1$: complete A-COW group versus incomplete A-COW group.

$P_2$: complete P-COW group versus incomplete P-COW group.

**Table 3-4. Association between the COW integrity and the plaque locations in asymptomatic and symptomatic intracranial atherosclerotic lesions.**

| | Plaques within complete A-COW (n=172) | Plaques within incomplete A-COW (n=120) | $P_1$ value | Plaques within complete P-COW (n=50) | Plaques within incomplete P-COW (n=242) | $P_2$ value |
|---|---|---|---|---|---|---|
| **Asymptomatic lesions** | | | | | | |
| Distribution | | | 0.882 | | | 0.912 |
| M1 segment, n (%) | 45 (33.8%) | 31 (34.1%) | 1 | 13 (34.2%) | 63 (33.9%) | 1 |
| M2 segment, n (%) | 17 (12.8%) | 9 (9.9%) | 0.534 | 5 (13.2%) | 21 (11.3%) | 0.781 |
| Basilar artery, n (%) | 17 (12.8%) | 14 (15.4%) | 0.694 | 6 (15.8%) | 25 (13.4%) | 0.796 |
| Vertebral artery, n (%) | 54 (40.6%) | 37 (40.7%) | 1 | 14 (36.8%) | 77 (41.4%) | 0.718 |
| **Symptomatic lesions** | | | | | | |
| Distribution | | | **0.012** | | | 0.555 |
| M1 segment, n (%) | 19 (48.7%) | 24 (82.8%) | **0.005** | 7 (58.3%) | 36 (64.3%) | 0.748 |
| M2 segment, n (%) | 7 (17.9%) | 1 (3.4%) | 0.125 | 1 (8.3%) | 7 (12.5%) | 1 |
| Basilar artery, n (%) | 2 (5.1%) | 2 (6.9%) | 1 | 0 (0.0%) | 4 (7.1%) | 1 |
| Vertebral artery, n (%) | 11 (28.2%) | 2 (6.9%) | 0.032 | 4 (33.3%) | 9 (16.1%) | 0.223 |

COW, circle of Willis; A-COW, anterior COW; P-COW, posterior COW.

$P_1$: complete A-COW group versus incomplete A-COW group.

$P_2$: complete P-COW group versus incomplete P-COW group.

### 3.3.4 Reliability of evaluation

The intra- and inter-observer agreement of assessing the COW completeness and the vascular location of the intracranial atherosclerotic plaques in the major intracranial large arteries were shown in **Table 3-5**. The intra- and inter-observer reliability were excellent for the assessments.

**Table 3-5. Intra- and inter-observer reliability of evaluating the COW integrity and the vascular location of the intracranial atherosclerotic plaques.**

| | Intra-observer agreement Coefficient (95% CI) | Inter-observer agreement Coefficient (95% CI) |
|---|---|---|
| COW integrity | 0.939 (0.931-0.947) | 0.909 (0.901-0.917) |
| Plaque location | 0.955 (0.950-0.960) | 0.933 (0.928-0.938) |

CI, confidence interval; COW, circle of Willis.

## 3.4 Discussion

In this hospital-based study, firstly, we found that the MCA-M1 segment was the most common site to develop symptomatic atherosclerotic lesions among the major intracranial arteries in patients with ICAS. Secondly, the incomplete A-COW subtype was significantly associated with the occurrence of symptomatic atherosclerotic lesions in the MCA-M1 segment. Our investigation may help with the knowledge of the underlying cerebrovascular pathogenesis of ICAS in acute patients with IS.

Our previous postmortem findings showed that the MCA had the severest stenotic degree and the most plaques with eccentric wall distribution, compared with the BA and the VA [17]. Via three-dimensional T1w VISTA imaging, the MCA-M1 segment was identified as the most common vascular site to occur symptomatic atherosclerosis among patients with ICAS

in this study. This result, along with other evidence of growing atherosclerosis among the intracranial large arteries [4], demonstrated that the MCA was the most likely to develop atherosclerosis and cause the subsequent ischemic events. Then, the influence of the COW variations on the arterial locations of the intracranial atherosclerotic plaques was explored, which may ascertain the underlying role of the cerebrovascular structural pattern in forming atherosclerotic plaques that induce ICAS [6, 18].

The anatomical patterns of the COW were reliably revealed in patients with ICAS through TOF MRA imaging. Our observations suggested that the incomplete COW subtypes were prevalent among ICAS patients, which was in accord with other MRA studies on the COW integrity [15, 19]. Yet, the different study populations might cause the fluctuation in the incident rates of each incomplete COW subtype [15, 20]. Significant difference in the vascular locations of the symptomatic intracranial atherosclerotic plaques was then found between the complete and incomplete A-COW structures in our study, which might be achieved by the hemodynamic role depending on the COW structure [18, 21]. Two causes could be postulated: First, the distribution of CBF within the intracranial arteries might be directly affected by the structural variance in the COW [16, 22]. Second, the COW anomalies might also largely modify the pattern of WSS acting on the intracranial arterial walls [18, 23]. Both might further worsen the vessel wall condition of the intracranial arteries, and thus accelerate the progression of unstable plaques [18, 21, 24, 25].

This hypothesis may be supported by our main result that the occurrence of symptomatic atherosclerosis in the MCA-M1 segment had significant relevance to the incomplete A-COW subtype. Briefly, the integrity of the COW might determine the hemodynamic status of the intracranial arteries [8, 26, 27]. Particularly, the collateral blood flow to the territories of ischemia might also be provided immediately and persistently via recruiting the anastomotic pathways from the complete A-COW to the MCA [28]. In this study, we thus speculate that the

incomplete A-COW structure may deteriorate the vessel wall condition of the MCA-M1 segment via affecting the patterns of CBF and WSS, and eventually induce plaque rupture in the MCA-M1 segment. This speculation may inspire future research. In our study, the incomplete P-COW subtype was commonly detectable among patients with ICAS as well. However, we did not identify any significant relationship between the incomplete P-COW and the arterial locations of the symptomatic intracranial atherosclerotic plaques, which needs more studies to verify.

We should consider some limitations to this study. First, the sample size was relatively small. Based on the previous MRA imaging research, the classification of the COW completeness was general in the current study [15]. Further research with a larger study population could apply a detailed subdivision of the COW structures [9], clarifying the potential role of each COW variant on the plaque formation. Second, TOF MRA was used to analyze the COW completeness in our study, but this imaging modality was reported relatively insensitive to the detection of low CBF and intracranial small arteries [29]. Consequently, we might overestimate the incidence of each incomplete COW subtype. Third, the ICA was not included. Our previous study showed that coexistent high-grade ICA stenosis might significantly change the velocity of CBF within other intracranial atherosclerotic arteries [30]. Accordingly, the ICA should be excluded to avoid the underlying confounding factors in the present study.

### 3.5 Conclusions

The MCA-M1 segment was more likely to grow symptomatic atherosclerotic lesions among patients with ICAS, compared to the MCA-M2 segment, the BA, and the VA. Importantly, the occurrence of the symptomatic atherosclerotic lesions in the MCA-M1 segment was found in significant association with the incomplete A-COW subtype. Our

findings implied that the structural variations of the COW might affect the progression of the intracranial atherosclerotic plaques via hemodynamic changes in the MCA-M1 segment, which should be further validated through other intracranial imaging methods.

## References


1. Holmstedt CA, Turan TN, Chimowitz MI. Atherosclerotic intracranial arterial stenosis: Risk factors, diagnosis, and treatment. *Lancet Neurol*. 2013;12:1106-1114
2. Wang Y, Zhao X, Liu L, Soo YO, Pu Y, Pan Y, et al. Prevalence and outcomes of symptomatic intracranial large artery stenoses and occlusions in china: The chinese intracranial atherosclerosis (cicas) study. *Stroke*. 2014;45:663-669
3. Lange MC, Ribas G, Scavasine V, Ducci RD, Mendes DC, Zetola VHF, et al. Stroke recurrence in the different subtypes of ischemic stroke. The importance of the intracranial disease. *Arq Neuropsiquiatr*. 2018;76:649-653
4. Banerjee C, Chimowitz MI. Stroke caused by atherosclerosis of the major intracranial arteries. *Circ Res*. 2017;120:502-513
5. Qureshi AI, Caplan LR. Intracranial atherosclerosis. *Lancet*. 2014;383:984-998
6. Ritz K, Denswil NP, Stam OC, van Lieshout JJ, Daemen MJ. Cause and mechanisms of intracranial atherosclerosis. *Circulation*. 2014;130:1407-1414
7. Vrselja Z, Brkic H, Mrdenovic S, Radic R, Curic G. Function of circle of willis. *J Cereb Blood Flow Metab*. 2014;34:578-584
8. Ginsberg MD. The cerebral collateral circulation: Relevance to pathophysiology and treatment of stroke. *Neuropharmacology*. 2018;134:280-292
9. Qiu C, Zhang Y, Xue C, Jiang S, Zhang W. Mra study on variation of the circle of willis in healthy chinese male adults. *Biomed Res Int*. 2015;2015:976340
10. Klimek-Piotrowska W, Rybicka M, Wojnarska A, Wojtowicz A, Koziej M, Holda MK. A multitude of variations in the configuration of the circle of willis: An autopsy study. *Anat Sci Int*. 2016;91:325-333

11. Yeniceri IO, Cullu N, Deveer M, Yeniceri EN. Circle of willis variations and artery diameter measurements in the turkish population. *Folia Morphol (Warsz)*. 2017;76:420-425

12. Leng X, Wong KS, Liebeskind DS. Evaluating intracranial atherosclerosis rather than intracranial stenosis. *Stroke*. 2014;45:645-651

13. Wang M, Wu F, Yang Y, Miao H, Fan Z, Ji X, et al. Quantitative assessment of symptomatic intracranial atherosclerosis and lenticulostriate arteries in recent stroke patients using whole-brain high-resolution cardiovascular magnetic resonance imaging. *J Cardiovasc Magn Reson*. 2018;20:35

14. Qiao Y, Zeiler SR, Mirbagheri S, Leigh R, Urrutia V, Wityk R, et al. Intracranial plaque enhancement in patients with cerebrovascular events on high-spatial-resolution mr images. *Radiology*. 2014;271:534-542

15. Zhou C, Yuan C, Li R, Wang W, Li C, Zhao X, et al. Association between incomplete circle of willis and carotid vulnerable atherosclerotic plaques. *Arterioscler Thromb Vasc Biol*. 2018;38:2744-2749

16. Zarrinkoob L, Ambarki K, Wahlin A, Birgander R, Eklund A, Malm J. Blood flow distribution in cerebral arteries. *J Cereb Blood Flow Metab*. 2015;35:648-654

17. Yang WJ, Fisher M, Zheng L, Niu CB, Paganini-Hill A, Zhao HL, et al. Histological characteristics of intracranial atherosclerosis in a chinese population: A postmortem study. *Front Neurol*. 2017;8:488

18. Nixon AM, Gunel M, Sumpio BE. The critical role of hemodynamics in the development of cerebral vascular disease. *J Neurosurg*. 2010;112:1240-1253

19. Zhou H, Sun J, Ji X, Lin J, Tang S, Zeng J, et al. Correlation between the integrity of the circle of willis and the severity of initial noncardiac cerebral infarction and clinical prognosis. *Medicine (Baltimore)*. 2016;95:e2892

20. Goksu EO, Koc P, Kucukseymen E, Unal A, Genc F, Gencer ES, et al. The association of the circle of willis anomaly and risk of stroke in patients with carotid artery disease. *Arq Neuropsiquiatr*. 2017;75:429-432

21. Frangos SG, Gahtan V, Sumpio B. Localization of atherosclerosis: Role of hemodynamics. *Arch Surg*. 1999;134:1142-1149

22. Pascalau R, Padurean VA, Bartos D, Bartos A, Szabo BA. The geometry of the circle of willis anatomical variants as a potential cerebrovascular risk factor. *Turk Neurosurg*. 2019;29:151-158

23. Alnaes MS, Isaksen J, Mardal KA, Romner B, Morgan MK, Ingebrigtsen T. Computation of hemodynamics in the circle of willis. *Stroke*. 2007;38:2500-2505

24. Schirmer CM, Malek AM. Prediction of complex flow patterns in intracranial atherosclerotic disease using computational fluid dynamics. *Neurosurgery*. 2007;61:842-851; discussion 852

25. Schirmer CM, Malek AM. Estimation of wall shear stress dynamic fluctuations in intracranial atherosclerotic lesions using computational fluid dynamics. *Neurosurgery*. 2008;63:326-334; discussion 334-325

26. Ryu J, Hu X, Shadden SC. A coupled lumped-parameter and distributed network model for cerebral pulse-wave hemodynamics. *J Biomech Eng*. 2015;137:101009

27. Leger PL, Bonnin P, Lacombe P, Couture-Lepetit E, Fau S, Renolleau S, et al. Dynamic spatio-temporal imaging of early reflow in a neonatal rat stroke model. *J Cereb Blood Flow Metab*. 2013;33:137-145

28. Armitage GA, Todd KG, Shuaib A, Winship IR. Laser speckle contrast imaging of collateral blood flow during acute ischemic stroke. *J Cereb Blood Flow Metab*. 2010;30:1432-1436

29. Hartkamp MJ, van Der Grond J, van Everdingen KJ, Hillen B, Mali WP. Circle of willis collateral flow investigated by magnetic resonance angiography. *Stroke*. 1999;30:2671-2678

30. Zhong J, Chen XY, Leung TW, Ou A, Shi X, Cai Y, et al. Significance of raised flow velocity in basilar artery in patients with acute ischemic stroke: Focal stenosis, coexistent stenosis, and collateral flow. *J Neuroimaging*. 2015;25:922-926

# Chapter 4. The pattern of plaque wall distribution in middle cerebral artery atherosclerosis is correlated with the incomplete circle of Willis

## 4.1 Background

As major etiology of IS, ICAS brings heavy neurological burden to the public health all over the world [1-3]. Compared to other intracranial large arteries, the MCA is more vulnerably exposed to atherosclerosis, and has higher luminal narrowing percentages and more plaques distributed eccentrically [1, 4]. In general, the occurrence and development of MCA atherosclerosis may be affected by the anatomical variability in the intracranial vasculature [5, 6]. Substantial variations in the structural patterns of the COW are identified within normal individuals [7-9], which may make a direct impact on the process of intracranial atherosclerotic lesions [10, 11]. Yet little is known about the relevance of the COW anatomical integrity to the plaque characters of MCA atherosclerosis.

HR-MRI can noninvasively describe the typical vessel wall morphology of the intracranial atherosclerotic arteries [12, 13]. The fundamental feature of the plaque wall distribution in the MCA delineated by HR-MRI was shown in correlation with the cerebrovascular pathogenesis of ICAS, and might even help with precise interventional therapy in the clinical practice [5, 14]. This study aimed to explore the underlying relationship between the incomplete COW structures and the pattern of the plaque wall distribution in MCA atherosclerosis through utilizing HR-MRI.

## 4.2 Methods

### 4.2.1 Study subjects

In this hospital-based prospective dataset, consecutive adult patients were recruited from a single medical institution between 2014 and 2020. Subjects with MCA atherosclerotic plaques identified by HR-MRI were included in the current study, when they were also diagnosed as first-ever acute IS or TIA in a week; atherosclerotic stenosis of at least one intracranial large artery verified by MRA or DSA. The exclusion criteria were as follows: no atherosclerotic plaques in the MCAs confirmed by HR-MRI; non-atherosclerotic stenosis (dissection, moyamoya disease, or vasculitis); clinical evidence of cardio-embolism (atrial fibrillation or valvular heart diseases); coexistence of over 50% stenosis in the ICA and/or the ECA; any known brain tumor or vascular malformation; history of cerebral artery surgical/interventional procedure or recurrent stroke; any contraindications to MRI. Baseline clinical information of all the included patients were documented during hospitalization, such as age, sex, hypertension, hyperlipidemia, diabetes and smoking status. This study was approved by the institutional review board, and followed the Declaration of Helsinki. Each subject signed the written informed consent.

### 4.2.2 Imaging protocol

A 3.0-Tesla Achieva magnetic resonance system with a standardized eight-channel head coil (Philips Healthcare, Cleveland, OH, USA) was utilized to scan all the subjects. The imaging protocol comprised a TOF MRA sequence and a transverse three-dimensional T1w VISTA sequence before and after administrating a contrast agent containing gadolinium with 0.1 mL/kg to every patient (Dotarem, Gadoteric acid 0.5 mmol/mL, Guerbet, Roissy CdG Cedex, France). The TOF MRA sequence parameters included FOV 200*200*56$mm^3$, acquired resolution 0.4*0.6*0.7$mm^3$, TR/TE 23/3.5ms, and scan duration 3:07min. The imaging parameters for the T1w VISTA sequence were as follows: FOV 200*167*45$mm^3$, acquired resolution 0.6*0.6*1.0$mm^3$, reconstructed resolution 0.5*0.5*0.5 $mm^3$ with zero

filling, TR 1500ms, TE 36ms, turbo-spin-echo + startup echoes 56+6, echo spacing 4.0ms, SENSE factor 1.5 with phase-encode direction, and scan duration 6:51min.

### 4.2.3 Imaging evaluation

Visual image assessment was performed on the source images with axial orientation, as well as on the three-dimensional reconstructed images. Image quality evaluation was based on a three-point scale (3: excellent, 2: adequate, and 1: poor). Images graded more than two were used for the subsequent imaging analyses.

Two observers were blind to the clinical information of all the study subjects, and assessed the intra- and inter-observer agreement. Thirty subjects were randomly selected. One observer analyzed the images two times over a three-month period between the first and the second analysis. Another observer independently analyzed the images of the same thirty subjects once.

### 4.2.4 The anatomical completeness of the COW

The structural patterns of the COW integrity were analyzed on the basis of the information from MRA imaging [15, 16]. The COW was separated into the A-COW and the P-COW (**Figure 4-1**). An incomplete structure of the A-COW or the P-COW was featured as any dysplastic or absent component artery within one of the two anatomical parts, the threshold diameter of which was < 0.8mm shown on the MRA images [16]. For instance, the A-COW part was identified as incomplete, when any segment of the bilateral ACA-A1 and the ACoA was dysplastic or absent. The evaluation of the COW completeness was conducted independently of the following imaging analyses.

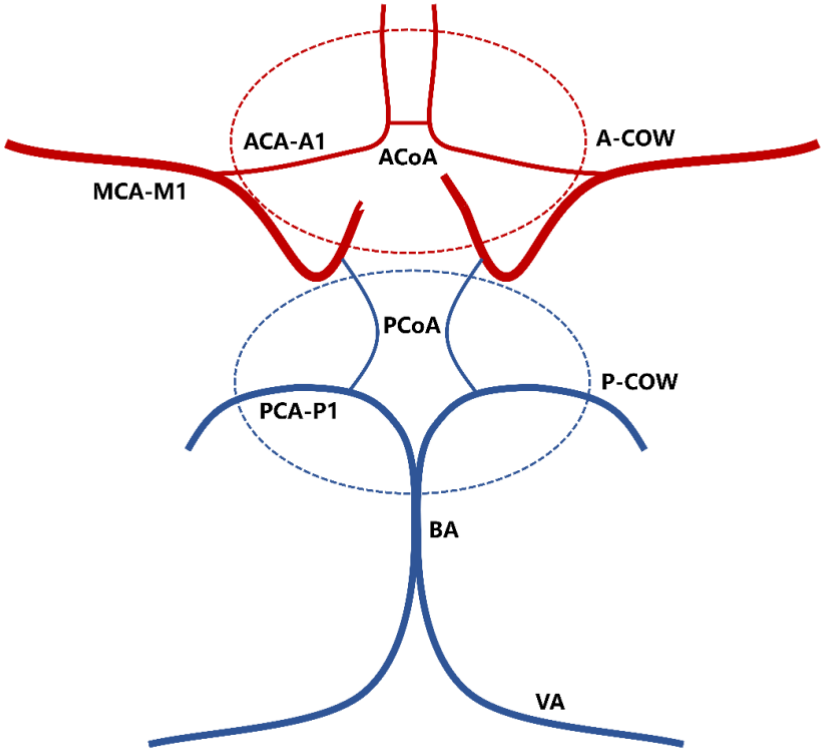


**Figure 4-1. The COW has two structural sections: the A-COW and the P-COW.** The A-COW in red: the ACoA and the first segments of the bilateral ACAs. The P-COW in blue: the bilateral PCoAs and the first segments of the bilateral PCAs. ACA, anterior cerebral artery; ACoA, anterior communicating artery; A-COW, anterior circle of Willis; BA, basilar artery; COW, circle of Willis; MCA, middle cerebral artery; PCA, posterior cerebral artery; PCoA, posterior communicating artery; P-COW, posterior circle of Willis; VA, vertebral artery.

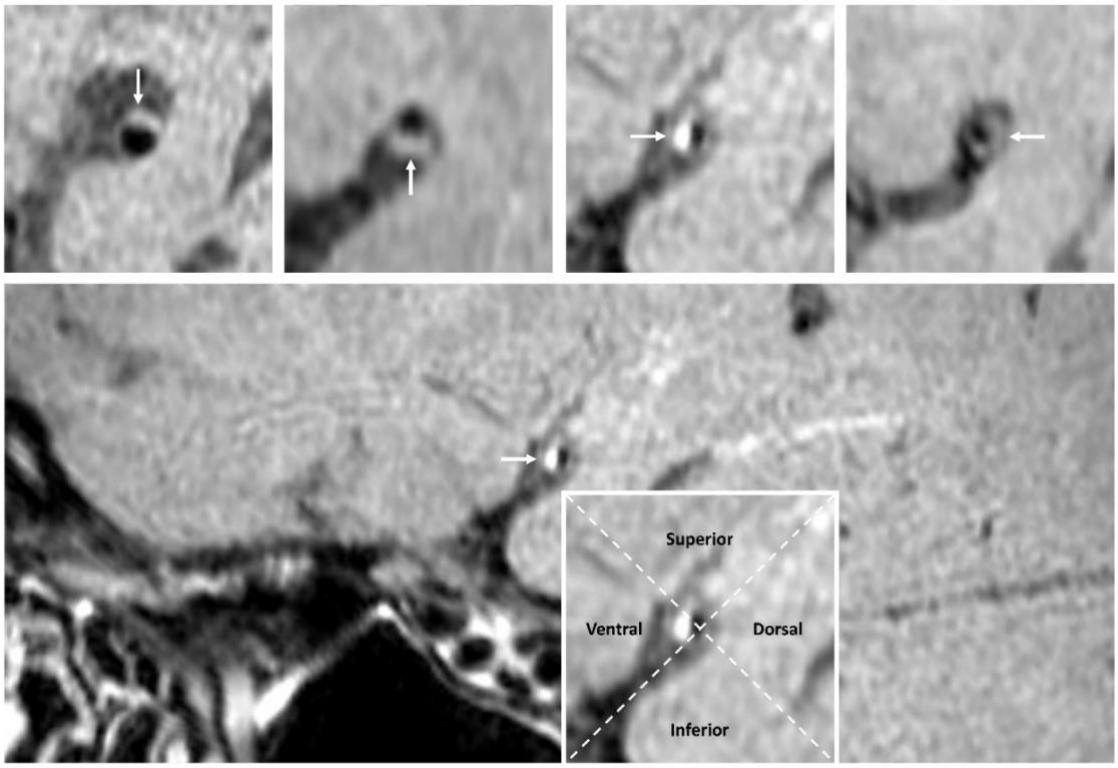


**Figure 4-2. High-resolution vessel wall imaging shows the patterns of plaque wall distribution in MCA atherosclerosis [17].** A white arrow highlights the MCA atherosclerotic plaque in an individual imaging cross-section. Two dashed lines intersect at the center of the MCA lumen, and categorize every imaging cross-section into superior, inferior, ventral, and dorsal vascular sides. The plaque in the cross-sectional image may be distributed on one of the four quadrants. MCA, middle cerebral artery.

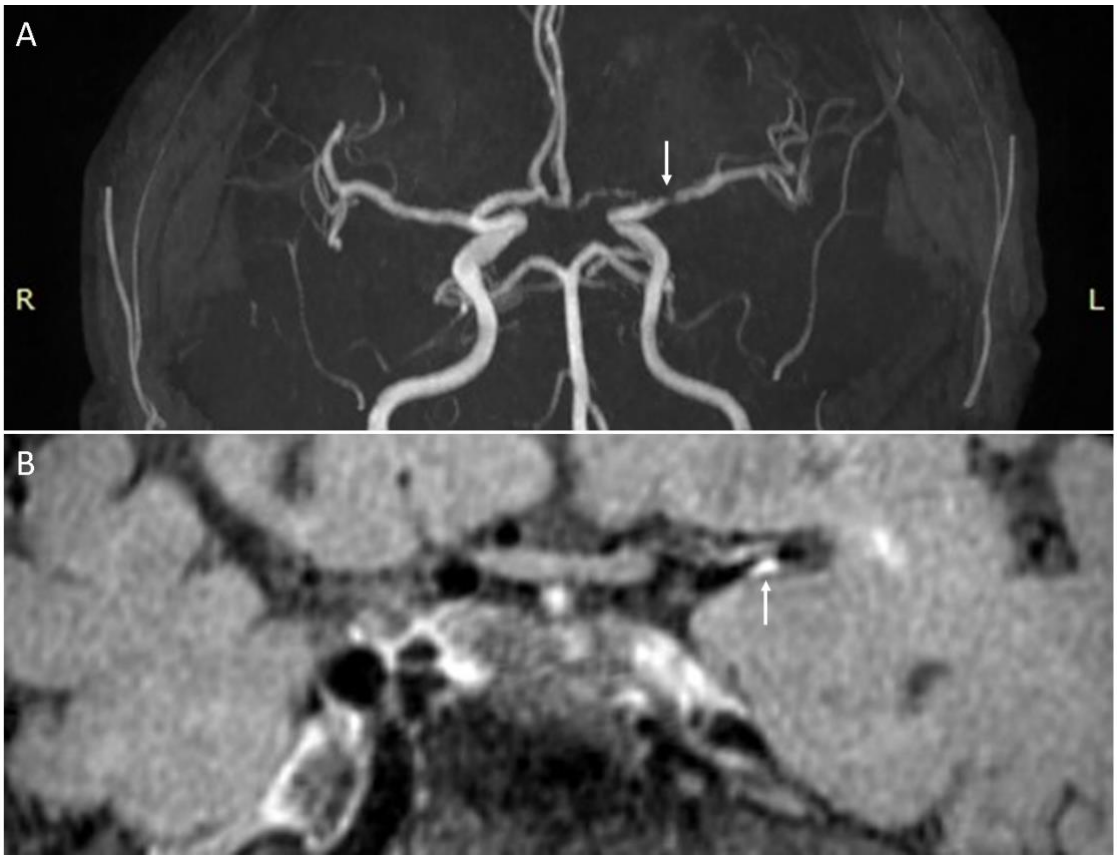


**Figure 4-3. A 61-year-old male patient with acute infarct in the left anterior circulation.** **A**, a symptomatic atherosclerotic stenosis of the left MCA-M1 segment on the MRA image (white arrow). **B**, an eccentric, focal plaque in the left MCA-M1 segment as a symptomatic atherosclerotic lesion on the T1w image (white arrow). MCA, middle cerebral artery; MRA, magnetic resonance angiography; T1w, T1-weighted.

### 4.2.5 The pattern of MCA plaque wall distribution

An atherosclerotic plaque in the first segment of the MCA was recognized through visual inspection on the three-dimensional T1w VISTA images, when focal thickening appeared on the vessel wall (the thickest point was over double the thinnest site) [14]. All the imaging cross-sections of the MCA-M1 plaque were sorted, according to the vessel wall distribution of the plaque on the superior, inferior, ventral, or dorsal side (**Figure 4-2**). Every cross-section of the plaque was categorized into one quadrant. Only the quadrant of the maximum wall thickness was considered in this study, when two or more quadrants were covered by the plaque.

Every plaque was then classified into symptomatic or asymptomatic, based on the situation that the plaque might or might not lead to the downstream ischemia in the territory of the MCA-M1 segment (symptoms of neurological dysfunction and/or acute infarctions on DWI) [18] (**Figure 4-3**). If the plaque was the only or the most stenotic/enhanced in the IS/TIA territory of the ipsilateral MCA-M1 segment, this lesion was found as symptomatic. If the plaque was not in the ischemic territory of the ipsilateral MCA-M1 segment, or it was in the ischemic territory but not the most stenotic/enhanced, the lesion was identified as asymptomatic.

### 4.2.6 Statistical analysis

SPSS version 26.0 (IBM, NY, USA) was used to perform all statistical analyses. Data were summarized as means ± SD or percentages, where appropriate. For every atherosclerotic plaque, the individual percentage of plaque wall distribution was determined. Then, the mean percentages of superior, inferior, ventral, and dorsal wall distribution were calculated in the total groups of complete and incomplete COW subtypes, respectively [14]. Mann-Whitney U test was utilized to compare the mean percentages of each plaque wall orientation between

complete and incomplete COW subtypes. Statistical significance was defined as P value < 0.05. Cohen κ or intraclass correlation coefficient with 95% CIs was used to evaluate intra- and inter-observer agreement. A coefficient over 0.81 referred to excellence.

## 4.3 Results

### 4.3.1 Baseline demographic and clinical features of subjects

One hundred and seven patients with atherosclerotic plaques in the MCA-M1 segments were included in this study. The patient demographic and clinical characteristics at admission were presented in **Table 4-1**. Mean age was 62.50 ± 11.69 years old. Sixty-seven subjects were male. Among all the patients, the incident rate of hypertension was 74.8%, and higher than that of hyperlipidemia, diabetes, or current smoking status. The prevalence of TIA was only 13.1%, while that of IS reached 86.9%.

**Table 4-1. Baseline clinical characters of patients with MCA atherosclerosis.**

| Parameters | Subjects (n=107) |
|---|---|
| Age, years, mean ± SD | 62.50 ± 11.69 |
| Male/Female, n | 67/40 |
| Hypertension, n (%) | 80 (74.8%) |
| Hyperlipidemia, n (%) | 62 (57.9%) |
| Diabetes, n (%) | 35 (32.7%) |
| Smoking, n (%) | 28 (26.2%) |
| Index event | |
| Stroke, n (%) | 93 (86.9%) |
| TIA, n (%) | 14 (13.1%) |
| COW integrity | |
| Incomplete A-COW, n (%) | 46 (43.0%) |
| Incomplete P-COW, n (%) | 91 (85.0%) |

A-COW, anterior circle of Willis; COW, circle of Willis; MCA, middle cerebral artery; P-COW, posterior circle of Willis; TIA, transient ischemic attack.

**Table 4-2. Association of the incomplete COW with the plaque wall distribution in the atherosclerotic MCAs.**

| Wall orientation | Plaques without incomplete A-COW | Plaques with incomplete A-COW | P value | Plaques without incomplete P-COW | Plaques with incomplete P-COW | P value |
|---|---|---|---|---|---|---|
| **All lesions (158)** | | | | | | |
| Superior wall | 15.49% | 15.33% | 0.684 | 10.71% | 16.27% | 0.331 |
| Inferior wall | 22.73% | 46.81% | **0.000** | 52.73% | 29.39% | **0.011** |
| Ventral wall | 51.57% | 21.75% | **0.000** | 28.13% | 40.86% | 0.318 |
| Dorsal wall | 10.22% | 16.11% | 0.253 | 8.44% | 13.49% | 0.709 |
| **Asymptomatic lesions (96)** | | | | | | |
| Superior wall | 16.10% | 18.92% | 0.617 | 14.29% | 17.68% | 0.679 |
| Inferior wall | 20.88% | 47.64% | **0.003** | 46.75% | 28.54% | 0.085 |
| Ventral wall | 50.39% | 15.49% | **0.000** | 25.93% | 38.82% | 0.516 |
| Dorsal wall | 12.63% | 17.96% | 0.546 | 13.04% | 14.96% | 0.879 |
| **Symptomatic lesions (62)** | | | | | | |
| Superior wall | 14.36% | 10.91% | 0.977 | 5.70% | 14.04% | 0.314 |
| Inferior wall | 26.13% | 45.78% | 0.067 | 61.10% | 30.74% | 0.057 |
| Ventral wall | 53.73% | 29.47% | **0.019** | 31.20% | 44.07% | 0.433 |
| Dorsal wall | 5.78% | 13.83% | 0.253 | 2.00% | 11.15% | 0.421 |

A-COW, anterior circle of Willis; COW, circle of Willis; MCA, middle cerebral artery; P-COW, posterior circle of Willis.

### 4.3.2 The COW structural integrity

As illuminated in **Table 4-1**, the incidence of the incomplete A-COW type was 43.0% in all the subjects with MCA atherosclerosis, whereas that of the incomplete P-COW type went up to 85.0%.

### 4.3.3 Relationship between the incomplete COW and the plaque wall distribution in MCA atherosclerosis

In the current study, we detected 158 MCA atherosclerotic plaques overall (96 plaques were asymptomatic, and 62 were symptomatic). In total, 612 imaging slices from HR-MRI were utilized to determine the pattern of plaque wall distribution in MCA atherosclerosis.

As shown in **Table 4-2**, the mean percentages of each plaque orientation side in the atherosclerotic MCA-M1 segments were compared between complete and incomplete COW subgroups. Compared to the complete A-COW, within all MCA atherosclerotic lesions, the incomplete A-COW had more plaques on the inferior wall (46.81% versus 22.73%, $P < 0.001$, **Table 4-2**), but fewer plaques on the ventral wall (21.75% versus 51.57%, $P < 0.001$, **Table 4-2**). Asymptomatic MCA plaques in the incomplete A-COW were more likely to be located on the inferior wall (47.64% versus 20.88%, $P = 0.003$, **Table 4-2**), but less likely to be located on the ventral wall (15.49% versus 50.39%, $P < 0.001$, **Table 4-2**), compared with those in the complete A-COW. Similarly, symptomatic MCA plaques in the incomplete A-COW were located less commonly on the ventral wall than those in the complete A-COW (29.47% versus 53.73%, $P = 0.019$, **Table 4-2**).

Within all lesions of MCA atherosclerosis, besides, the incomplete P-COW had fewer plaques distributed on the inferior wall than the complete P-COW (29.39% versus 52.73%, $P = 0.011$, **Table 4-2**). Nevertheless, both asymptomatic and symptomatic MCA plaques were

evenly distributed on the four vascular sides between the complete and incomplete P-COW subtypes (all P values > 0.05, **Table 4-2**).

### 4.3.4 Reliability of assessment

The intra- and inter-observer agreement of analyzing the COW completeness and the MCA plaque wall distribution were shown in **Table 4-3**. The intra- and inter-observer reliability were excellent for the evaluations.

**Table 4-3. Intra- and inter-observer reliability of evaluating the COW integrity and the MCA plaque wall orientation.**

| | Intra-observer agreement Coefficient (95% CI) | Inter-observer agreement Coefficient (95% CI) |
|---|---|---|
| COW integrity | 0.939 (0.931-0.947) | 0.909 (0.901-0.917) |
| Plaque wall distribution | 0.950 (0.906-0.974) | 0.912 (0.838-0.953) |

CI, confidence interval; COW, circle of Willis; MCA, middle cerebral artery.

## 4.4 Discussion

In this study, we verified that the occurrence of an incomplete COW structure was common among patients with MCA atherosclerosis. Via the utilization of HR-MRI, the characteristic pattern of the plaque wall orientation in MCA atherosclerosis could be differentiated between complete and incomplete COW subtypes. Our findings suggested that the incomplete A-COW had more inferior-wall plaques, but fewer ventral-wall plaques in the atherosclerotic MCA-M1 segments. Meanwhile, fewer MCA plaques in the incomplete P-COW were distributed on the inferior wall. Our investigations might further our knowledge of the pathological process of MCA atherosclerosis owing to the structural variations in the cerebral vasculature.

The anatomical variability in the COW has occurred since the beginning of the COW formation among normal individuals [19]. Prior MRA research indicated that the prevalence of the incomplete A-COW was 21.42% in the healthy male populations, and that of the incomplete P-COW was found to be 83.93% [7]. Furthermore, the incomplete COW structures were also prevalent among patients with stroke [15, 16]. One of the MRA findings demonstrated that the incomplete A-COW was detected in 40.7% of patients with symptomatic carotid artery atherosclerosis, while the incomplete P-COW in 79.7% [15]. In the present study, 43.0% of patients with MCA atherosclerosis had an incomplete A-COW type, and 85.0% possessed an incomplete P-COW type. Despite the fluctuation in the rates of each incomplete COW structure caused by different study populations, our observations were in line with the results from previous studies.

The pattern of the plaque wall orientation in the MCA has its own distinctive feature. The MCA atherosclerotic plaques were reported to be primarily located on the inferior and ventral vessel walls, of which the asymptomatic plaques were more possible to be located on the inferior wall of the MCA than the symptomatic plaques [14]. In this study, we further found that the incomplete A-COW structure was significantly associated with more inferior-wall plaques, but fewer ventral-wall plaques in MCA atherosclerosis than the complete A-COW structure. The significant differences in the vessel wall distribution of the MCA plaques between complete and incomplete A-COW structures might be resulted from the change to the hemodynamic force within the atherosclerotic MCA. Firstly, the structural variations in the COW could predominantly influence the pattern of CBF in the MCA [11, 20, 21]. Secondly, the local alteration in the hemodynamic status of the MCA might subsequently impact upon the spatial distribution of the WSS on the vessel walls [20, 22, 23]. Notably, the reduced levels of the WSS might result in the dysfunction and inflammation of endothelial cells, which finally accelerated the formation and development of the MCA plaques [24-26]. This hypothesis might

be supported by our observations. Meanwhile, we also identified that the incomplete P-COW type was negatively related to the existence of the inferior-wall plaques in MCA atherosclerosis. However, a larger sample size is needed for confirmation.

Our findings have potential value for the clinical practice. The anatomical features of the intracranial vasculature were revealed to affect the outcomes of endovascular treatment [27, 28]. Consequently, the basic assessment of the COW structure prior to the interventional procedures may be beneficial to localizing the atherosclerotic plaques non-randomly distributed within the MCA and help with the improvement of endovascular therapy [29, 30]. The clinical importance of evaluating the COW integrity for patients with MCA atherosclerosis requires further validation in the follow-up research.

This study had several limitations. First, all the subjects were recruited from a single stroke center, and thus our results should be applied with caution to other races and geography. Second, the current study could introduce a selection bias. We did not include patients with chronic and subacute IS/TIA to avoid the possible confounders, since medical treatment, lifestyle improvement and time course might have a major effect on the development of the intracranial atherosclerotic plaques [31]. Third, we hypothesized, according to our investigation, the hemodynamic function of the incomplete A-COW geometry on the plaque wall distribution of MCA atherosclerosis via affecting the CBF and WSS levels, which needs subsequent verification through other intracranial imaging techniques.

### 4.5 Conclusion

Among patients with MCA atherosclerosis, the existence of an incomplete COW structure was common. The incomplete A-COW type was revealed in significant association with more inferior-wall plaques, but fewer ventral-wall plaques in MCA atherosclerosis. Besides, the incomplete P-COW type was correlated with fewer inferior-wall plaques in the

atherosclerotic MCAs. The patterns of MCA plaque wall distribution related to the incomplete COW may be important to understand the cerebrovascular pathogenesis of MCA atherosclerosis and conduct precision medicine for patients with ICAS.

## References


1. Banerjee C, Chimowitz MI. Stroke caused by atherosclerosis of the major intracranial arteries. *Circ Res*. 2017;120:502-513
2. Balla SR, Cyr DD, Lokhnygina Y, Becker RC, Berkowitz SD, Breithardt G, et al. Relation of risk of stroke in patients with atrial fibrillation to body mass index (from patients treated with rivaroxaban and warfarin in the rivaroxaban once daily oral direct factor xa inhibition compared with vitamin k antagonism for prevention of stroke and embolism trial in atrial fibrillation trial). *Am J Cardiol*. 2017;119:1989-1996
3. Collaborators GBDN. Global, regional, and national burden of neurological disorders, 1990-2016: A systematic analysis for the global burden of disease study 2016. *Lancet Neurol*. 2019;18:459-480
4. Yang WJ, Fisher M, Zheng L, Niu CB, Paganini-Hill A, Zhao HL, et al. Histological characteristics of intracranial atherosclerosis in a chinese population: A postmortem study. *Front Neurol*. 2017;8:488
5. Yu YN, Li ML, Xu YY, Meng Y, Trieu H, Villablanca JP, et al. Middle cerebral artery geometric features are associated with plaque distribution and stroke. *Neurology*. 2018;91:e1760-e1769
6. Kim BJ, Yoon Y, Lee DH, Kang DW, Kwon SU, Kim JS. The shape of middle cerebral artery and plaque location: High-resolution mri finding. *Int J Stroke*. 2015;10:856-860
7. Qiu C, Zhang Y, Xue C, Jiang S, Zhang W. Mra study on variation of the circle of willis in healthy chinese male adults. *Biomed Res Int*. 2015;2015:976340

8. Klimek-Piotrowska W, Rybicka M, Wojnarska A, Wojtowicz A, Koziej M, Holda MK. A multitude of variations in the configuration of the circle of willis: An autopsy study. *Anat Sci Int*. 2016;91:325-333

9. Yeniceri IO, Cullu N, Deveer M, Yeniceri EN. Circle of willis variations and artery diameter measurements in the turkish population. *Folia Morphol (Warsz)*. 2017;76:420-425

10. Ginsberg MD. The cerebral collateral circulation: Relevance to pathophysiology and treatment of stroke. *Neuropharmacology*. 2018;134:280-292

11. Pascalau R, Padurean VA, Bartos D, Bartos A, Szabo BA. The geometry of the circle of willis anatomical variants as a potential cerebrovascular risk factor. *Turk Neurosurg*. 2019;29:151-158

12. Bodle JD, Feldmann E, Swartz RH, Rumboldt Z, Brown T, Turan TN. High-resolution magnetic resonance imaging: An emerging tool for evaluating intracranial arterial disease. *Stroke*. 2013;44:287-292

13. Dieleman N, van der Kolk AG, Zwanenburg JJ, Harteveld AA, Biessels GJ, Luijten PR, et al. Imaging intracranial vessel wall pathology with magnetic resonance imaging: Current prospects and future directions. *Circulation*. 2014;130:192-201

14. Xu WH, Li ML, Gao S, Ni J, Zhou LX, Yao M, et al. Plaque distribution of stenotic middle cerebral artery and its clinical relevance. *Stroke*. 2011;42:2957-2959

15. Zhou C, Yuan C, Li R, Wang W, Li C, Zhao X, et al. Association between incomplete circle of willis and carotid vulnerable atherosclerotic plaques. *Arterioscler Thromb Vasc Biol*. 2018;38:2744-2749

16. Zhou H, Sun J, Ji X, Lin J, Tang S, Zeng J, et al. Correlation between the integrity of the circle of willis and the severity of initial noncardiac cerebral infarction and clinical prognosis. *Medicine (Baltimore)*. 2016;95:e2892

17. Li J, Zheng L, Yang WJ, Sze-To CY, Leung TW, Chen XY. Plaque wall distribution pattern of the atherosclerotic middle cerebral artery associates with the circle of willis completeness. *Front Neurol*. 2020;11:599459

18. Qiao Y, Zeiler SR, Mirbagheri S, Leigh R, Urrutia V, Wityk R, et al. Intracranial plaque enhancement in patients with cerebrovascular events on high-spatial-resolution mr images. *Radiology*. 2014;271:534-542

19. Furuichi K, Ishikawa A, Uwabe C, Makishima H, Yamada S, Takakuwa T. Variations of the circle of willis at the end of the human embryonic period. *Anat Rec (Hoboken)*. 2018;301:1312-1319

20. Nixon AM, Gunel M, Sumpio BE. The critical role of hemodynamics in the development of cerebral vascular disease. *J Neurosurg*. 2010;112:1240-1253

21. Zarrinkoob L, Ambarki K, Wahlin A, Birgander R, Eklund A, Malm J. Blood flow distribution in cerebral arteries. *J Cereb Blood Flow Metab*. 2015;35:648-654

22. Alnaes MS, Isaksen J, Mardal KA, Romner B, Morgan MK, Ingebrigtsen T. Computation of hemodynamics in the circle of willis. *Stroke*. 2007;38:2500-2505

23. Chen Z, Qin H, Liu J, Wu B, Cheng Z, Jiang Y, et al. Characteristics of wall shear stress and pressure of intracranial atherosclerosis analyzed by a computational fluid dynamics model: A pilot study. *Front Neurol*. 2019;10:1372

24. Costopoulos C, Timmins LH, Huang Y, Hung OY, Molony DS, Brown AJ, et al. Impact of combined plaque structural stress and wall shear stress on coronary plaque progression, regression, and changes in composition. *Eur Heart J*. 2019;40:1411-1422

25. Chistiakov DA, Orekhov AN, Bobryshev YV. Effects of shear stress on endothelial cells: Go with the flow. *Acta Physiol (Oxf)*. 2017;219:382-408

26. Stone PH, Coskun AU, Kinlay S, Clark ME, Sonka M, Wahle A, et al. Effect of endothelial shear stress on the progression of coronary artery disease, vascular

remodeling, and in-stent restenosis in humans: In vivo 6-month follow-up study. *Circulation*. 2003;108:438-444

27. Schwaiger BJ, Gersing AS, Zimmer C, Prothmann S. The curved mca: Influence of vessel anatomy on recanalization results of mechanical thrombectomy after acute ischemic stroke. *AJNR Am J Neuroradiol*. 2015;36:971-976

28. Zhu L, Liebeskind DS, Jahan R, Starkman S, Salamon N, Duckwiler G, et al. Thrombus branching and vessel curvature are important determinants of middle cerebral artery trunk recanalization with merci thrombectomy devices. *Stroke*. 2012;43:787-792

29. Banga PV, Varga A, Csobay-Novak C, Kolossvary M, Szanto E, Oderich GS, et al. Incomplete circle of willis is associated with a higher incidence of neurologic events during carotid eversion endarterectomy without shunting. *J Vasc Surg*. 2018;68:1764-1771

30. Millesi K, Mutzenbach JS, Killer-Oberpfalzer M, Hecker C, Machegger L, Bubel N, et al. Influence of the circle of willis on leptomeningeal collateral flow in anterior circulation occlusive stroke: Friend or foe? *J Neurol Sci*. 2019;396:69-75

31. Leung TW, Wang L, Soo YO, Ip VH, Chan AY, Au LW, et al. Evolution of intracranial atherosclerotic disease under modern medical therapy. *Ann Neurol*. 2015;77:478-486

# Chapter 5. The circle of Willis anomaly in symptomatic middle cerebral artery atherosclerosis: Dysplasia or absence of the anterior communicating artery

## 5.1 Background

ICAS accounts for huge numbers of the events of acute ischemic stroke in all parts of the world, and burdens the society with a high risk of stroke-related disability and mortality [1-3]. Among the major intracranial large arteries, the MCA is the most likely to be affected by atherosclerosis, with the highest degree of luminal stenosis and the most plaques of eccentric morphology [4, 5]. Growing evidence confirmed a strong relationship between MCA atherosclerosis and the structural variance in the intracranial arterial system [6-8], which may gain some insights into the pathological process of MCA atherosclerotic plaques depending on the geometric characters of the cerebral vasculature.

Among the general populations, the COW is characterized by varying patterns of anatomical structure [9-11]. The geometric variability in the COW was found in robust relevance to the occurrence and progression of intracranial large-artery atherosclerotic stenosis [12, 13]. Interestingly, our previous study verified a higher prevalence of the incomplete COW subtypes among patients with MCA atherosclerotic plaques, which could influence the MCA plaque wall orientation [8]. Nonetheless, the clinical impact of the incomplete COW structures on the process of MCA atherosclerosis still remains unknown.

In the present study, we further explored the structural patterns of each incomplete COW geometry among patients with MCA atherosclerosis. With the utilization of HR-MRI, moreover, we differentiated quantitatively and qualitatively between the asymptomatic and symptomatic MCA atherosclerotic lesions. Importantly, this study was initiated to investigate

the potential effect of the anatomical patterns of the COW anomaly on the progression of symptomatic MCA atherosclerosis.

## 5.2 Methods

### 5.2.1 Study subjects

This study was based in a single medical institution, and recruited adult subjects consecutively between 2014 and 2020. Patients with MCA atherosclerotic plaques recognized by HR-MRI were included in this study, if they were clinically diagnosed with first-ever acute IS or TIA in seven days; not less than one intracranial large artery confirmed as atherosclerotic stenosis through the routine cerebral angiographic modality. Patients were excluded, when they had the following condition: no atherosclerotic plaque in the bilateral MCAs identified by HR-MRI; non-atherosclerotic stenosis (dissection, vasculitis, or moyamoya disease); cardio-embolism (atrial fibrillation or valvular heart diseases); coexisting over 50% stenosis of the ICA and/or the ECA; any history of brain tumor, vascular malformation, cerebral surgical/interventional procedure, or recurrent stroke; or contraindications to MRI. The patient clinical data at admission were registered (age, sex, hypertension, hyperlipidemia, diabetes mellitus, and present smoking status). The current study was approved by the institutional review board, following the Declaration of Helsinki. The written informed consents were signed by all the subjects or family members.

### 5.2.2 Imaging protocol

A 3.0-Tesla Achieva magnetic resonance system with a standardized eight-channel head coil (Philips Healthcare, Cleveland, OH, USA) was utilized to scan all the subjects. The imaging protocol contained a TOF MRA sequence and a transverse three-dimensional T1w VISTA sequence before and after administrating a contrast agent containing gadolinium (Dotarem, Gadoteric acid 0.5 mmol/mL, Guerbet, Roissy CdG Cedex, France) with 0.1

mL/kg to every subject. The TOF MRA sequence parameters were as follows: FOV 200*200*56$mm^3$, acquired resolution 0.4*0.6*0.7$mm^3$, TR/TE 23/3.5ms, and scan duration 3:07min. The imaging parameters for the T1w VISTA sequence included FOV 200*167*45$mm^3$, acquired resolution 0.6*0.6*1.0$mm^3$, reconstructed resolution 0.5*0.5*0.5 $mm^3$ with zero filling, TR 1500ms, TE 36ms, turbo-spin-echo + startup echoes 56+6, echo spacing 4.0ms, SENSE factor 1.5 with phase-encode direction, and scan duration 6:51min.

### 5.2.3 Imaging assessment

The source images with axial orientation and the three-dimensional reconstructed images were used to carry out the visual image quality evaluation, according to a three-point scale (1: poor, 2: adequate, and 3: excellent). The images graded as one point were excluded from this study.

Two examiners were blind to the patient clinical information, and independently evaluated the intra- and inter-observer agreement. Thirty patients were chosen at random. One examiner analyzed the images two times over a period of three months between the two measurements. Another examiner analyzed the images of the same thirty patients once.

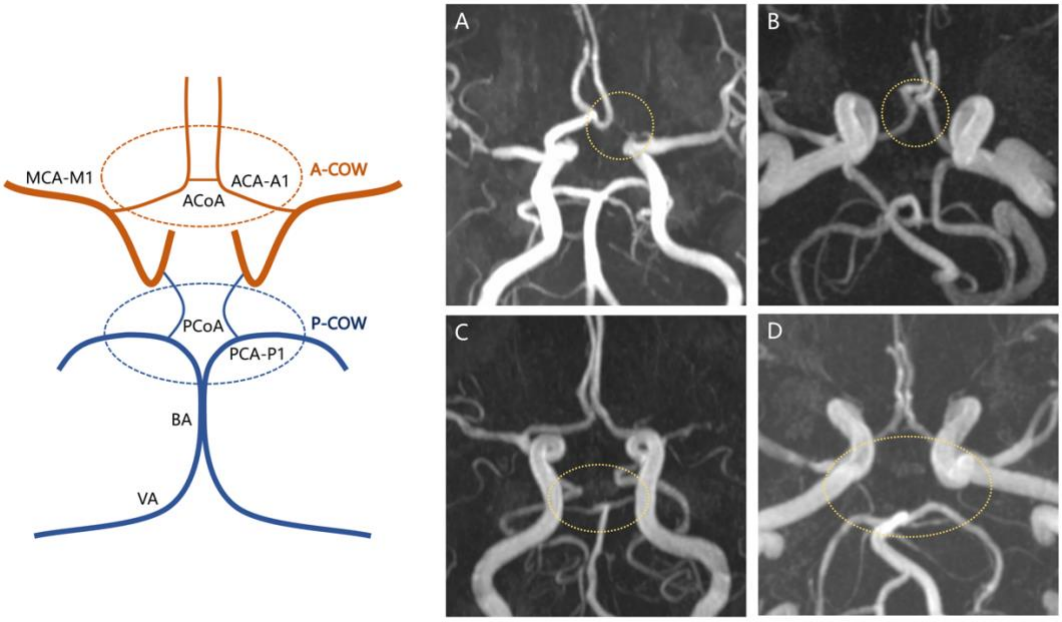


**Figure 5-1. A complete geometry of both A-COW and P-COW (Left) and four representative patterns of the incomplete COW subtypes on TOF MRA imaging (Right, A to D). A**, dysplasia or absence of the ACA as an incomplete A-COW pattern (yellow dashed outline). **B**, dysplasia or absence of the ACoA as an incomplete A-COW pattern (yellow dashed outline). **C**, dysplasia or absence of the PCA as an incomplete P-COW pattern (yellow dashed outline). **D**, dysplasia or absence of the PCoA as an incomplete P-COW pattern (yellow dashed outline). ACA, anterior cerebral artery; ACoA, anterior communicating artery; A-COW, anterior circle of Willis; BA, basilar artery; MCA, middle cerebral artery; PCA, posterior cerebral artery; PCoA, posterior communicating artery; P-COW, posterior circle of Willis; TOF MRA, Time-Of-Flight magnetic resonance angiography; VA, vertebral artery.

### 5.2.4 Determining the pattern of the incomplete COW geometry

The geometric patterns of the incomplete COW were discovered, based on the findings from TOF MRA imaging [8, 14]. The COW was split up into two anatomical sections: the A-COW and the P-COW (**Figure 5-1**). An incomplete pattern of the A-COW geometry was characterized as dysplasia or absence of any segment of the ACoA and the ACA-A1, while an incomplete pattern of the P-COW structure was featured as dysplasia or absence of any segment of the PCoA and the PCA-P1. A dysplastic or absent intracranial artery was defined as the threshold diameter less than 0.8mm displayed on TOF MRA imaging [8, 14]. The analysis of the incomplete COW patterns was independent of the quantitative and qualitative measurements of the MCA atherosclerotic plaques.

### 5.2.5 Quantitatively measuring the MCA atherosclerotic plaques

An atherosclerotic plaque was designated as focal thickening on the vessel wall along the bilateral segments of the MCA-M1 from both pre- and post-contrast T1w imaging (**Figure 5-2** and **Figure 5-3**), utilizing a definition reported previously [15]. VesselMass software (Leiden University Medical Center, the Netherlands) was used to measure the MCA atherosclerotic plaques quantitatively (luminal stenosis percentage, plaque burden degree, wall area index, remodeling index, and enhancement index) on the basis of the algorithms published by previous research [16-18].

The imaging cross-section of the MCA atherosclerotic lesion at the most narrowing lumen was used for measuring the area of the MCA plaque, and the reference site referred to the adjacent vascular segment (plaque-free, non-tortuous and normal) proximal or distal to the atherosclerotic lesion [16, 19]. The vessel area (VA) was determined by manually tracing the vessel-cerebrospinal fluid interface, and the lumen area (LA) was measured through the

blood-intima interface. Moreover, both maximal and minimal wall thicknesses were measured at the most stenotic luminal lesion. The formulas were as follows:

The wall area (WA) = VA – LA;

The degree of luminal stenosis = (1 – lesion LA / reference LA) × 100%;

The plaque burden percentage = (lesion WA / lesion VA) × 100%;

The wall area index = lesion WA / reference WA;

The remodeling index = lesion VA / reference VA (If the index was ≥ 1.05, the arterial remodeling was a positive pattern. Otherwise, the pattern of arterial remodeling was non-positive.).

Besides, the plaque signal intensity (SI) was measured on the matched pre- and post-contrast T1w imaging, after manually tracing both vascular lumen and outer wall boundary at the most narrowing lesion of MCA atherosclerosis [16]. The gray-matter SI was measured on the matched pre- and post-contrast T1w imaging as well via manually drawing a circle of 10 to 12 $mm^2$ at the normal tissue of gray matter next to the MCA atherosclerotic lesion [16]. The plaque contrast enhancement was quantified, using the following formula:

The enhancement index = [(plaque SI / gray-matter SI on post-contrast T1w imaging) – (plaque SI / gray-matter SI on pre-contrast T1w imaging)] / (plaque SI / gray-matter SI on pre-contrast T1w imaging) × 100%.


**Figure 5-2. A 68-year-old male patient with acute infarction in the left anterior circulation. A**, a symptomatic atherosclerotic stenosis of the left MCA-M1 on MRA imaging (white arrow). **B**, acute infarction in the left MCA-M1 territory on DWI (white arrow). **C** and **D**, an eccentric, focal plaque in the left MCA-M1 as a symptomatic atherosclerotic lesion before and after administrating contrast on T1w imaging, respectively (white arrows). DWI, diffusion-weighted imaging; MCA, middle cerebral artery; MRA, magnetic resonance angiography; T1w, T1-weighted.

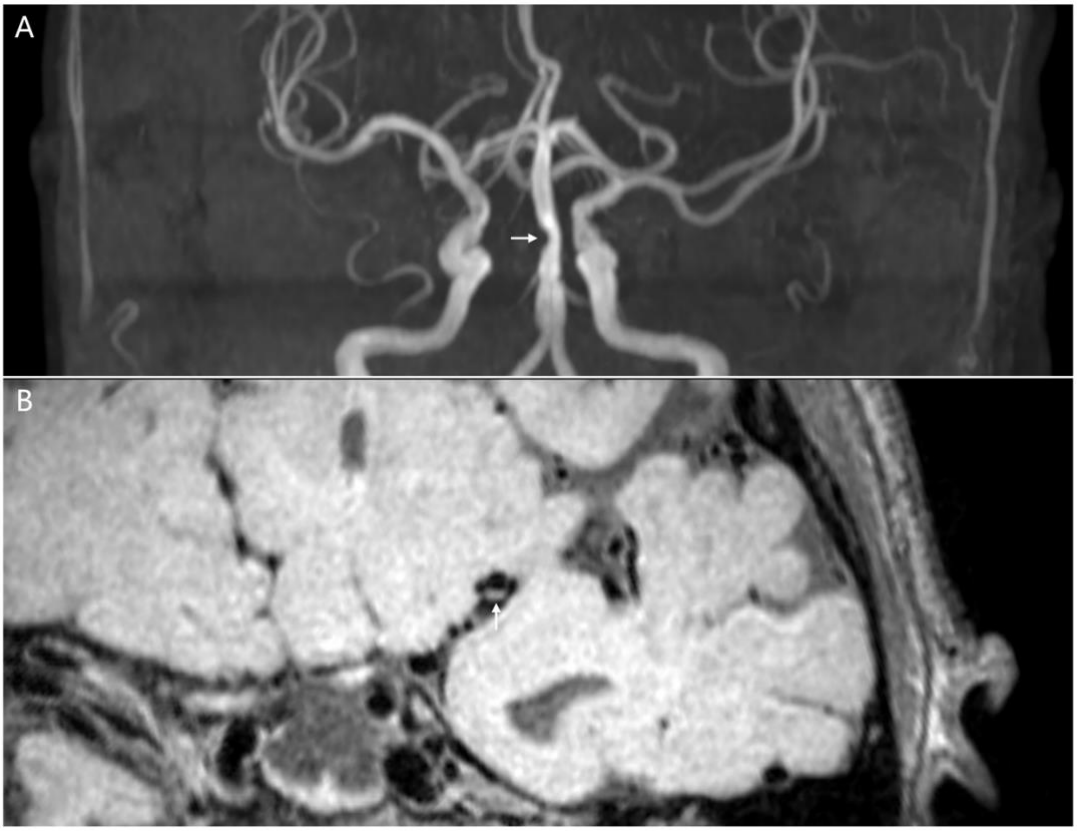


**Figure 5-3. A 72-year-old male patient with acute infarction in posterior circulation. A**, a symptomatic atherosclerotic stenosis of the BA on MRA imaging (white arrow). **B**, an eccentric, focal plaque in the right MCA-M1 as an asymptomatic atherosclerotic lesion on T1w imaging (white arrow). BA, basilar artery; MCA, middle cerebral artery; MRA, magnetic resonance angiography; T1w, T1-weighted.

### 5.2.6 Qualitatively measuring the MCA atherosclerotic plaques

The MCA atherosclerotic plaques were then assessed qualitatively (plaque hyperintensity signal, plaque hypointensity signal, IPH, and symptomatic status), according to the definitions reported by our prior research [16, 20].

The plaque SI was also classified as hyperintensity or hypointensity on the pre-contrast T1w imaging, compared to the normal gray-matter SI nearest to the MCA atherosclerotic lesion [20]. The occurrence of IPH was described as a high signal area within the plaque on the pre-contrast T1w imaging (more than 150% of the adjacent muscle SI) [16].

The MCA atherosclerotic plaque was designated as symptomatic or asymptomatic lesion on the basis of the clinical event of acute ischemia in the corresponding MCA territory directly caused by the plaque or not (acute cerebral infarction on DWI and/or acute symptom of neurological dysfunction) [16]. The MCA plaque was regarded as symptomatic lesion, when this plaque was the only or the most stenotic/enhanced in the ipsilateral MCA territory of acute infarct. The MCA plaque was considered as asymptomatic lesion, if this plaque was out of the MCA territory of acute infarction, or not the most stenotic/enhanced within the acute ischemic MCA territory.

### 5.2.7 Statistical analysis

SPSS version 26.0 (IBM, NY, USA) was used to analyze all statistical data. Categorical variables were expressed as percentages, while continuous variables were listed as means ± SD or medians (interquartile range, IQR). Chi-squared test, Fisher's exact test, or Mann-Whitney U test was utilized to compare the imaging features of the MCA atherosclerotic plaques between asymptomatic and symptomatic lesions. Chi-squared test or Fisher's exact test was used for determining the relationship between the patterns of the incomplete COW geometry and symptomatic MCA atherosclerosis. Univariate and multivariate logistic

regression analyses were carried out to further estimate the correlation of the incomplete COW structure with symptomatic MCA atherosclerosis. Two-tailed P value less than 0.05 was indicated as significant difference. Intraclass correlation or Cohen κ coefficient with 95% CIs was used to analyze intra- and inter-observer agreement. A coefficient more than 0.81 was known as excellence.

## 5.3 Results

### 5.3.1 Subject demographic and clinical characteristics on admission

This study included a total of one hundred and seven subjects with MCA atherosclerotic plaques. **Table 5-1** showed the baseline demographic and clinical features of all the subjects (mean age = 62.50 ± 11.69 years old; 62.6% were male). Among patients with MCA atherosclerosis, the occurrence of hypertension was the most prevalent (74.8%), followed by hyperlipidemia (57.9%), diabetes mellitus (32.7%), and present smoking status (26.2%). The incidence of TIA (13.1%) as an index stroke event was lower than that of IS (86.9%).

### 5.3.2 The anatomical patterns of the incomplete COW

**Table 5-1** also displayed the prevalence of each geometric pattern of the incomplete COW subtype among patients with MCA atherosclerosis. The incident rate of the ACA dysplasia or absence as an incomplete A-COW structure was observed to be 34.6%, and that of the ACoA dysplasia/absence was 29.9%. The incidence of the dysplastic or absent PCA as an incomplete P-COW structure was only 27.1%, whereas that of the dysplastic/absent PCoA was up to 80.4%.

**Table 5-1. Demographic and clinical characteristics of patients with MCA atherosclerosis.**

| Parameters | Subjects (n=107) |
|---|---|
| Age, years, mean ± SD | 62.50 ± 11.69 |
| Male/Female, n | 67/40 |
| Hypertension, n (%) | 80 (74.8%) |
| Hyperlipidemia, n (%) | 62 (57.9%) |
| Diabetes, n (%) | 35 (32.7%) |
| Smoking, n (%) | 28 (26.2%) |
| Index event | |
| Stroke, n (%) | 93 (86.9%) |
| TIA, n (%) | 14 (13.1%) |
| Incomplete A-COW | |
| ACA dysplasia/absence, n (%) | 37 (34.6%) |
| ACoA dysplasia/absence, n (%) | 32 (29.9%) |
| Incomplete P-COW | |
| PCA dysplasia/absence, n (%) | 29 (27.1%) |
| PCoA dysplasia/absence, n (%) | 86 (80.4%) |

ACA, anterior cerebral artery; ACoA, anterior communicating artery; A-COW, anterior circle of Willis; MCA, middle cerebral artery; PCA, posterior cerebral artery; PCoA, posterior communicating artery; P-COW, posterior circle of Willis; TIA, transient ischemic attack.

### 5.3.3 Comparison of the plaque imaging characters between asymptomatic and symptomatic MCA atherosclerotic lesions

In this study, one hundred and fifty-eight MCA atherosclerotic plaques were identified in total, of which ninety-six were asymptomatic and sixty-two were symptomatic. **Table 5-2** and **Figure 5-4** illustrated the differences of the quantitative and qualitative measurements of the atherosclerotic plaques between the asymptomatic and symptomatic MCA lesions, respectively.

As listed in **Table 5-2**, the symptomatic MCA atherosclerotic lesions possessed significantly smaller LA (1.50mm$^2$ [IQR, 0.83-2.46] versus 2.57mm$^2$ [IQR, 1.43-4.17], P <

0.001), but significantly larger maximal wall thickness (1.79mm [IQR, 1.23-2.14] versus 1.42mm [IQR, 1.16-1.71], P = 0.001) than the asymptomatic MCA atherosclerotic lesions. Besides, the symptomatic MCA atherosclerotic lesions had significantly higher degree of luminal stenosis (77.62% [IQR, 60.98-85.25] versus 60.51% [IQR, 37.94-75.45], P < 0.001), higher plaque burden percentage (85.70% [IQR, 78.02-92.19] versus 76.86% [IQR, 69.72-86.27], P < 0.001), and larger enhancement index value (32.23% [IQR, 17.83-46.82] versus 12.34% [IQR, 3.88-31.72], P < 0.001), compared to the asymptomatic MCA atherosclerotic lesions. However, the wall area index and the remodeling index in MCA atherosclerosis were not significantly different between the two groups (both P values > 0.05).

**Table 5-2. Quantitative plaque imaging features of MCA atherosclerosis between asymptomatic and symptomatic lesions.**

| Characters | Asymptomatic MCA lesions (n=96) | Symptomatic MCA lesions (n=62) | P value |
|---|---|---|---|
| **At the maximal narrowing lumen site** | | | |
| Lumen area, $mm^2$, median (IQR) | 2.57 (1.43-4.17) | 1.50 (0.83-2.46) | **0.000** |
| Vessel area, $mm^2$, median (IQR) | 11.80 (8.80-15.16) | 10.59 (7.92-13.52) | 0.126 |
| Wall area, $mm^2$, median (IQR) | 9.23 (7.18-11.40) | 9.36 (6.50-11.47) | 0.912 |
| Maximum wall thickness, mm, median (IQR) | 1.42 (1.16-1.71) | 1.79 (1.23-2.14) | **0.001** |
| Minimum wall thickness, mm, median (IQR) | 0.67 (0.44-0.84) | 0.60 (0.36-0.80) | 0.188 |
| Stenosis percentage, %, median (IQR) | 60.51 (37.94-75.45) | 77.62 (60.98-85.25) | **0.000** |
| Plaque burden, %, median (IQR) | 76.86 (69.72-86.27) | 85.70 (78.02-92.19) | **0.000** |
| Wall area index, median (IQR) | 18.92 (5.05-43.15) | 11.13 (3.17-37.91) | 0.168 |
| Remodeling index, median (IQR) | 1.34 (0.97-1.93) | 1.12 (0.87-1.79) | 0.146 |
| Enhancement index, %, median (IQR) | 12.34 (3.88-31.72) | 32.23 (17.83-46.82) | **0.000** |
| **At the reference site** | | | |
| Lumen area, $mm^2$, median (IQR) | 6.75 (4.82-9.74) | 6.42 (4.76-7.72) | 0.214 |
| Vessel area, $mm^2$, median (IQR) | 9.12 (6.38-12.29) | 8.39 (6.18-12.67) | 0.950 |

MCA, middle cerebral artery; IQR, interquartile range.

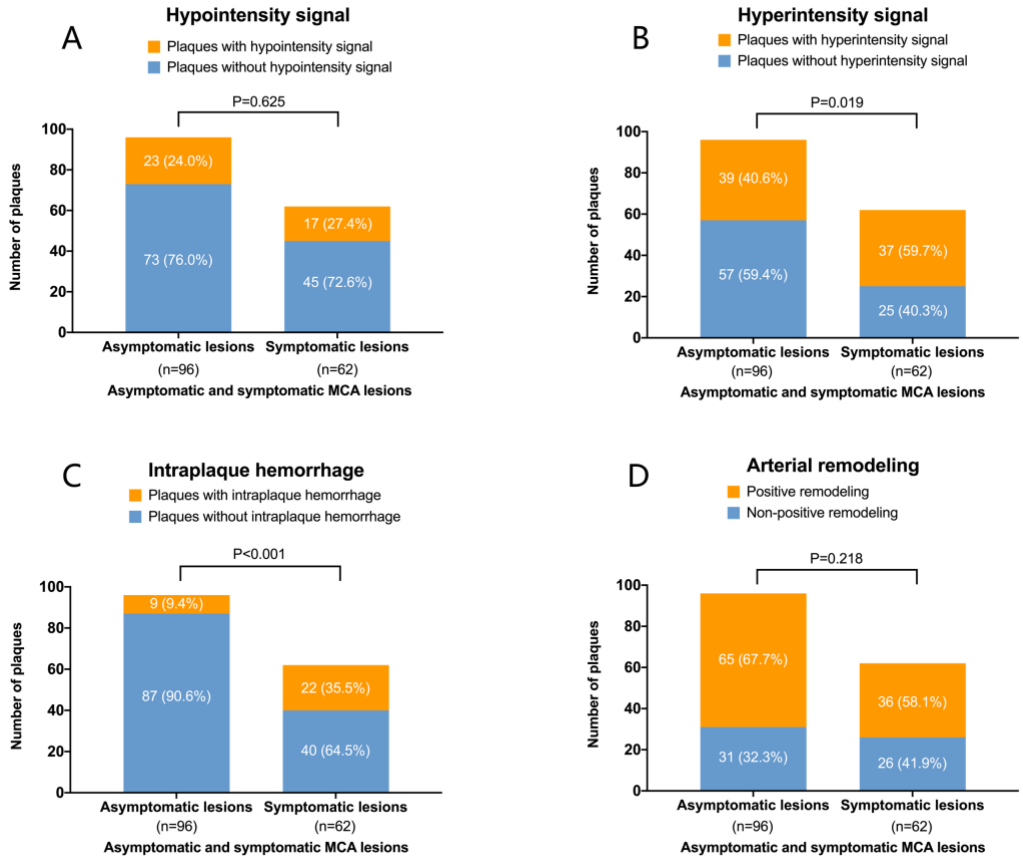


**Figure 5-4. Other MCA plaque imaging features are compared between asymptomatic and symptomatic atherosclerotic lesions. A**, plaque hypointensity signal. **B**, plaque hyperintensity signal. **C**, intraplaque hemorrhage. **D**, arterial remodeling pattern. MCA, middle cerebral artery.

As exhibited in **Figure 5-4**, the MCA atherosclerotic plaques with hyperintensity signal (59.7% versus 40.6%, P = 0.019) and IPH (35.5% versus 9.4%, P < 0.001) were more frequently found in the symptomatic lesions, instead of the asymptomatic lesions. Nevertheless, no significant differences of the plaque hypointensity signal and the arterial remodeling pattern in the atherosclerotic MCAs were observed between the asymptomatic and symptomatic lesions (both P values > 0.05).

### 5.3.4 Relationship between the incomplete COW patterns and symptomatic MCA atherosclerosis

Our understanding of the progression of symptomatic MCA atherosclerosis depending upon the four anatomical patterns of the incomplete COW subtypes was advanced in **Table 5-3** and **Table 5-4**.

As shown in **Table 5-3**, the dysplasia or absence of the ACoA as an incomplete A-COW pattern was significantly associated with the symptomatic MCA atherosclerotic lesions, rather than the asymptomatic MCA lesions (43.5% versus 19.8%, P = 0.001). Yet, we did not observe any significant association between the dysplastic/absent ACA and the symptomatic MCA atherosclerotic lesions (P value > 0.05). Similarly, the dysplasia/absence of the PCA or the PCoA as an incomplete P-COW pattern was not found to be correlated with symptomatic MCA atherosclerosis as well (both P values > 0.05).

**Table 5-3. Association of the COW anomalies with the symptomatic status of MCA atherosclerosis.**

| COW anomaly | Asymptomatic MCA lesions (n=96) | Symptomatic MCA lesions (n=62) | P value |
|---|---|---|---|
| A-COW | | | 0.221 |
| Complete, n (%) | 59 (61.5%) | 32 (51.6%) | |
| Incomplete, n (%) | 37 (38.5%) | 30 (48.4%) | |
| ACA | | | 0.830 |
| Normal, n (%) | 62 (64.6%) | 39 (62.9%) | |
| Dysplastic/absent, n (%) | 34 (35.4%) | 23 (37.1%) | |
| ACoA | | | **0.001** |
| Normal, n (%) | 77 (80.2%) | 35 (56.5%) | |
| Dysplastic/absent, n (%) | 19 (19.8%) | 27 (43.5%) | |
| P-COW | | | 0.792 |
| Complete, n (%) | 14 (14.6%) | 10 (16.1%) | |
| Incomplete, n (%) | 82 (85.4%) | 52 (83.9%) | |
| PCA | | | 0.312 |
| Normal, n (%) | 69 (71.9%) | 49 (79.0%) | |
| Dysplastic/absent, n (%) | 27 (28.1%) | 13 (21.0%) | |
| PCoA | | | 0.925 |
| Normal, n (%) | 18 (18.8%) | 12 (19.4%) | |
| Dysplastic/absent, n (%) | 78 (81.3%) | 50 (80.6%) | |

ACA, anterior cerebral artery; ACoA, anterior communicating artery; A-COW, anterior circle of Willis; COW, circle of Willis; MCA, middle cerebral artery; PCA, posterior cerebral artery; PCoA, posterior communicating artery; P-COW, posterior circle of Willis

As suggested in **Table 5-4**, the ACoA dysplasia or absence was strongly related to the symptomatic MCA atherosclerotic lesions in the univariate logistic regression model (odds ratio, 3.126, [95%CI, 1.537-6.359]; P = 0.002). Moreover, the dysplastic or absent ACoA was also independently associated with symptomatic MCA atherosclerosis in the multivariate logistic regression model (odds ratio, 3.132, [95%CI, 1.412-6.946]; P = 0.005) controlling the potential confounders, including dysplastic/absent ACA, dysplastic/absent PCA, dysplastic/absent PCoA, IPH, luminal stenosis percentage, and plaque enhancement index.

**Table 5-4. Regression models for independent association of the ACoA dysplasia/absence with symptomatic MCA atherosclerosis.**

| | Univariate regression | | Multivariate regression [#] | |
|---|---|---|---|---|
| | **OR 95% CI** | **P value** | **OR 95% CI** | **P value** |
| Normal ACoA | 1 (ref.) | | 1 (ref.) | |
| Dysplastic/absent ACoA | 3.126 (1.537-6.359) | 0.002 | 3.132 (1.412-6.946) | 0.005 |

ACA, anterior cerebral artery; ACoA, anterior communicating artery; CI, confidential interval; MCA, middle cerebral artery; OR, odds ratio; PCA, posterior cerebral artery; PCoA, posterior communicating artery.

[#], adjusted for dysplastic/absent ACA, dysplastic/absent PCA, dysplastic/absent PCoA, intraplaque hemorrhage, luminal stenosis percentage, and plaque enhancement index.

### 5.3.5 Reliability of measurement

The intra-observer reliability was excellent for determining the patterns of the COW structure (coefficient = 0.939, 95% CI 0.931-0.947). The inter-observer reliability was excellent as well for analyzing the patterns of the COW geometry (coefficient = 0.909, 95% CI 0.901-0.917). The intra- and inter-observer reliability were substantial to excellent for evaluating the plaque imaging characters quantitatively and qualitatively, which was previously published by our HR-MRI research [20, 21].

## 5.4 Discussion

In our hospital-based study, firstly, we described the geometric pattern of each incomplete COW subtype in patients with MCA atherosclerosis, among which the PCoA dysplasia or absence was the most prevalent, followed by the dysplasia/absence of the ACA, the ACoA, and the PCA. With the help of HR-MRI, secondly, we distinguished the fundamental imaging features of the MCA atherosclerotic plaques between asymptomatic and symptomatic lesions.

Apparently, the symptomatic MCA atherosclerotic lesions were robustly associated with a worse vessel wall state. Thirdly, as a representative anatomical pattern of an incomplete A-COW subtype, the dysplastic or absent ACoA was revealed in independent correlation with symptomatic MCA atherosclerosis, after adjusted for the possible confounding factors.

TOF MRA imaging reliably disclosed the detailed patterns of the COW anomaly among patients with MCA atherosclerotic plaques. In this study, we found that the dysplastic/absent PCoA was the most common variation in the incomplete COW geometry, while the dysplastic/absent PCA was the least. This observation showed consistency with other earlier results from the autopsy and MRA imaging [9, 13, 22]. We also revealed a high prevalence of the dysplasia/absence of the ACA and the ACoA as the typical patterns of the incomplete A-COW geometry, which accorded with previous studies [10, 23]. It was obvious that each rate of the incomplete COW patterns might be fluctuating among various study populations in virtue of the differences of the ethnics and the available technical modalities [24-26].

Accumulative evidence from HR-MRI studies point to a striking difference in the quantitative and qualitative imaging characteristics of MCA atherosclerosis between asymptomatic and symptomatic lesions [27-29]. Our findings also affirmed that symptomatic MCA atherosclerosis was in a poorer vessel wall condition. Firstly, a significant increase in severity of the MCA stenotic lumen was detected in the symptomatic atherosclerotic lesions, such as larger maximum wall width, severer narrowing lumen, and heavier plaque burden. Both values of luminal stenosis and plaque burden were highlighted due to the clinical importance of risk stratification for symptomatic MCA atherosclerotic disease and recurrent stroke [27, 30, 31]. Secondly, a larger plaque enhancement index featured prominently in symptomatic MCA atherosclerosis. This imaging index might serve as a reliable marker that was highly suggestive of acute cerebral infarcts within the ipsilateral vascular territory [32-34]. Interestingly, our previous MRI study further indicated that the MCA plaque contrast

enhancement was even gradually decreased in the time course of MCA atherosclerosis [16]. Thirdly, both IPH and plaque hyperintensity signal on pre-contrast T1w imaging existed more commonly in symptomatic MCA atherosclerosis. Of note, as a crucial imaging indicator of unstable plaques, IPH might independently predict the increasing risks of plaque rupture and subsequent ischemic events [35, 36].

The aim of a focus for discriminating the symptomatic MCA atherosclerotic lesions from the asymptomatic lesions was to offer an overview of the MCA plaque imaging features. The underlying influence of the COW anomaly patterns on symptomatic MCA atherosclerosis was then investigated. Among the four patterns of the incomplete COW geometry, in our study, the ACoA dysplasia or absence was robustly related to the occurrence of the symptomatic MCA atherosclerotic lesions. More importantly, an independent association of the ACoA dysplasia/absence with an ascending risk of developing symptomatic MCA atherosclerosis was ascertained, after adjustment for the potential confounders.

Our results lent plausibility to the hypothesis that the COW anomaly, particularly the dysplasia/absence of the ACoA, might alter the MCA hemodynamics and thus accelerate the development of symptomatic MCA atherosclerosis [37-39]. Causes could be provided: Firstly, the CBF pattern in the MCA might be changed to a great extent without the ACoA collateral supply owing to the ACoA dysplasia/absence [38, 39]. Secondly, the low WSS level spatially acting on the vessel walls might be mostly induced by the local alteration in the MCA hemodynamic force [40, 41]. This process might directly worsen the MCA wall condition through endothelial inflammation and dysfunction, thereby leading to the growth of unstable atherosclerotic plaques [42, 43]. Briefly, the ACoA dysplasia/absence might increase the risk of occurring symptomatic MCA atherosclerotic lesions, largely via affecting the local hemodynamic condition in the MCA. Our speculation could provide new insight into future studies.

We should take some limitations into consideration. Firstly, our sample size was relatively small, and was from a single stroke center. Therefore, our findings should be applied with caution to other study populations. Secondly, we could not include other unnoticed and remaining confounding factors in the regression model.

## 5.5 Conclusion

The structural anomaly of the COW was prevalent among patients with MCA atherosclerotic plaques, including the dysplasia or absence of the PCoA, the ACA, the ACoA, and the PCA. The ACoA dysplasia or absence was independently correlated with the symptomatic MCA atherosclerotic lesions. These findings could further our knowledge of the pathogenesis of MCA atherosclerosis depending on the anatomical feature of the COW anomaly.

## References


1. Battistella V, Elkind M. Intracranial atherosclerotic disease. *Eur J Neurol*. 2014;21:956-962
2. Al Kasab S, Derdeyn CP, Guerrero WR, Limaye K, Shaban A, Adams HP, Jr. Intracranial large and medium artery atherosclerotic disease and stroke. *J Stroke Cerebrovasc Dis*. 2018;27:1723-1732
3. Huang H, Zheng H, Zhang D, Yu N, Hu J, Xie M, et al. Ethnic differences in characteristics and outcome of acute ischemic stroke in china: A single center experience. *J Clin Neurosci*. 2020;79:113-117
4. Banerjee C, Chimowitz MI. Stroke caused by atherosclerosis of the major intracranial arteries. *Circ Res*. 2017;120:502-513
5. Yang WJ, Fisher M, Zheng L, Niu CB, Paganini-Hill A, Zhao HL, et al. Histological characteristics of intracranial atherosclerosis in a chinese population: A postmortem study. *Front Neurol*. 2017;8:488
6. Kim BJ, Yoon Y, Lee DH, Kang DW, Kwon SU, Kim JS. The shape of middle cerebral artery and plaque location: High-resolution mri finding. *Int J Stroke*. 2015;10:856-860
7. Yu YN, Li ML, Xu YY, Meng Y, Trieu H, Villablanca JP, et al. Middle cerebral artery geometric features are associated with plaque distribution and stroke. *Neurology*. 2018;91:e1760-e1769
8. Li J, Zheng L, Yang WJ, Sze-To CY, Leung TW, Chen XY. Plaque wall distribution pattern of the atherosclerotic middle cerebral artery associates with the circle of willis completeness. *Front Neurol*. 2020;11:599459

9. Jones JD, Castanho P, Bazira P, Sanders K. Anatomical variations of the circle of willis and their prevalence, with a focus on the posterior communicating artery: A literature review and meta-analysis. *Clin Anat*. 2020

10. Shatri J, Cerkezi S, Ademi V, Reci V, Bexheti S. Anatomical variations and dimensions of arteries in the anterior part of the circle of willis. *Folia Morphol (Warsz)*. 2019;78:259-266

11. Cui Y, Xu T, Chen J, Tian H, Cao H. Anatomic variations in the anterior circulation of the circle of willis in cadaveric human brains. *Int J Clin Exp Med*. 2015;8:15005-15010

12. Kim KM, Kang HS, Lee WJ, Cho YD, Kim JE, Han MH. Clinical significance of the circle of willis in intracranial atherosclerotic stenosis. *J Neurointerv Surg*. 2016;8:251-255

13. Pascalau R, Padurean VA, Bartos D, Bartos A, Szabo BA. The geometry of the circle of willis anatomical variants as a potential cerebrovascular risk factor. *Turk Neurosurg*. 2019;29:151-158

14. Zhou C, Yuan C, Li R, Wang W, Li C, Zhao X, et al. Association between incomplete circle of willis and carotid vulnerable atherosclerotic plaques. *Arterioscler Thromb Vasc Biol*. 2018;38:2744-2749

15. Qiao Y, Zeiler SR, Mirbagheri S, Leigh R, Urrutia V, Wityk R, et al. Intracranial plaque enhancement in patients with cerebrovascular events on high-spatial-resolution mr images. *Radiology*. 2014;271:534-542

16. Yang WJ, Abrigo J, Soo YO, Wong S, Wong KS, Leung TW, et al. Regression of plaque enhancement within symptomatic middle cerebral artery atherosclerosis: A high-resolution mri study. *Front Neurol*. 2020;11:755

17. Wang M, Wu F, Yang Y, Miao H, Fan Z, Ji X, et al. Quantitative assessment of symptomatic intracranial atherosclerosis and lenticulostriate arteries in recent stroke patients using whole-brain high-resolution cardiovascular magnetic resonance imaging. *J Cardiovasc Magn Reson*. 2018;20:35

18. Guo R, Zhang X, Zhu X, Liu Z, Xie S. Morphologic characteristics of severe basilar artery atherosclerotic stenosis on 3d high-resolution mri. *BMC Neurol*. 2018;18:206

19. Samuels OB, Joseph GJ, Lynn MJ, Smith HA, Chimowitz MI. A standardized method for measuring intracranial arterial stenosis. *AJNR Am J Neuroradiol*. 2000;21:643-646

20. Yang WJ, Chen XY, Zhao HL, Niu CB, Zhang B, Xu Y, et al. Postmortem study of validation of low signal on fat-suppressed t1-weighted magnetic resonance imaging as marker of lipid core in middle cerebral artery atherosclerosis. *Stroke*. 2016;47:2299-2304

21. Dieleman N, Yang W, Abrigo JM, Chu WC, van der Kolk AG, Siero JC, et al. Magnetic resonance imaging of plaque morphology, burden, and distribution in patients with symptomatic middle cerebral artery stenosis. *Stroke*. 2016;47:1797-1802

22. Klimek-Piotrowska W, Rybicka M, Wojnarska A, Wojtowicz A, Koziej M, Holda MK. A multitude of variations in the configuration of the circle of willis: An autopsy study. *Anat Sci Int*. 2016;91:325-333

23. Zaki SM, Shaaban MH, Abd Al Galeel WA, El Husseiny AAW. Configuration of the circle of willis and its two parts among egyptian: A magnetic resonance angiographic study. *Folia Morphol (Warsz)*. 2019;78:703-709

24. Hindenes LB, Haberg AK, Johnsen LH, Mathiesen EB, Robben D, Vangberg TR. Variations in the circle of willis in a large population sample using 3d tof angiography: The tromso study. *PLoS One*. 2020;15:e0241373

25. Klimek-Piotrowska W, Kopec M, Kochana M, Krzyzewski RM, Tomaszewski KA, Brzegowy P, et al. Configurations of the circle of willis: A computed tomography angiography based study on a polish population. *Folia Morphol (Warsz)*. 2013;72:293-299

26. Krabbe-Hartkamp MJ, van der Grond J, de Leeuw FE, de Groot JC, Algra A, Hillen B, et al. Circle of willis: Morphologic variation on three-dimensional time-of-flight mr angiograms. *Radiology*. 1998;207:103-111

27. Lin GH, Song JX, Fu NX, Huang X, Lu HX. Quantitative and qualitative analysis of atherosclerotic stenosis in the middle cerebral artery using high-resolution magnetic resonance imaging. *Can Assoc Radiol J*. 2020:846537120961312

28. Meng Y, Li M, Yu Y, Xu Y, Gao S, Feng F, et al. Quantitative score of the vessel morphology in middle cerebral artery atherosclerosis. *J Neurol Sci*. 2019;399:111-117

29. Zhao DL, Deng G, Xie B, Ju S, Yang M, Chen XH, et al. High-resolution mri of the vessel wall in patients with symptomatic atherosclerotic stenosis of the middle cerebral artery. *J Clin Neurosci*. 2015;22:700-704

30. Ran Y, Wang Y, Zhu M, Wu X, Malhotra A, Lei X, et al. Higher plaque burden of middle cerebral artery is associated with recurrent ischemic stroke: A quantitative magnetic resonance imaging study. *Stroke*. 2020;51:659-662

31. Cao Y, Sun Y, Zhou B, Zhao H, Zhu Y, Xu J, et al. Atherosclerotic plaque burden of middle cerebral artery and extracranial carotid artery characterized by mri in patients with acute ischemic stroke in china: Association and clinical relevance. *Neurol Res*. 2017;39:344-350

32. Gupta A, Baradaran H, Al-Dasuqi K, Knight-Greenfield A, Giambrone AE, Delgado D, et al. Gadolinium enhancement in intracranial atherosclerotic plaque and ischemic stroke: A systematic review and meta-analysis. *J Am Heart Assoc*. 2016;5

33. Lu SS, Ge S, Su CQ, Xie J, Mao J, Shi HB, et al. Mri of plaque characteristics and relationship with downstream perfusion and cerebral infarction in patients with symptomatic middle cerebral artery stenosis. *J Magn Reson Imaging*. 2018;48:66-73

34. Skarpathiotakis M, Mandell DM, Swartz RH, Tomlinson G, Mikulis DJ. Intracranial atherosclerotic plaque enhancement in patients with ischemic stroke. *AJNR Am J Neuroradiol*. 2013;34:299-304

35. Song JW, Wasserman BA. Vessel wall mr imaging of intracranial atherosclerosis. *Cardiovasc Diagn Ther*. 2020;10:982-993

36. Wu F, Yu H, Yang Q. Imaging of intracranial atherosclerotic plaques using 3.0 t and 7.0 t magnetic resonance imaging-current trends and future perspectives. *Cardiovasc Diagn Ther*. 2020;10:994-1004

37. Hillen B. The variability of the circle of willis: Univariate and bivariate analysis. *Acta Morphol Neerl Scand*. 1986;24:87-101

38. Wu HM, Chuang YM. The clinical relevance of fetal variant of the circle of willis and its influence on the cerebral collateral circulation. *Acta Neurol Taiwan*. 2011;20:232-242

39. Wei W, Yi X, Ruan J, Duan X, Luo H, Lv Z. Influence of collateral circulation on cerebral blood flow and frontal lobe cognitive function in patients with severe internal carotid artery stenosis. *BMC Neurol*. 2019;19:151

40. Alnaes MS, Isaksen J, Mardal KA, Romner B, Morgan MK, Ingebrigtsen T. Computation of hemodynamics in the circle of willis. *Stroke*. 2007;38:2500-2505

41. Chen Z, Qin H, Liu J, Wu B, Cheng Z, Jiang Y, et al. Characteristics of wall shear stress and pressure of intracranial atherosclerosis analyzed by a computational fluid dynamics model: A pilot study. *Front Neurol*. 2019;10:1372

42. Costopoulos C, Timmins LH, Huang Y, Hung OY, Molony DS, Brown AJ, et al. Impact of combined plaque structural stress and wall shear stress on coronary plaque progression, regression, and changes in composition. *Eur Heart J*. 2019;40:1411-1422

43. Chistiakov DA, Orekhov AN, Bobryshev YV. Effects of shear stress on endothelial cells: Go with the flow. *Acta Physiol (Oxf)*. 2017;219:382-408

# PART THREE

# Chapter 6. Relationship between the vertebrobasilar junction angle over 90° and the pattern of plaque wall distribution in vertebrobasilar artery atherosclerosis

## 6.1 Background

Intracranial large artery atherosclerosis is a major causative factor in acute ischemic stroke (AIS), and still imposes huge medical and economic burdens on the whole world [1-3]. The brain tissue fed by the vertebrobasilar circulation is implicated in over 20% of all cerebral infarctions, which is even at high risk of stroke recurrence and mortality [4-6].

The anatomical variation is commonly found in the vertebrobasilar circulation, and may play an important role in the process of vertebrobasilar artery atherosclerotic plaques, especially affecting the plaque location on the vessel walls [7-9]. Previous studies reported the wide-ranging degrees of the confluence angles of the vertebrobasilar junction in the human brain samples [10, 11]. Interestingly, the experimental and numerical findings then suggested that the development of vertebrobasilar artery atherosclerosis might be largely influenced by the structure of the VBJ angle [10-12]. As yet little evidence could be further corroborated from patients with AIS to indicate the relationship between the VBJ angle magnitude and the vertebrobasilar plaque wall location.

HR-MRI takes a detailed approach to a pathological description of the vessel wall changes to the intracranial large arteries [13]. Notably, determining the vessel wall locations of the intracranial atherosclerotic plaques via HR-MRI not only helps to illuminate the underlying stroke mechanisms, but also has clinical potentiality to guide therapeutic strategy [14, 15]. In this study, we aimed to investigate the morphological feature of the vertebrobasilar plaque wall

distribution depending upon the VBJ angle over 90° among AIS patients with vertebrobasilar artery atherosclerosis.

## 6.2 Methods

### 6.2.1 Study subjects

In this prospective database from a single stroke center, adult subjects were consecutively recruited between 2014 and 2020. The subject inclusion criteria included 1) first-ever AIS or TIA in a week; 2) at least one intracranial large artery identified as atherosclerotic stenosis by MRA or DSA; 3) atherosclerotic plaques in the vertebrobasilar arteries detected by HR-MRI; 4) the existence of the bilateral VAs and the BA shown on MRA. The subject exclusion criteria were as follows: 1) no atherosclerotic plaque in the vertebrobasilar arteries detected by HR-MRI; 2) absence of the VAs or the BA shown on MRA; 3) non-atherosclerotic stenosis, such as vasculitis, dissection, and moyamoya disease; 4) clinical evidence of cardio-embolism (atrial fibrillation or valvular heart disease); 5) coexisting more than 50% stenosis of the ICA and/or the ECA; 6) history of known brain tumor, vascular malformation, cerebral surgical/interventional procedure or recurrent stroke; 7) contraindications to MRI; 8) incomplete imaging scan of the intracranial segments of the bilateral VAs. The patient clinical information on admission were recorded during hospitalization, including age, sex, hypertension, hyperlipidemia, diabetes and smoking status. The institutional review board approved this study, which followed the Declaration of Helsinki. The written informed consent was signed by each subject.

### 6.2.2 Imaging protocol

A 3.0-Tesla Achieva magnetic resonance system with a standardized eight-channel head coil (Philips Healthcare, Cleveland, OH, USA) was utilized to scan all the subjects. The imaging protocol included a TOF MRA sequence and a transverse three-dimensional T1w

VISTA sequence before and after administrating a contrast agent containing gadolinium (Dotarem, Gadoteric acid 0.5 mmol/mL, Guerbet, Roissy CdG Cedex, France) with 0.1 mL/kg to every subject. The TOF MRA sequence parameters included FOV 200*200*56$mm^3$, acquired resolution 0.4*0.6*0.7$mm^3$, TR/TE 23/3.5ms, and scan duration 3:07min. The imaging parameters for the T1w VISTA sequence were as follows: FOV 200*167*45$mm^3$, acquired resolution 0.6*0.6*1.0$mm^3$, reconstructed resolution 0.5*0.5*0.5 $mm^3$ with zero filling, TR 1500ms, TE 36ms, turbo-spin-echo + startup echoes 56+6, echo spacing 4.0ms, SENSE factor 1.5 with phase-encode direction, and scan duration 6:51min.

### 6.2.3 Imaging assessment

The source images with axial orientation and the three-dimensional reconstructed images were used for conducting visual image quality evaluation, according to a three-point scale (3 = excellent, 2 = adequate, and 1 = poor). The images graded as one point were excluded in the following imaging analyses.

Two independent examiners were blind to the patient clinical information, and evaluated the intra- and inter-observer agreement. Thirty patients were randomly chosen. One examiner analyzed the images twice over a three-month period between the two imaging analyses. Another examiner analyzed the images of the same thirty patients once.

### 6.2.4 The degree of the VBJ angle

The three-dimensional reconstructed cross-sections from TOF MRA imaging were oriented towards the best visualization to determine the degree of the VBJ angle, through utilizing OsiriX DICOM Viewer (Geneva, Switzerland) (**Figure 6-1**). The confluence angle of the VBJ was described as the space where the two inner walls of the bilateral VAs joined [11]. The measurement of the VBJ angle was independent of the imaging analysis of the plaque wall distribution in the atherosclerotic vertebrobasilar arteries.

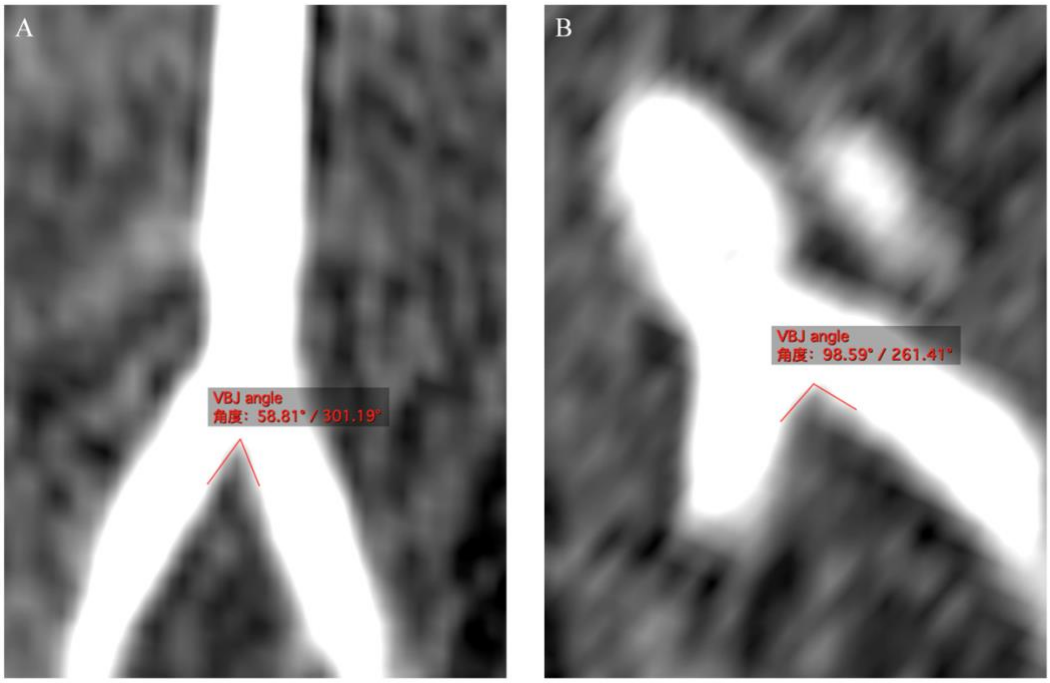


**Figure 6-1. Measuring the degrees of the VBJ confluence angles on the three-dimensional reconstructed cross-sections from TOF MRA imaging. A**, the VBJ angle is classified into the group with the angles less than 90°. **B**, the VBJ angle is classified into the group with the angles more than 90°. TOF MRA, Time-Of-Flight magnetic resonance angiography; VBJ, vertebrobasilar junction.

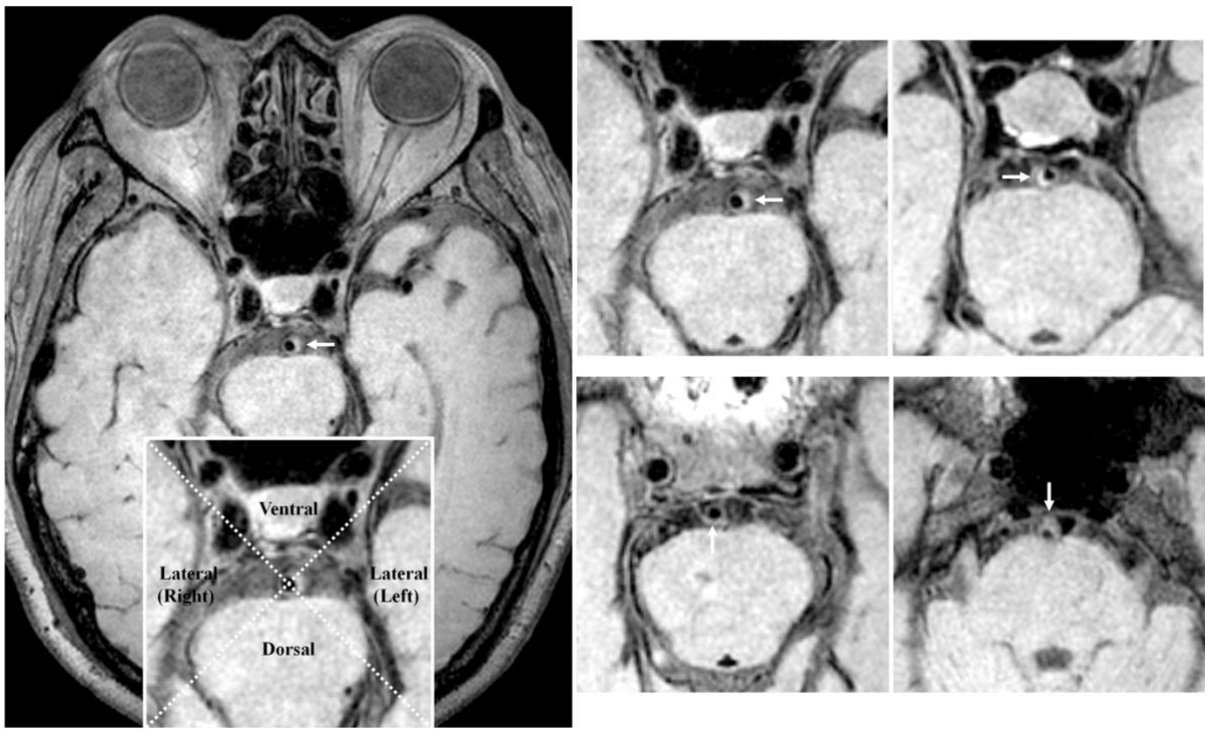


**Figure 6-2. The pattern of the plaque wall distribution in the atherosclerotic BAs is shown on high-resolution vessel wall MRI.** The BA atherosclerotic plaque is highlighted in an individual cross-sectional image (white arrow). The BA lumen is centrally intersected by the two dashed lines. Every cross-sectional image of the plaque is divided into four vascular quadrants: ventral, dorsal, right, and left. The plaque in this cross-sectional image may be located on one of the four vascular sides. BA, basilar artery; MRI, magnetic resonance imaging.

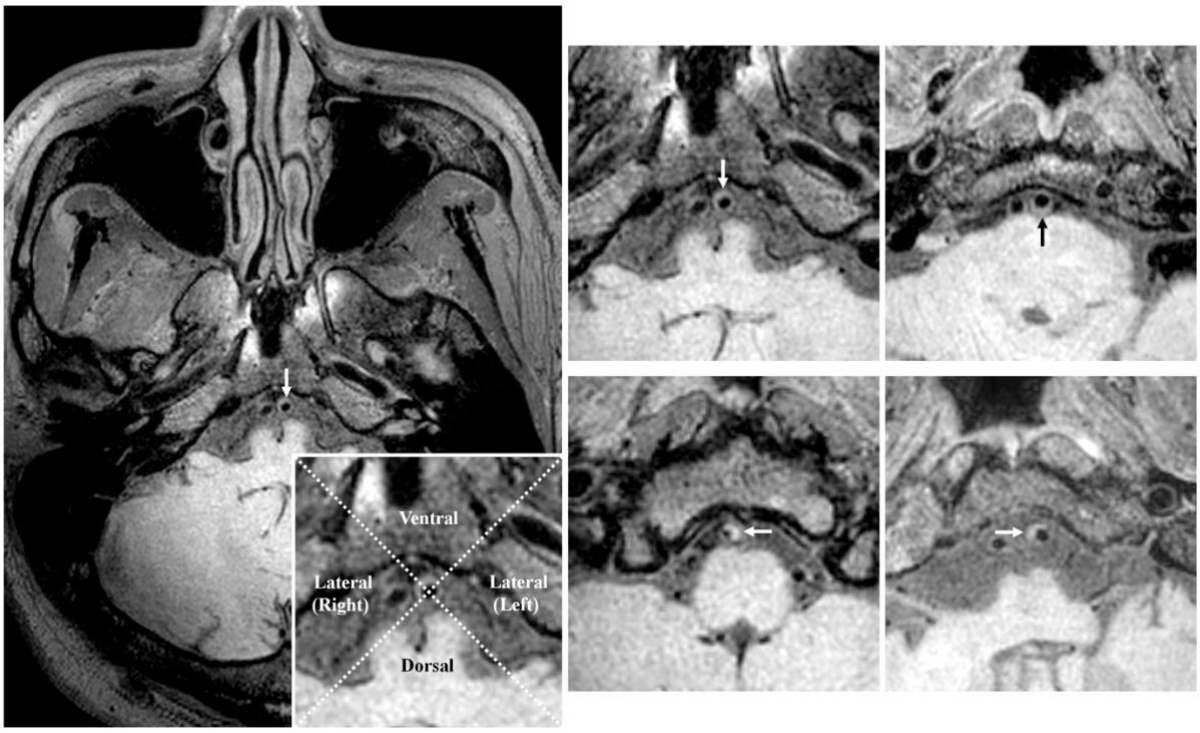


**Figure 6-3. The examples of the VA plaques distributed on the ventral, dorsal, left, and right walls, respectively.** Every cross-section of the VA plaque is separated into the four quadrants by two dashed lines intersecting at the luminal center (T1-weighted imaging). VA, vertebral artery.

### 6.2.5 The pattern of plaque wall distribution in vertebrobasilar artery atherosclerosis

The atherosclerotic plaque was visually detected along the intracranial segments of the bilateral VAs and the BA on the three-dimensional reconstructed T1w imaging, if identified as focal thickening on the vessel walls [16]. All the cross-sectional images of the vertebrobasilar plaque were categorized according to the plaque locations being centrally distributed on the different vascular sides: dorsal, ventral, and lateral (right or left) (**Figure 6-2** and **Figure 6-3**). Every cross-sectional image of the plaque was sorted into one of the four quadrants. Considering that the vertebrobasilar plaque might cover two or more quadrants, the quadrant at the thickest point of the vessel wall was used in the current study.

### 6.2.6 Statistical analysis

SPSS version 26.0 (IBM, NY, USA) was utilized to analyze the statistical data. Qualitative variables were summarized as percentages, while quantitative variables were shown as means ± SD. Chi-squared test or Fisher's exact test was used for comparing the VBJ angles above 90° between patients with and without vertebrobasilar atherosclerosis. The individual percentage of the plaque wall orientation was calculated for each vertebrobasilar plaque [16]. The mean percentages of the plaque locations on the dorsal, ventral, and lateral walls were then produced in the group of all vertebrobasilar plaques, the group of the VBJ angles above 90°, as well as the group of the angles below 90°, respectively. Mann-Whitney U test was used for comparing the mean percentages of every plaque wall location between the two groups of the VBJ angles above 90° and the angles below 90°. P value less than 0.05 referred to statistical significance. Cohen κ or intraclass correlation coefficient with 95% CIs was utilized to assess intra- and inter-observer agreement. A coefficient more than 0.81 was regarded as excellence.

## 6.3 Results

### 6.3.1 The geometric variation of the VBJ angle in subjects with and without vertebrobasilar atherosclerosis

The VBJ angles ranged in magnitude between 29.45° and 124.20° among patients with vertebrobasilar atherosclerosis (data not shown). The VBJ angle degrees varied from 38.95° to 117.89° among patients without vertebrobasilar atherosclerosis (data not shown).

According to the degree of the VBJ angle greater than 90° or not, patients with and without vertebrobasilar atherosclerosis were then classified into two subgroups, respectively. 48.5% of patients with vertebrobasilar atherosclerosis had the VBJ angles ≥ 90°, while 51.5% possessed the VBJ angles < 90°. The VBJ angles ≥ 90° were found in 40.0% of patients without vertebrobasilar atherosclerosis, whereas the VBJ angles < 90° in 60.0%. As displayed in **Table 6-1**, however, there was no significant difference in the VBJ angle magnitude (above and below 90°) between patients with and without vertebrobasilar artery atherosclerosis (P value > 0.05).

**Table 6-1. Comparison of the VBJ angle degrees between subjects with and without vertebrobasilar atherosclerosis.**

| VBJ angle | Patients with vertebrobasilar atherosclerosis (n=68) | Patients without vertebrobasilar atherosclerosis (n=20) | P value |
|---|---|---|---|
| ≥ 90°, n (%) | 33 (48.5%) | 8 (40.0%) | 0.613 |
| < 90°, n (%) | 35 (51.5%) | 12 (60.0%) | |

VBJ angle, vertebrobasilar junction angle.

### 6.3.2 Baseline demographic and clinical characteristics of subjects with vertebrobasilar atherosclerosis

The present study included sixty-eight subjects with vertebrobasilar atherosclerotic plaques in total for subsequent analyses. The demographic and clinical characters of the subjects at admission were summarized in **Table 6-2**. Mean age was 63.53 ± 9.42 years old; 63.2% were male patients. The prevalence of hypertension was found to be 79.4% among patients with vertebrobasilar atherosclerosis, which was higher than that of hyperlipidemia, diabetes, or current smoking status. The occurrence of IS as an index stroke event was more prevalent than that of TIA (89.7% versus 10.3%).

**Table 6-2. Demographic and clinical features of patients with vertebrobasilar artery atherosclerosis.**

| Parameters | Subjects (n=68) |
|---|---|
| Age, years, mean ± SD | 63.53 ± 9.42 |
| Male/Female, n | 43/25 |
| Hypertension, n (%) | 54 (79.4%) |
| Hyperlipidemia, n (%) | 39 (57.4%) |
| Diabetes, n (%) | 27 (39.7%) |
| Smoking, n (%) | 18 (26.5%) |
| Index event | |
| Stroke, n (%) | 61 (89.7%) |
| TIA, n (%) | 7 (10.3%) |
| VBJ angle | |
| ≥ 90°, n (%) | 33 (48.5%) |
| < 90°, n (%) | 35 (51.5%) |

TIA, transient ischemic attack; VBJ angle, vertebrobasilar junction angle.

### 6.3.3 Relationship between the VBJ angle over 90° and the plaque wall distribution in the atherosclerotic vertebrobasilar arteries

One hundred and thirty-one atherosclerotic plaques were identified in the vertebrobasilar arteries of the included patients. The pattern of the plaque location on the vessel wall of the atherosclerotic vertebrobasilar arteries was determined on HR-MRI, by using a total of 659 imaging slices.

The overall feature of the plaque wall distribution in the atherosclerotic vertebrobasilar arteries was shown in **Table 6-3**. The vertebrobasilar plaques were evenly distributed on the lateral (38.64%), ventral (38.66%), and dorsal (22.70%) walls.

The mean percentages of each plaque distribution side in vertebrobasilar artery atherosclerosis were subsequently compared between the group of the VBJ angles ≥ 90° and the group of the VBJ angles < 90°. As illustrated in **Table 6-4**, the vertebrobasilar plaques within the VBJ angles ≥ 90° were more likely to be located on the ventral walls than those within the VBJ angles < 90° (50.14% versus 25.49%, P = 0.003). On the other hand, the VBJ angles ≥ 90° had fewer vertebrobasilar plaques distributed on the dorsal walls, compared to the VBJ angles < 90° (7.32% versus 40.34%, P < 0.001).

**Table 6-3. The overall pattern of plaque wall distribution in vertebrobasilar artery atherosclerosis.**

| Wall orientation | Vertebrobasilar plaques (n=131) |
|---|---|
| Lateral wall | 38.64% |
| Ventral wall | 38.66% |
| Dorsal wall | 22.70% |

**Table 6-4. Association of the VBJ angle with the plaque wall distribution in vertebrobasilar artery atherosclerosis.**

| Wall orientation | Plaques within VBJ angle ≥ 90° (n=70) | Plaques within VBJ angle < 90° (n=61) | P value |
|---|---|---|---|
| Lateral wall | 42.54% | 34.17% | 0.396 |
| Ventral wall | 50.14% | 25.49% | **0.003** |
| Dorsal wall | 7.32% | 40.34% | **0.000** |

VBJ angle, vertebrobasilar junction angle.

### 6.3.4 Reliability of evaluation

The intra- and inter-observer agreement of measuring the VBJ angle and determining the vertebrobasilar plaque location on the vessel wall were presented in **Table 6-5**. The intra- and inter-observer reliability were excellent for the imaging analyses.

**Table 6-5. Intra- and inter-observer reliability of analyzing the VBJ angle and the plaque wall distribution in vertebrobasilar artery atherosclerosis.**

| | Intra-observer agreement Coefficient (95% CI) | Inter-observer agreement Coefficient (95% CI) |
|---|---|---|
| VBJ angle | 0.907 (0.814-0.955) | 0.860 (0.728-0.931) |
| Plaque wall orientation | 0.911 (0.852-0.947) | 0.842 (0.743-0.905) |

CI, confidence interval; VBJ angle, vertebrobasilar junction angle.

## 6.4 Discussion

In this hospital-based study, firstly, we found that there commonly existed the geometric variations in the magnitude of the VBJ angles among patients with vertebrobasilar artery atherosclerosis. Secondly, the pattern of the plaque location on the vessel wall was depicted

in the atherosclerotic vertebrobasilar arteries by using HR-MRI. Importantly, the feature of the vertebrobasilar plaque wall distribution was further revealed depending on the structure of the VBJ angle over 90°. Our study showed that the VBJ angles exceeding 90° possessed more ventral-wall plaques, but had fewer dorsal-wall plaques in the atherosclerotic vertebrobasilar arteries.

Through TOF MRA imaging, the VBJ angles were displayed with varying magnitude from 29.45° to 124.20° among patients with vertebrobasilar atherosclerotic plaques in the current study. This result was observed in line with the previous autopsy finding from eighty-five human brains, in which the degrees of the VBJ angles were measured ranging between 10° and 160° [10]. Yet, the other MR imaging research investigated this anatomical variation among twelve healthy adult individuals, reporting that the degrees of the VBJ angles varied from 54° to 86° [17]. Of note, the differences in the range of the VBJ-angle degrees among various studies may be attributed to the different study populations.

The vessel wall distribution of atherosclerotic plaque in vertebrobasilar circulation may have its unique pattern. Among healthy subjects over 20 years old, the asymptomatic BA plaques in the early stage were mainly distributed on the ventral and dorsal walls, and these plaques might extend to the right or left wall in the progression of atherosclerosis [9]. Not surprisingly, the atherosclerotic plaques of less than 50% BA stenosis were found to be evenly located on the ventral, dorsal and lateral walls [16]. However, the plaque distribution of 70-99% BA atherosclerotic stenosis were predominantly on the dorsal and lateral walls [18]. The exact mechanism determining the plaque wall distribution in vertebrobasilar circulation atherosclerosis is still unknown. Growing evidence implied that the pattern of vertebrobasilar plaque location on the vessel walls might be strongly correlated with the anatomical structure of the vertebrobasilar arteries, largely via the role of hemodynamics [9, 17, 19, 20].

In this study, we also confirmed the even distribution of the total vertebrobasilar plaques on the vessel walls, and nearly two thirds of these plaques involved the ventral and dorsal walls, regardless of the stenotic degrees of the vertebrobasilar arteries. Our observations further demonstrated that the VBJ angles over 90° were positively related to the vertebrobasilar plaques on the ventral wall, but negatively to the plaques on the dorsal wall. This significant difference in the vertebrobasilar plaque wall distribution between the VBJ angles above 90° and the angles below 90° might be induced by the local changes in the hemodynamics and the vascular ability of the vertebrobasilar arteries. The possible explanations could be offered: First, the larger VBJ angles could bring about the complex CBF pattern and the decreased WSS level in the corresponding area of the vertebrobasilar arteries to form atherosclerosis [10, 11]. Second, the VBJ angle of 90° could significantly attenuate the functional response of the vascular smooth muscle cells (VSMCs) to the hemodynamic alteration [12]. Thus, it would seem reasonable to speculate that the VBJ angles ≥ 90° were more likely to worsen the ventral-wall condition of the vertebrobasilar arteries to develop atherosclerosis, mainly by altering the hemodynamic force and the vascular function of the vertebrobasilar arteries. Our findings could inspire future research direction.

Our results have potential clinical value. Prior HR-MRI study suggested that the plaques in the atherosclerotic BA were primarily located on the ventral wall among symptomatic patients with vertebrobasilar circulation infarction [21, 22]. Moreover, various infarct mechanisms could contribute to symptomatic vertebrobasilar circulation atherosclerotic disease [23, 24]. Accordingly, subsequent study with a larger sample size can explore whether the vertebrobasilar plaque wall distribution depending on the VBJ angle over 90° is independently correlated with the stroke patterns among these symptomatic patients.

Our study had some limitations. Firstly, a relatively small sample size and a lack of further validation of the clinical value of our findings. Secondly, our results should be cautiously

applied to other study populations. Thirdly, the relationship between the vertebrobasilar plaque wall distribution and the VBJ angle over 90° was not causal in this research, which requires verification by other cerebral fluid dynamics studies.

## 6.5 Conclusion

The degrees of the VBJ angles varied considerably among patients with vertebrobasilar artery atherosclerosis. The pattern of the vertebrobasilar plaque location on the vessel wall was robustly associated with the geometry of the VBJ angle over 90°. Further research is warranted to verify our observations.

## References


1. Lakomkin N, Dhamoon M, Carroll K, Singh IP, Tuhrim S, Lee J, et al. Prevalence of large vessel occlusion in patients presenting with acute ischemic stroke: A 10-year systematic review of the literature. *J Neurointerv Surg*. 2019;11:241-245
2. Zhou W, Chen R, Hopkins A, Wang Y, Tang J, Chen X, et al. Association between socioeconomic status and incident stroke in china. *J Epidemiol Community Health*. 2020;74:519-526
3. Wang W, Jiang B, Sun H, Ru X, Sun D, Wang L, et al. Prevalence, incidence, and mortality of stroke in china: Results from a nationwide population-based survey of 480 687 adults. *Circulation*. 2017;135:759-771
4. Prognosis of patients with symptomatic vertebral or basilar artery stenosis. The warfarin-aspirin symptomatic intracranial disease (wasid) study group. *Stroke*. 1998;29:1389-1392
5. Marquardt L, Kuker W, Chandratheva A, Geraghty O, Rothwell PM. Incidence and prognosis of > or = 50% symptomatic vertebral or basilar artery stenosis: Prospective population-based study. *Brain*. 2009;132:982-988
6. Compter A, van der Worp HB, Algra A, Kappelle LJ, Second Manifestations of AdSG. Prevalence and prognosis of asymptomatic vertebral artery origin stenosis in patients with clinically manifest arterial disease. *Stroke*. 2011;42:2795-2800
7. Xu Z, Li M, Hou Z, Lyu J, Zhang N, Lou X, et al. Association between basilar artery configuration and vessel wall features: A prospective high-resolution magnetic resonance imaging study. *BMC Med Imaging*. 2019;19:99
8. Liu L, Zhang XB, Lu S, Liu ZJ, Zhu XJ. Plaque distribution of basilar artery fenestration by 3d high-resolution mr vessel wall imaging. *Cell Transplant*. 2019;28:851-855

9. Kim BJ, Kim HY, Jho W, Kim YS, Koh SH, Heo SH, et al. Asymptomatic basilar artery plaque distribution and vascular geometry. *J Atheroscler Thromb*. 2019;26:1007-1014

10. Ravensbergen J, Krijger JK, Hillen B, Hoogstraten HW. The influence of the angle of confluence on the flow in a vertebro-basilar junction model. *J Biomech*. 1996;29:281-299

11. Ravensbergen J, Ravensbergen JW, Krijger JK, Hillen B, Hoogstraten HW. Localizing role of hemodynamics in atherosclerosis in several human vertebrobasilar junction geometries. *Arterioscler Thromb Vasc Biol*. 1998;18:708-716

12. Zhang Y, Menon NV, Li C, Chan V, Kang Y. The role of bifurcation angles on collective smooth muscle cell biomechanics and the implication in atherosclerosis development. *Biomater Sci*. 2016;4:430-438

13. Young CC, Bonow RH, Barros G, Mossa-Basha M, Kim LJ, Levitt MR. Magnetic resonance vessel wall imaging in cerebrovascular diseases. *Neurosurg Focus*. 2019;47:E4

14. de Havenon A, Mossa-Basha M, Shah L, Kim SE, Park M, Parker D, et al. High-resolution vessel wall mri for the evaluation of intracranial atherosclerotic disease. *Neuroradiology*. 2017;59:1193-1202

15. Wu F, Yu H, Yang Q. Imaging of intracranial atherosclerotic plaques using 3.0 t and 7.0 t magnetic resonance imaging-current trends and future perspectives. *Cardiovasc Diagn Ther*. 2020;10:994-1004

16. Yu J, Li ML, Xu YY, Wu SW, Lou M, Mu XT, et al. Plaque distribution of low-grade basilar artery atherosclerosis and its clinical relevance. *BMC Neurol*. 2017;17:8

17. Wake-Buck AK, Gatenby JC, Gore JC. Hemodynamic characteristics of the vertebrobasilar system analyzed using mri-based models. *PLoS One*. 2012;7:e51346

18. Guo R, Zhang X, Zhu X, Liu Z, Xie S. Morphologic characteristics of severe basilar artery atherosclerotic stenosis on 3d high-resolution mri. *BMC Neurol*. 2018;18:206

19. Yu J, Zhang S, Li ML, Ma Y, Dong YR, Lou M, et al. Relationship between the geometry patterns of vertebrobasilar artery and atherosclerosis. *BMC Neurol*. 2018;18:83

20. Kim BJ, Lee KM, Kim HY, Kim YS, Koh SH, Heo SH, et al. Basilar artery plaque and pontine infarction location and vascular geometry. *J Stroke*. 2018;20:92-98

21. Huang B, Yang WQ, Liu XT, Liu HJ, Li PJ, Lu HK. Basilar artery atherosclerotic plaques distribution in symptomatic patients: A 3.0t high-resolution mri study. *Eur J Radiol*. 2013;82:e199-203

22. Wang W, Yang Q, Li D, Fan Z, Bi X, Du X, et al. Incremental value of plaque enhancement in patients with moderate or severe basilar artery stenosis: 3.0 t high-resolution magnetic resonance study. *Biomed Res Int*. 2017;2017:4281629

23. Samaniego EA, Shaban A, Ortega-Gutierrez S, Roa JA, Hasan DM, Derdeyn C, et al. Stroke mechanisms and outcomes of isolated symptomatic basilar artery stenosis. *Stroke Vasc Neurol*. 2019;4:189-197

24. Schaafsma JD, Silver FL, Kasner SE, Caplan LR, Rose-Finnell L, Charbel FT, et al. Infarct patterns in patients with atherosclerotic vertebrobasilar disease in relation to hemodynamics. *Cerebrovasc Dis Extra*. 2019;9:123-128

# Chapter 7. The vertebrobasilar junction angle exceeding 90° is related to the progressive atherosclerotic lesions in patients with vertebrobasilar artery atherosclerosis

## 7.1 Background

IS owing to intracranial large-artery atherosclerotic stenosis is threatening the public health and bringing huge socio-economic burden all over the world [1-3]. Approximately one fourth of acute cerebral infarcts involve the tissues depending on a blood supply from the vertebrobasilar circulation system, which are also associated with high risks of recurrent stroke and stroke-related disability [4, 5].

There commonly exists a wide variety of anatomical variances in the vertebrobasilar circulation system, which may be strongly related to the occurrence and development of vertebrobasilar atherosclerotic plaques [6-8]. Of note, the degrees of the VBJ confluence angles in the human brain samples were reported to vary between 10° and 160° [9, 10]. The experimental and numerical models subsequently revealed that the vertebrobasilar arteries were more likely to show proneness to atherosclerosis in the larger degrees of the VBJ angles, mainly through the hemodynamic changes affected by the VBJ-angle structure [9-11]. Nonetheless, few data could be directly offered from patients with acute IS to ascertain the relevance of the VBJ angle magnitude to the progression of vertebrobasilar artery atherosclerosis.

With the help of HR-MRI, the present study aimed to describe the essential imaging characteristics of the vertebrobasilar atherosclerotic plaques quantitatively and qualitatively among AIS patients with vertebrobasilar artery atherosclerosis; and to explore the correlation

between the VBJ angles more than 90° and the plaque imaging features of vertebrobasilar artery atherosclerosis.

## 7.2 Methods

### 7.2.1 Study subjects

This was a hospital-based study from a single medical institution, recruiting consecutive subjects from 2014 to 2020. Adult patients were included in this study, if they met the following conditions: first-ever AIS or TIA in 7 days; at least one intracranial large artery diagnosed as atherosclerotic stenosis via routine cerebral angiography; vertebrobasilar atherosclerotic plaques identified by HR-MRI; both the bilateral VAs and the BA displayed on MRA; complete imaging scan from the intracranial segments of the bilateral VAs. Patients were excluded, if they suffered from non-atherosclerotic stenosis (dissection, vasculitis, or moyamoya disease); cardio-embolism (atrial fibrillation or valvular heart diseases); coexistent exceeding 50% stenosis of the ICA and/or the ECA; history of known brain tumor, vascular malformation, cerebral surgical/interventional procedure, or recurrent stroke; absence of the VA or the BA displayed on MRA; no vertebrobasilar atherosclerotic plaque detected by HR-MRI; or any contraindication to MRI. The baseline clinical information of all the patients were noted down, like age, sex, hypertension, hyperlipidemia, diabetes mellitus, or present smoking status. This study was approved by the institutional review board, following the Declaration of Helsinki. The written informed consents were provided by all the patients or family members.

### 7.2.2 Imaging protocol

A 3.0-Tesla Achieva magnetic resonance system with a standardized eight-channel head coil (Philips Healthcare, Cleveland, OH, USA) was utilized to scan all the subjects. The imaging protocol contained a TOF MRA sequence and a transverse three-dimensional T1w

VISTA sequence before and after administrating a contrast agent containing gadolinium (Dotarem, Gadoteric acid 0.5 mmol/mL, Guerbet, Roissy CdG Cedex, France) with 0.1 mL/kg to every subject. The TOF MRA sequence parameters were as follows: FOV 200*200*56mm$^3$, acquired resolution 0.4*0.6*0.7mm$^3$, TR/TE 23/3.5ms, and scan duration 3:07min. The imaging parameters for the T1w VISTA sequence included FOV 200*167*45mm$^3$, acquired resolution 0.6*0.6*1.0mm$^3$, reconstructed resolution 0.5*0.5*0.5 mm$^3$ with zero filling, TR 1500ms, TE 36ms, turbo-spin-echo + startup echoes 56+6, echo spacing 4.0ms, SENSE factor 1.5 with phase-encode direction, and scan duration 6:51min.

### 7.2.3 Imaging evaluation

The source images with axial orientation and the three-dimensional reconstructed images were utilized to perform visual image quality evaluation, according to a three-point scale (1 = poor, 2 = adequate, and 3 = excellent). The images graded as two to three points were included in the subsequent imaging analyses.

Two examiners were blind to the patient clinical data, and independently assessed the intra- and inter-observer agreement. Thirty subjects were chosen at random. One examiner analyzed the images twice over a period of three months between the two measurements. Another examiner analyzed the images of the same thirty subjects once.

### 7.2.4 Measuring the degrees of the VBJ angles

Via the usage of OsiriX DICOM Viewer (Geneva, Switzerland), the degrees of the VBJ angles were measured on the three-dimensional reconstructed cross-sections from TOF MRA imaging with the best-oriented visualization (**Figure 7-1**). The VBJ confluence angle was defined as the corresponding space joined by the two inner arterial walls of the right and left VAs [10]. Measuring the VBJ-angle degrees was independent of the quantitative and qualitative imaging analyses of vertebrobasilar artery atherosclerosis.

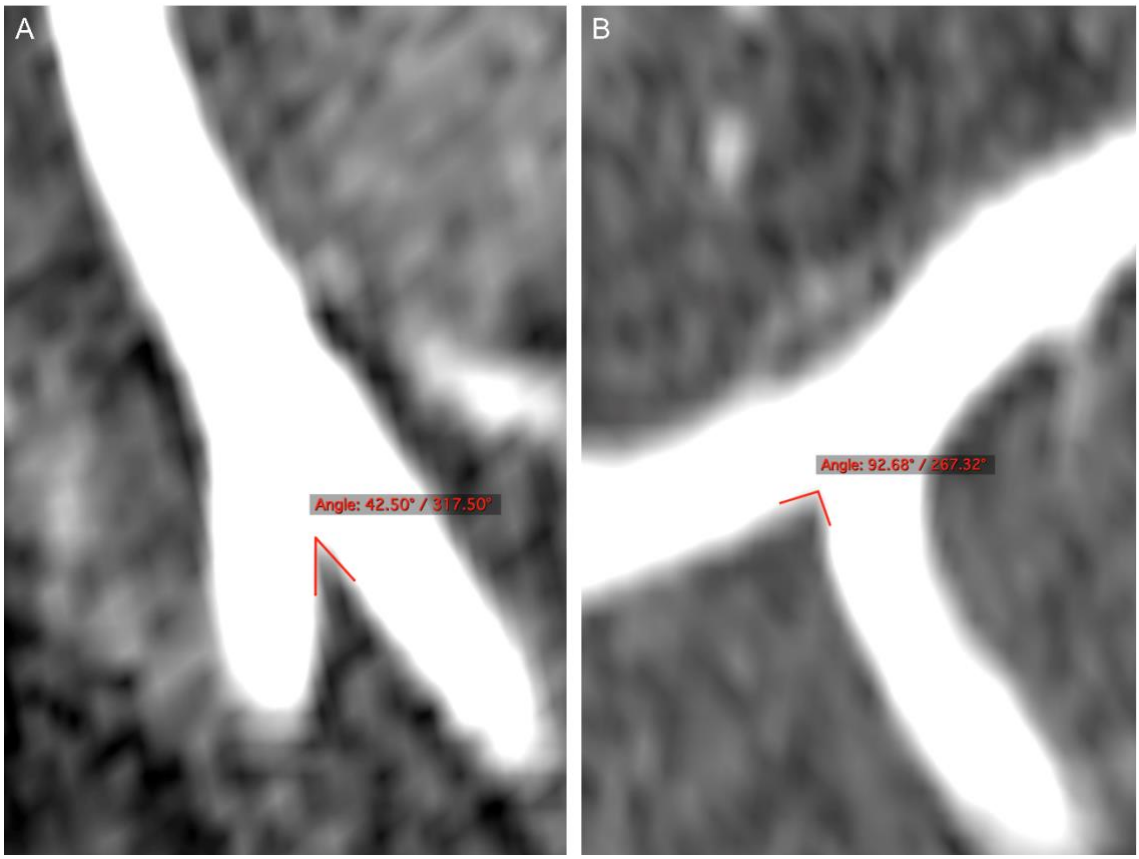


**Figure 7-1. The measurement of the VBJ-angle degrees on the three-dimensional reconstructed cross-sections from TOF MRA imaging. A**, the VBJ angle is grouped into the category of the angles below 90°. **B**, the VBJ angle is grouped into the category of the angles above 90°. TOF MRA, Time-Of-Flight magnetic resonance angiography; VBJ, vertebrobasilar junction.

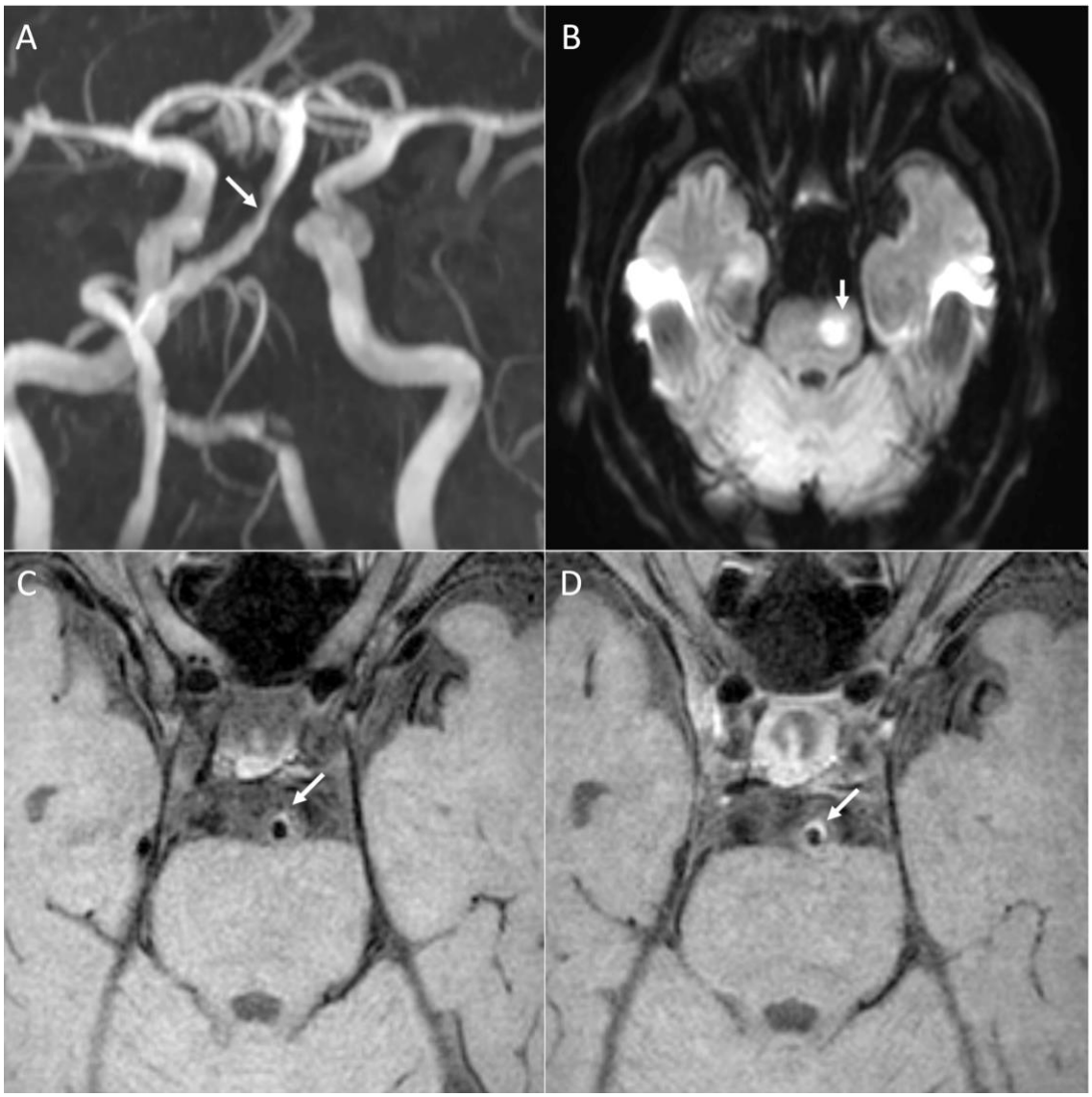


**Figure 7-2. A typical case of a symptomatic atherosclerotic plaque in the BA. A**, a symptomatic atherosclerotic stenosis of the BA on MRA imaging (white arrow). **B**, acute infarction in the BA territory on DWI (white arrow). **C** and **D**, an eccentric, focal plaque in the BA as a symptomatic atherosclerotic lesion before and after administrating contrast on T1w imaging, respectively (white arrows). BA, basilar artery; DWI, diffusion-weighted imaging; MRA, magnetic resonance angiography; T1w, T1-weighted.

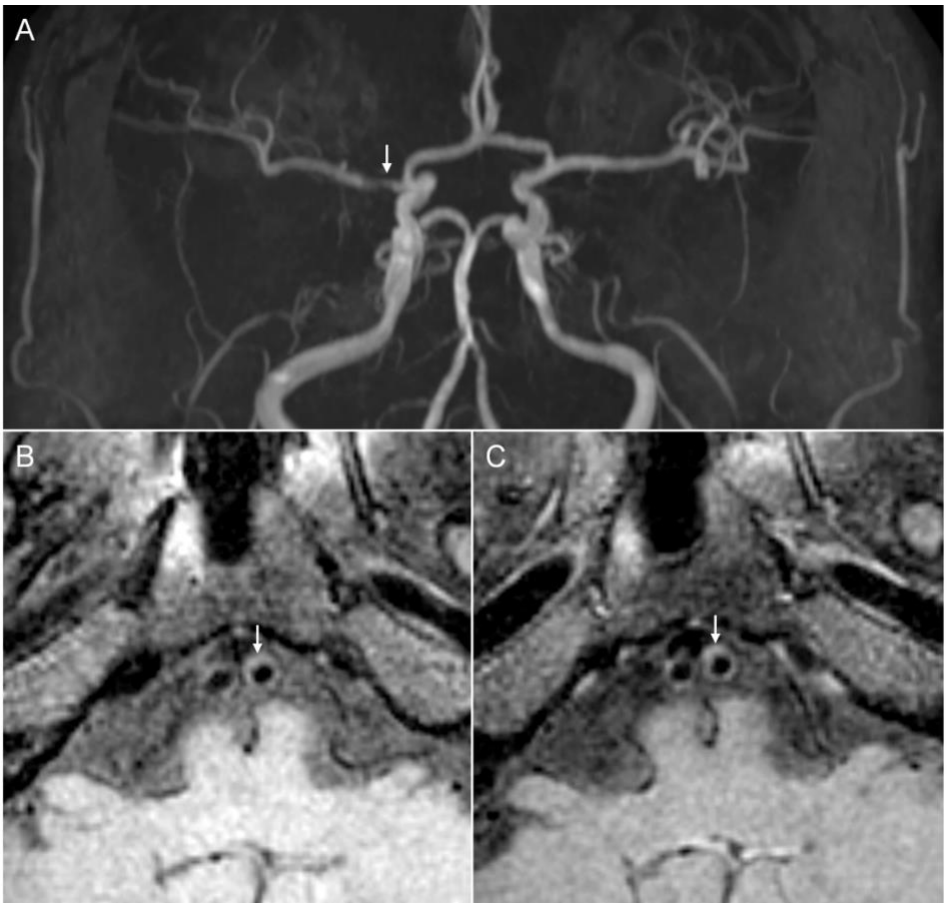


**Figure 7-3. A typical case of an asymptomatic atherosclerotic plaque in the VA. A**, a symptomatic atherosclerotic stenosis of the right MCA-M1 segment on MRA imaging (white arrow). **B** and **C**, an eccentric, focal plaque in the left VA as an asymptomatic atherosclerotic lesion before and after administrating contrast on T1w imaging, respectively (white arrows). MCA, middle cerebral artery; MRA, magnetic resonance angiography; T1w, T1-weighted; VA, vertebral artery.

### 7.2.5 Quantitatively measuring the vertebrobasilar atherosclerotic plaques

An atherosclerotic plaque was recognized by focal thickening on the vessel wall along the intracranial segments of the bilateral VAs and the BA from both pre- and post-contrast T1w imaging (**Figure 7-2** and **Figure 7-3**), based on a definition reported previously [12]. VesselMass software (Leiden University Medical Center, the Netherlands) was used to perform the quantitative measurements of the atherosclerotic plaques in the vertebrobasilar arteries (luminal stenosis degree, plaque burden percentage, wall area index, remodeling index, and enhancement index), according to the algorithms from previous research [13-15].

The imaging cross-section of the vertebrobasilar atherosclerotic lesion at the most narrowing lumen was used to measure the area of the vertebrobasilar plaque, while the reference site referred to the adjacent vascular segment proximal or distal to the atherosclerotic lesion, which was plaque-free, non-tortuous and normal [13, 16]. The vessel area was measured via manually tracing the vessel-cerebrospinal fluid interface, and the lumen area was determined by the blood-intima interface. Besides, both maximal and minimal wall thicknesses were measured at the most stenotic luminal lesion. The formulas were as follows:

The wall area = VA – LA;

The degree of luminal stenosis = (1 – lesion LA / reference LA) × 100%;

The plaque burden percentage = (lesion WA / lesion VA) × 100%;

The wall area index = lesion WA / reference WA;

The remodeling index = lesion VA / reference VA (If the index was ≥ 1.05, the arterial remodeling was a positive pattern; if the index was < 1.05, the pattern of arterial remodeling was non-positive.).

Moreover, the plaque signal intensity was measured on the matched pre- and post-contrast T1w imaging, after manually tracing both vascular lumen and outer wall boundary at the most narrowing lesion of vertebrobasilar artery atherosclerosis [13]. The gray-matter SI was also measured on the matched pre- and post-contrast T1w imaging via manually drawing a circle of 10 to 12 $mm^2$ at the normal tissue of gray matter next to the atherosclerotic lesion [13]. The plaque contrast enhancement was quantified on a basis of the following formula:

The enhancement index = [(plaque SI / gray-matter SI on post-contrast T1w imaging) – (plaque SI / gray-matter SI on pre-contrast T1w imaging)] / (plaque SI / gray-matter SI on pre-contrast T1w imaging) × 100%.

### 7.2.6 Qualitatively measuring the vertebrobasilar atherosclerotic plaques

The atherosclerotic plaques in the vertebrobasilar arteries were then evaluated qualitatively (plaque hyperintensity signal, plaque hypointensity signal, IPH, and symptomatic status), based on the methodologies from our prior research [13, 17].

The plaque SI was also designated as hyperintensity or hypointensity on the pre-contrast T1w imaging in comparison with the normal gray-matter SI nearest to the atherosclerotic lesion [17]. If a high signal area was found within the plaque on the pre-contrast T1w imaging (exceeding 150% of the adjacent muscle SI), the occurrence of IPH was considered [13].

Furthermore, the vertebrobasilar plaque was described as symptomatic or asymptomatic according to whether this plaque could make a direct contribution to acute ischemia within the corresponding vertebrobasilar territory (the positive findings of DWI and/or acute symptoms of neurological dysfunction) [13]. The symptomatic vertebrobasilar lesion was defined by the situation that the plaque was the only or the most stenotic/enhanced in the same vertebrobasilar territory of acute infarction. The asymptomatic vertebrobasilar lesion was determined by the circumstance that the plaque was out of the vertebrobasilar territory of

acute infarct, or not the most stenotic/enhanced within the acute ischemic vertebrobasilar territory.

### 7.2.7 Statistical analysis

SPSS version 26.0 (IBM, NY, USA) was used for conducting statistical analyses. Statistical data were displayed as percentages, means ± SD, or medians (IQR), where appropriate. Chi-squared test, Fisher's exact test, or T-test was utilized to compare the patient baseline clinical characters between the group with the VBJ angles ≥ 90° and the group with the angles < 90°. Chi-squared test, Fisher's exact test, or Mann-Whitney U test was used to compare the plaque imaging features of vertebrobasilar artery atherosclerosis between the group with the VBJ angles ≥ 90° and the group with the angles < 90°. P value below 0.05 was considered as statistical significance. Intraclass correlation or Cohen κ coefficient with 95% CIs was utilized for determining intra- and inter-observer agreement. A coefficient above 0.81 was identified as excellence.

## 7.3 Results

### 7.3.1 Baseline demographic and clinical characteristics of all the subjects

In the current study, sixty-eight patients with atherosclerotic plaques in the vertebrobasilar arteries were included. The baseline clinical features of all the patients (mean age = 63.53 ± 9.42 years old; 43 male patients) were shown in **Table 7-1**. Among all the patients, the incidence of hypertension was observed to be 79.4%, and higher than that of hyperlipidemia, diabetes mellitus, or present smoking status. The prevalence of AIS (89.7%) was higher than that of TIA (10.3%).

All the patients were then classified into two categories according to whether the degrees of the VBJ angles exceeded 90°: 33 in the category of the VBJ angles ≥ 90°; 35 in the

category of the VBJ angles < 90°. As presented in **Table 7-1**, no significant differences of the patient baseline clinical characters were found between the two categories (all P values > 0.05).

**Table 7-1. Baseline clinical characteristics of subjects with vertebrobasilar atherosclerosis between the VBJ angles ≥ 90° and the angles < 90°.**

| Parameters | All patients (n=68) | Patients with VBJ angle ≥ 90° (n=33) | Patients with VBJ angle < 90° (n=35) | P value[#] |
|---|---|---|---|---|
| Age, years, mean ± SD | 63.53 ± 9.42 | 62.97 ± 9.69 | 64.06 ± 9.25 | 0.638 |
| Male/Female, n | 43/25 | 22/11 | 21/14 | 0.569 |
| Hypertension, n (%) | 54 (79.4%) | 26 (78.8%) | 28 (80.0%) | 0.902 |
| Hyperlipidemia, n (%) | 39 (57.4%) | 21 (63.6%) | 18 (51.4%) | 0.309 |
| Diabetes, n (%) | 27 (39.7%) | 11 (33.3%) | 16 (45.7%) | 0.297 |
| Smoking, n (%) | 18 (26.5%) | 9 (27.3%) | 9 (25.7%) | 0.884 |
| Index event | | | | 0.107 |
| Stroke, n (%) | 61 (89.7%) | 32 (97.0%) | 29 (82.9%) | |
| TIA, n (%) | 7 (10.3%) | 1 (3.0%) | 6 (17.1%) | |

TIA, transient ischemic attack; VBJ angle, vertebrobasilar junction angle.

[#] P value: the group of the VBJ angle ≥ 90° versus the group of the VBJ angle < 90°.

### 7.3.2 Overall imaging characters of the vertebrobasilar atherosclerotic plaques

A total of one hundred and thirty-one plaques were recognized as atherosclerotic in the vertebrobasilar arteries among all the patients. The plaque imaging characteristics of all the vertebrobasilar atherosclerotic lesions were summarized in **Table 7-2**.

The incident rate of the vertebrobasilar plaques with hypointensity signal was found to be 42.0%, while that of the plaques with hyperintensity signal was 25.2%. Only 10.7% of all the vertebrobasilar plaques had IPH, while up to 74.0% showed positive pattern of arterial remodeling. Notably, 13.0% of the vertebrobasilar plaques were identified as symptomatic,

which induced acute infarctions on DWI and/or acute stroke signs in vertebrobasilar circulation.

At the narrowest luminal lesion, vertebrobasilar artery atherosclerosis showed a maximal wall width of 1.86mm (IQR, 1.46-2.29) and a minimal wall width of 0.85mm (IQR, 0.70-0.99). The degree of luminal stenosis in the atherosclerotic vertebrobasilar arteries was calculated to be 57.96% (IQR, 41.89-77.99), and the plaque burden percentage was 77.47% (IQR, 69.94-86.30). Besides, the wall area index reached 33.10 (IQR, 12.50-52.90) in vertebrobasilar artery atherosclerosis. The remodeling index was 1.37 (IQR, 1.04-1.77). The enhancement index was measured to be 34.34% (IQR, 16.05-54.16).

**Table 7-2. Plaque imaging features of vertebrobasilar atherosclerosis in all lesions.**

| Characters | Vertebrobasilar plaques (n=131) |
|---|---|
| Symptomatic status, n (%) | 17 (13.0%) |
| Hypointensity, n (%) | 55 (42.0%) |
| Hyperintensity, n (%) | 33 (25.2%) |
| Intraplaque hemorrhage, n (%) | 14 (10.7%) |
| Arterial remodeling | |
| Positive, n (%) | 97 (74.0%) |
| Non-positive, n (%) | 34 (26.0%) |
| **At the maximal narrowing lumen site** | |
| Lumen area, $mm^2$, median (IQR) | 3.84 (2.09-6.79) |
| Vessel area, $mm^2$, median (IQR) | 18.75 (13.87-26.05) |
| Wall area, $mm^2$, median (IQR) | 14.95 (11.03-19.96) |
| Maximum wall thickness, mm, median (IQR) | 1.86 (1.46-2.29) |
| Minimum wall thickness, mm, median (IQR) | 0.85 (0.70-0.99) |
| Stenosis percentage, %, median (IQR) | 57.96 (41.89-77.99) |
| Plaque burden, %, median (IQR) | 77.47 (69.94-86.30) |
| Wall area index, median (IQR) | 33.10 (12.50-52.90) |
| Remodeling index, median (IQR) | 1.37 (1.04-1.77) |
| Enhancement index, %, median (IQR) | 34.34 (16.05-54.16) |
| **At the reference site** | |
| Lumen area, $mm^2$, median (IQR) | 11.53 (7.88-16.66) |
| Vessel area, $mm^2$, median (IQR) | 14.59 (9.68-20.49) |

IQR, interquartile range.

**Table 7-3. Quantitative imaging features of vertebrobasilar atherosclerosis between the VBJ angles ≥ 90° and the angles < 90°.**

| Characters | Plaques within VBJ angle ≥ 90° (n=70) | Plaques within VBJ angle < 90° (n=61) | P value |
|---|---|---|---|
| **At the maximal narrowing lumen site** | | | |
| Lumen area, $mm^2$, median (IQR) | 2.95 (1.65-5.07) | 5.83 (3.73-8.57) | **0.000** |
| Vessel area, $mm^2$, median (IQR) | 18.46 (13.32-24.39) | 19.74 (14.32-26.91) | 0.422 |
| Wall area, $mm^2$, median (IQR) | 16.02 (11.09-20.27) | 14.77 (10.70-18.65) | 0.223 |
| Maximum wall thickness, mm, median (IQR) | 2.03 (1.66-2.53) | 1.70 (1.25-2.05) | **0.000** |
| Minimum wall thickness, mm, median (IQR) | 0.88 (0.73-1.06) | 0.79 (0.63-0.98) | **0.039** |
| Stenosis percentage, %, median (IQR) | 73.89 (53.81-85.12) | 45.68 (35.24-66.32) | **0.000** |
| Plaque burden, %, median (IQR) | 84.35 (75.24-89.88) | 70.58 (64.89-77.73) | **0.000** |
| Wall area index, median (IQR) | 35.89 (12.43-63.88) | 31.80 (12.67-47.45) | 0.190 |
| Remodeling index, median (IQR) | 1.31 (1.03-1.98) | 1.45 (1.03-1.73) | 0.761 |
| Enhancement index, %, median (IQR) | 38.83 (18.42-57.91) | 32.43 (12.37-45.34) | 0.131 |
| **At the reference site** | | | |
| Lumen area, $mm^2$, median (IQR) | 10.55 (7.57-17.67) | 11.76 (8.41-15.36) | 0.631 |
| Vessel area, $mm^2$, median (IQR) | 14.92 (8.39-20.18) | 14.59 (10.46-20.67) | 0.580 |

IQR, interquartile range; VBJ angle, vertebrobasilar junction angle.

### 7.3.3 Association between the VBJ angle degrees and vertebrobasilar artery atherosclerosis

The vertebrobasilar atherosclerotic plaques were subsequently categorized into the groups of the VBJ angles ≥ 90° (70 plaques) and the angles < 90° (61 plaques). The comparisons of the plaque imaging characteristics in vertebrobasilar artery atherosclerosis between the VBJ angles ≥ 90° and the angles < 90° were displayed in **Table 7-3** and **Figure 7-4**, respectively.

As shown in **Table 7-3**, the LA of vertebrobasilar artery atherosclerosis in the VBJ angles ≥ 90° was significantly smaller than that in the angles < 90° (2.95$mm^2$ [IQR, 1.65-5.07] versus 5.83$mm^2$ [IQR, 3.73-8.57], P < 0.001). The vertebrobasilar plaques in the VBJ angles ≥ 90° had significantly larger maximal wall thickness (2.03mm [IQR, 1.66-2.53] versus

1.70mm [IQR, 1.25-2.05], P < 0.001) and larger minimal wall thickness (0.88mm [IQR, 0.73-1.06] versus 0.79mm [IQR, 0.63-0.98], P = 0.039), compared with those in the angles < 90°. Furthermore, the degree of vertebrobasilar luminal stenosis in the VBJ angles ≥ 90° was significantly higher than that in the VBJ angle < 90° (73.89% [IQR, 53.81-85.12] versus 45.68% [IQR, 35.24-66.32], P < 0.001). The vertebrobasilar plaques in the VBJ angles ≥ 90° possessed significantly heavier plaque burden than those in the VBJ angles < 90° (84.35% [IQR, 75.24-89.88] versus 70.58% [IQR, 64.89-77.73], P < 0.001). However, the differences of the wall area index, the remodeling index and the enhancement index in vertebrobasilar atherosclerosis were not significant between the groups of the VBJ angles ≥ 90° and the angles < 90° (all P values > 0.05).

As illustrated in **Figure 7-4**, the vertebrobasilar plaques with symptomatic status (20.0% versus 4.9%, P = 0.01), hypointensity signal (51.4% versus 31.1%, P = 0.019), and IPH (17.1% versus 3.3%, P = 0.01) were more likely to be found in the VBJ angles ≥ 90°, rather than the VBJ angles < 90°. Yet, there were no significant differences of the plaque hyperintensity signal and the arterial remodeling pattern in vertebrobasilar atherosclerosis between the groups of the VBJ angles ≥ 90° and the angles < 90° (both P values > 0.05).

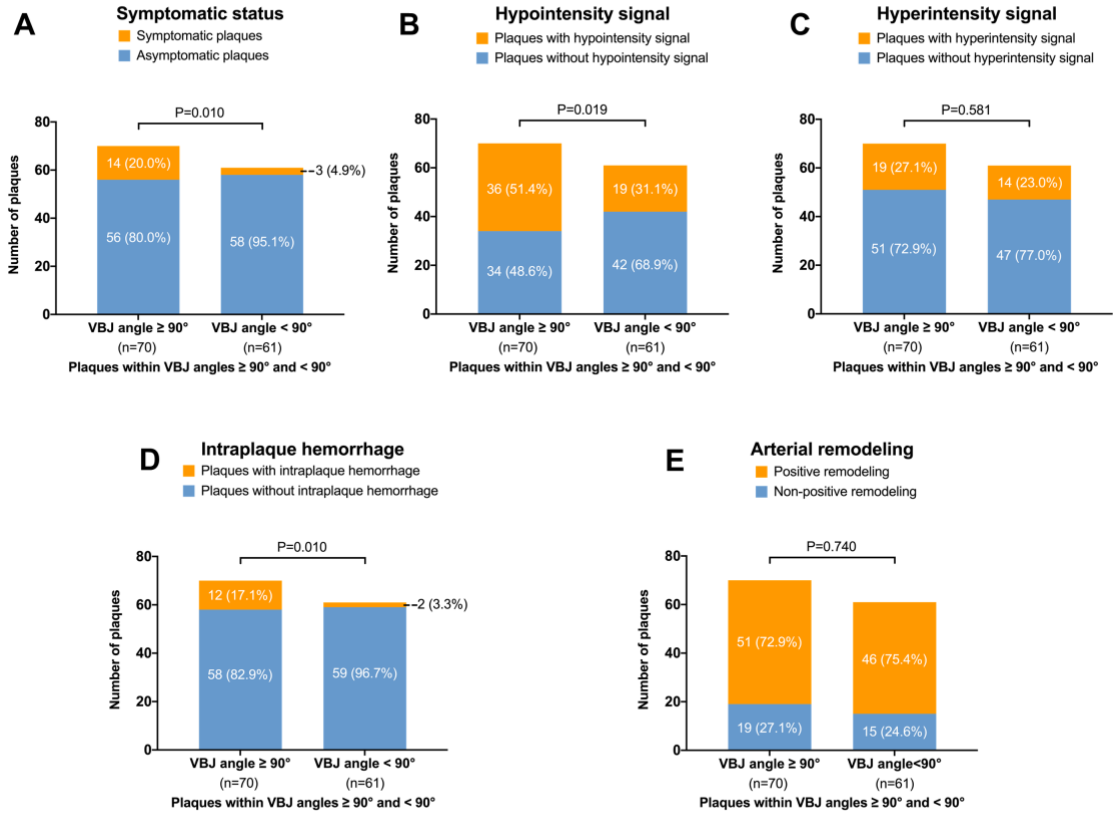


**Figure 7-4. The comparison of other vertebrobasilar plaque imaging features between the VBJ angles above 90° and the angles below 90°. A**, symptomatic status. **B**, plaque hypointensity signal. **C**, plaque hyperintensity signal. **D**, intraplaque hemorrhage. **E**, arterial remodeling pattern. VBJ, vertebrobasilar junction.

### 7.3.4 Reliability of measurement

The intra-observer reliability was excellent for measuring the VBJ-angle degrees (coefficient = 0.907, 95% CI 0.814-0.955). The inter-observer reliability was also excellent for measuring the VBJ-angle degrees (coefficient = 0.860, 95% CI 0.728-0.931). The intra- and inter-observer reliability were substantial to excellent for the quantitative and qualitative assessment of plaque imaging characters, which was previously reported by our HR-MRI research [17, 18].

## 7.4 Discussion

In this study, firstly, we utilized HR-MRI as an advanced intracranial vessel-wall imaging modality to depict the typical imaging features of the atherosclerotic plaques in the vertebrobasilar arteries. Secondly, we verified a strong correlation of the VBJ angles over 90° with vertebrobasilar artery atherosclerosis. The VBJ angles exceeding 90° were revealed in significant relevance to the increased values of wall thickness, luminal stenosis and plaque burden in vertebrobasilar artery atherosclerosis. Besides, the vertebrobasilar atherosclerotic plaques with hypointensity signal and IPH were more prevalent within the VBJ angles over 90°. Importantly, the atherosclerotic plaques within the VBJ angles exceeding 90° were more possible to result in acute infarctions and/or acute ischemia symptoms in vertebrobasilar circulation.

By using TOF MRA imaging, the marked anatomical variability in the VBJ-angle magnitude was observed among patients with vertebrobasilar atherosclerotic plaques, which ranged between 29.45° and 124.20° in our study (data not displayed). Our result was comparable to the prior post-mortem finding that the structural variation of the VBJ-angle degrees commonly existed in the human brains [9, 10]. The impact of a larger VBJ-angle degree on the progression of atherosclerosis was concluded numerically and experimentally in the

previous analytical models as well [9-11]. Notably, these studies suggested that the geometry of the larger VBJ-angle degrees might increase the risk of developing vertebrobasilar atherosclerotic plaques [9-11].

The reasonable explanation could be provided. Firstly, the VBJ-angle magnitude might have a strong influence on the hemodynamic force acting on the vertebrobasilar artery walls [9, 10, 19]. It was notable that the structure of the larger VBJ angles could induce the complex pattern of CBF and decrease the level of WSS on the vessel walls to grow atherosclerosis [9, 10]. Secondly, the magnitude of the VBJ angle might directly affect the function of the VSMCs in the vertebrobasilar arteries [11]. Particularly in the model of the VBJ angle of 90°, the VSMCs showed an attenuated reaction to the local alteration in hemodynamics and expressed the higher levels of pro-atherosclerotic cytokines [11]. Therefore, we speculated about the hemodynamic and vascular roles of the structure of the VBJ angles more than 90° in deteriorating the state of the vertebrobasilar artery walls to develop atherosclerosis.

Our observations could largely corroborate this hypothesis: First, the VBJ angles over 90° were found in robust association with the narrower condition of vertebrobasilar artery atherosclerosis, including larger wall thicknesses, severer luminal stenosis, and higher plaque burden percentages. Of note, compared to other routine imaging indexes, the plaque burden percentage was reported more reliable to indicate the severity of the narrowing lumen in the intracranial atherosclerotic large arteries [20-22]. Second, the vertebrobasilar atherosclerotic plaques within the VBJ angles exceeding 90° had the increased incidences of plaque hypointensity signal and IPH. On the pre-contrast T1w imaging, the plaque hypointensity signal might symbolize the presence of calcification within the plaque [23]. Our prior autopsy findings further confirmed that the occurrence of calcification was more prevalent in the vertebrobasilar circulation plaques, which was even related to the progressive atherosclerotic plaques [24, 25]. Regardless of the degrees of luminal stenosis, moreover, IPH was significantly

correlated with the unstable plaques and the plaque rupture in vertebrobasilar circulation atherosclerosis [26-28]. In our study, consequently, the VBJ angles more than 90° were validated in strong relevance to a worse vessel wall state of the atherosclerotic vertebrobasilar arteries.

Our study is of potential value to the clinical practice. Prior research suggested that the VBJ-angle degrees were significantly larger among patients with deep pontine lacunar infarction, compared with healthy subjects [29]. In this study, similarly, the symptomatic plaques inducing acute infarcts and/or acute stroke symptoms in vertebrobasilar circulation were mainly found within the VBJ angles more than 90°, instead of the angles less than 90°. Considering that various stroke patterns exist among patients with symptomatic vertebrobasilar artery atherosclerotic disease [30, 31], future study is required to confirm the independent association of the VBJ angles exceeding 90° with stroke occurrence or stroke mechanisms.

There are several limitations in the current study. First, we could not draw any causal conclusion regarding the VBJ-angle magnitude and vertebrobasilar atherosclerosis in virtue of the nature of our observational research. Second, although our finding was consistent with the previous studies reporting a low incident rate of symptomatic vertebrobasilar atherosclerotic disease [32, 33], a relatively small sample size in this study did not allow further investigation into the clinical impact of our results. Third, flow dynamic analysis is still needed to verify our observations.

### 7.5 Conclusion

Through using HR-MRI, the essential imaging features of the vertebrobasilar atherosclerotic plaques were described quantitatively and qualitatively in patients with vertebrobasilar artery atherosclerosis. The differences in the vertebrobasilar plaque imaging characteristics were found significant between the VBJ angles above 90° and the angles

below 90°. The VBJ angles exceeding 90° were strongly related to a worse condition of vertebrobasilar artery atherosclerosis.

## References


1. Kim J, Thayabaranathan T, Donnan GA, Howard G, Howard VJ, Rothwell PM, et al. Global stroke statistics 2019. *Int J Stroke*. 2020;15:819-838
2. Wang YJ, Li ZX, Gu HQ, Zhai Y, Jiang Y, Zhao XQ, et al. China stroke statistics 2019: A report from the national center for healthcare quality management in neurological diseases, china national clinical research center for neurological diseases, the chinese stroke association, national center for chronic and non-communicable disease control and prevention, chinese center for disease control and prevention and institute for global neuroscience and stroke collaborations. *Stroke Vasc Neurol*. 2020;5:211-239
3. Kaul S, Alladi S, Jabeen SA, Bandaru V, Ankem U, Mekala S, et al. Intracranial atherosclerosis is the most common stroke subtype: Ten-year data from hyderabad stroke registry (india). *Ann Indian Acad Neurol*. 2018;21:209-213
4. Savitz SI, Caplan LR. Vertebrobasilar disease. *N Engl J Med*. 2005;352:2618-2626
5. Sparaco M, Ciolli L, Zini A. Posterior circulation ischaemic stroke-a review part i: Anatomy, aetiology and clinical presentations. *Neurol Sci*. 2019;40:1995-2006
6. Xu Z, Li M, Hou Z, Lyu J, Zhang N, Lou X, et al. Association between basilar artery configuration and vessel wall features: A prospective high-resolution magnetic resonance imaging study. *BMC Med Imaging*. 2019;19:99
7. Zhou L, Yan Y, Du H, Ni X, Wang G, Wang Q. Plaque features and vascular geometry in basilar artery atherosclerosis. *Medicine (Baltimore)*. 2020;99:e19742
8. Yu J, Zhang S, Li ML, Ma Y, Dong YR, Lou M, et al. Relationship between the geometry patterns of vertebrobasilar artery and atherosclerosis. *BMC Neurol*. 2018;18:83

9. Ravensbergen J, Krijger JK, Hillen B, Hoogstraten HW. The influence of the angle of confluence on the flow in a vertebro-basilar junction model. *J Biomech*. 1996;29:281-299

10. Ravensbergen J, Ravensbergen JW, Krijger JK, Hillen B, Hoogstraten HW. Localizing role of hemodynamics in atherosclerosis in several human vertebrobasilar junction geometries. *Arterioscler Thromb Vasc Biol*. 1998;18:708-716

11. Zhang Y, Menon NV, Li C, Chan V, Kang Y. The role of bifurcation angles on collective smooth muscle cell biomechanics and the implication in atherosclerosis development. *Biomater Sci*. 2016;4:430-438

12. Qiao Y, Zeiler SR, Mirbagheri S, Leigh R, Urrutia V, Wityk R, et al. Intracranial plaque enhancement in patients with cerebrovascular events on high-spatial-resolution mr images. *Radiology*. 2014;271:534-542

13. Yang WJ, Abrigo J, Soo YO, Wong S, Wong KS, Leung TW, et al. Regression of plaque enhancement within symptomatic middle cerebral artery atherosclerosis: A high-resolution mri study. *Front Neurol*. 2020;11:755

14. Wang M, Wu F, Yang Y, Miao H, Fan Z, Ji X, et al. Quantitative assessment of symptomatic intracranial atherosclerosis and lenticulostriate arteries in recent stroke patients using whole-brain high-resolution cardiovascular magnetic resonance imaging. *J Cardiovasc Magn Reson*. 2018;20:35

15. Guo R, Zhang X, Zhu X, Liu Z, Xie S. Morphologic characteristics of severe basilar artery atherosclerotic stenosis on 3d high-resolution mri. *BMC Neurol*. 2018;18:206

16. Samuels OB, Joseph GJ, Lynn MJ, Smith HA, Chimowitz MI. A standardized method for measuring intracranial arterial stenosis. *AJNR Am J Neuroradiol*. 2000;21:643-646

17. Yang WJ, Chen XY, Zhao HL, Niu CB, Zhang B, Xu Y, et al. Postmortem study of validation of low signal on fat-suppressed t1-weighted magnetic resonance imaging as

marker of lipid core in middle cerebral artery atherosclerosis. *Stroke*. 2016;47:2299-2304

18. Dieleman N, Yang W, Abrigo JM, Chu WC, van der Kolk AG, Siero JC, et al. Magnetic resonance imaging of plaque morphology, burden, and distribution in patients with symptomatic middle cerebral artery stenosis. *Stroke*. 2016;47:1797-1802
19. Ritter MA, Ringelstein EB. The venturi effect and cerebrovascular ultrasound. *Cerebrovasc Dis*. 2002;14:98-104
20. Ran Y, Wang Y, Zhu M, Wu X, Malhotra A, Lei X, et al. Higher plaque burden of middle cerebral artery is associated with recurrent ischemic stroke: A quantitative magnetic resonance imaging study. *Stroke*. 2020;51:659-662
21. Wang Y, Liu X, Wu X, Degnan AJ, Malhotra A, Zhu C. Culprit intracranial plaque without substantial stenosis in acute ischemic stroke on vessel wall mri: A systematic review. *Atherosclerosis*. 2019;287:112-121
22. Wu F, Yu H, Yang Q. Imaging of intracranial atherosclerotic plaques using 3.0 t and 7.0 t magnetic resonance imaging-current trends and future perspectives. *Cardiovasc Diagn Ther*. 2020;10:994-1004
23. Song JW, Wasserman BA. Vessel wall mr imaging of intracranial atherosclerosis. *Cardiovasc Diagn Ther*. 2020;10:982-993
24. Yang WJ, Zheng L, Wu XH, Huang ZQ, Niu CB, Zhao HL, et al. Postmortem study exploring distribution and patterns of intracranial artery calcification. *Stroke*. 2018;49:2767-2769
25. Zheng L, Yang WJ, Niu CB, Zhao HL, Wong KS, Leung TWH, et al. Correlation of adventitial vasa vasorum with intracranial atherosclerosis: A postmortem study. *J Stroke*. 2018;20:342-349

26. Zhu C, Tian X, Degnan AJ, Shi Z, Zhang X, Chen L, et al. Clinical significance of intraplaque hemorrhage in low- and high-grade basilar artery stenosis on high-resolution mri. *AJNR Am J Neuroradiol*. 2018;39:1286-1292

27. Shi Z, Zhu C, Degnan AJ, Tian X, Li J, Chen L, et al. Identification of high-risk plaque features in intracranial atherosclerosis: Initial experience using a radiomic approach. *Eur Radiol*. 2018;28:3912-3921

28. Shi Z, Li J, Zhao M, Peng W, Meddings Z, Jiang T, et al. Quantitative histogram analysis on intracranial atherosclerotic plaques: A high-resolution magnetic resonance imaging study. *Stroke*. 2020;51:2161-2169

29. Jeong SK, Lee JH, Nam DH, Kim JT, Ha YS, Oh SY, et al. Basilar artery angulation in association with aging and pontine lacunar infarction: A multicenter observational study. *J Atheroscler Thromb*. 2015;22:509-517

30. Samaniego EA, Shaban A, Ortega-Gutierrez S, Roa JA, Hasan DM, Derdeyn C, et al. Stroke mechanisms and outcomes of isolated symptomatic basilar artery stenosis. *Stroke Vasc Neurol*. 2019;4:189-197

31. Schaafsma JD, Silver FL, Kasner SE, Caplan LR, Rose-Finnell L, Charbel FT, et al. Infarct patterns in patients with atherosclerotic vertebrobasilar disease in relation to hemodynamics. *Cerebrovasc Dis Extra*. 2019;9:123-128

32. Marquardt L, Kuker W, Chandratheva A, Geraghty O, Rothwell PM. Incidence and prognosis of > or = 50% symptomatic vertebral or basilar artery stenosis: Prospective population-based study. *Brain*. 2009;132:982-988

33. Kim YJ, Lee JH, Choi JW, Roh HG, Chun YI, Lee JS, et al. Long-term outcome of vertebral artery origin stenosis in patients with acute ischemic stroke. *BMC Neurol*. 2013;13:171

# PART FOUR

# Chapter 8. Summary and future directions

## 8.1 Summary of our findings in this thesis

Ischemic stroke accounts for nearly 82% of the Chinese in-patients with stroke, and brings about a large number of stroke-related disability and mortality [1-3]. Intracranial large artery atherosclerosis is the most common etiology of cerebrovascular ischemia, particularly among Asians [4]. Of note, patients with acute IS attributed to ICAS often run a high risk of stroke recurrence [5, 6].

As one of important mechanisms of developing ICAS, the anatomical structure of the intracranial vasculature plays a fundamental role in regulating the cerebral hemodynamic stress [7, 8]. It is notable that there exist considerable variability in the geometry of the intracranial vasculature among the normal populations, which may directly affect the hemodynamic pattern of the intracranial large arteries [9-12]. Nonetheless, little evidence could be provided from patients with acute IS to ascertain the relationship between the cerebral artery variations (the COW structural anomalies and the varying VBJ-angle degrees) and the formation of ICAS. Accordingly, in the current thesis, we mainly described the structural anomalies of the COW and the varying magnitude of the VBJ angles among Chinese stroke patients with ICAS through utilizing TOF MRA. Then, we explored the underlying influences of the two cerebral artery variations on the occurrence and progression of ICAS in these patients, via using high-resolution intracranial vessel-wall imaging.

Our observations in this thesis suggested that the cerebral artery variations could have an impact on the formation and development of intracranial large artery atherosclerosis, which may provide new insight into the early identification of stroke patients at high risks of developing ICAS and subsequent cerebral ischemia.

Firstly, the COW structural anomalies were prevalent among patients with ICAS, and could influence the formation and development of intracranial large artery atherosclerosis, especially MCA atherosclerosis. Among the major intracranial large arteries liable to atherosclerosis, the occurrence of the symptomatic atherosclerotic lesions in the first segment of the MCA was observed to be robustly related to the incomplete structure of the A-COW in patients with ICAS. Moreover, the incomplete A-COW could also strongly affect the MCA plaque location on the vessel walls in patients with MCA atherosclerosis. Among the four main patterns of the COW anomaly in patients with MCA atherosclerosis, the dysplasia or absence of the ACoA was shown in independent relevance to symptomatic MCA atherosclerosis. Accordingly, the incomplete geometry of the A-COW, particularly the dysplastic/absent ACoA, might serve as a potential risk factor for developing symptomatic MCA atherosclerotic lesions in Chinese stroke patients.

Secondly, substantial variations in the magnitude of the VBJ angles were identified in patients with ICAS as well. Among patients with vertebrobasilar artery atherosclerosis, the VBJ angles exceeding 90° were observed in robust association with more vertebrobasilar plaques on the ventral wall, but fewer vertebrobasilar plaques on the dorsal wall. When comparing the imaging features of the vertebrobasilar plaques between the VBJ angles above 90° and the angles below 90°, we found that the VBJ angles above 90° were significantly correlated with the progressive lesions of vertebrobasilar artery atherosclerosis. Consequently, the VBJ angles more than 90° might significantly increase the risk of developing vertebrobasilar artery atherosclerosis in Chinese stroke patients.

### 8.2 Future directions

In the present thesis, we observed that the occurrence and progression of intracranial large artery atherosclerosis might be largely influenced by the incomplete structure of the COW or

the larger magnitude of the VBJ angle. Despite some unavoidable limitations, our findings in this thesis give novel insight into the field of stroke, especially intracranial large artery atherosclerosis.

First, based on the significant relevance of the cerebral arterial variations to the occurrence of the intracranial atherosclerotic lesions, further studies are required to investigate the underlying hemodynamic mechanisms affected by the incomplete A-COW structure (especially the ACoA dysplasia/absence) or the VBJ angles above 90° in stroke patients with ICAS. Transcranial Doppler ultrasonography was reported to detect the pattern of cerebral blood flow in the intracranial atherosclerotic large arteries efficiently [13]. Thus, the use of this technology can further the knowledge of the flow features depending on the cerebral arterial variations in stroke patients with ICAS. Besides, the wall shear stress in the focal lesion of ICAS can be evaluated quantitatively in a computational fluid dynamics model on the basis of computed tomography angiography [14]. Accordingly, the focal pattern of wall shear stress influenced by the incomplete A-COW subtype or the VBJ angles over 90° can be explored in ICAS patients.

Second, clinicians and researchers can pay more attention to the common variability in the COW geometry or the VBJ-angle magnitude among the normal populations, which may help to stratify the individuals at high risks of developing ICAS and subsequent cerebrovascular ischemia. Multi-center follow-up research with a larger study population can facilitate our investigations into the effects of the two cerebral artery variations on the development of MCA or vertebrobasilar artery atherosclerosis among the healthy subjects in the long term.

### 8.3 Conclusion

As a major cause of acute ischemic stroke, intracranial large artery atherosclerosis has gained more interest and knowledge, since high-resolution intracranial vessel-wall imaging is

widely utilized in acute patients with IS. In the current thesis, we were primarily concerned with the plaque imaging characteristics of the intracranial atherosclerotic arteries depending on the cerebral artery variations in stroke patients with ICAS. We analyzed the incidences of the incomplete COW patterns and the VBJ angles over 90° among Chinese stroke patients owing to ICAS, and explored the potential clinical impact of both cerebral artery variations on the occurrence and progression of the intracranial atherosclerotic plaques. Future research is still needed to further our knowledge of the underlying hemodynamic mechanisms of developing ICAS that are directly attributed to the incomplete A-COW geometry or the VBJ angles exceeding 90° in acute stroke patients. Besides, a multi-center study with a larger sample size will enable the risk stratification for the normal individuals with the COW anomalies or the larger VBJ angles.

## References


1. Wang YJ, Li ZX, Gu HQ, Zhai Y, Jiang Y, Zhao XQ, et al. China stroke statistics 2019: A report from the national center for healthcare quality management in neurological diseases, china national clinical research center for neurological diseases, the chinese stroke association, national center for chronic and non-communicable disease control and prevention, chinese center for disease control and prevention and institute for global neuroscience and stroke collaborations. *Stroke Vasc Neurol*. 2020;5:211-239
2. Rajsic S, Gothe H, Borba HH, Sroczynski G, Vujicic J, Toell T, et al. Economic burden of stroke: A systematic review on post-stroke care. *Eur J Health Econ*. 2019;20:107-134
3. Diseases GBD, Injuries C. Global burden of 369 diseases and injuries in 204 countries and territories, 1990-2019: A systematic analysis for the global burden of disease study 2019. *Lancet*. 2020;396:1204-1222
4. Holmstedt CA, Turan TN, Chimowitz MI. Atherosclerotic intracranial arterial stenosis: Risk factors, diagnosis, and treatment. *Lancet Neurol*. 2013;12:1106-1114
5. Lange MC, Ribas G, Scavasine V, Ducci RD, Mendes DC, Zetola VHF, et al. Stroke recurrence in the different subtypes of ischemic stroke. The importance of the intracranial disease. *Arq Neuropsiquiatr*. 2018;76:649-653
6. Saber H, Thrift AG, Kapral MK, Shoamanesh A, Amiri A, Farzadfard MT, et al. Incidence, recurrence, and long-term survival of ischemic stroke subtypes: A population-based study in the middle east. *Int J Stroke*. 2017;12:835-843
7. Ritz K, Denswil NP, Stam OC, van Lieshout JJ, Daemen MJ. Cause and mechanisms of intracranial atherosclerosis. *Circulation*. 2014;130:1407-1414

8. Vrselja Z, Brkic H, Mrdenovic S, Radic R, Curic G. Function of circle of willis. *J Cereb Blood Flow Metab*. 2014;34:578-584

9. Routsonis KG, Stamboulis E, Christodoulaki M. Anomalies of the circle of willis and atherosclerosis. *Vasc Surg*. 1973;7:141-145

10. Hartkamp MJ, van Der Grond J, van Everdingen KJ, Hillen B, Mali WP. Circle of willis collateral flow investigated by magnetic resonance angiography. *Stroke*. 1999;30:2671-2678

11. Ravensbergen J, Krijger JK, Hillen B, Hoogstraten HW. The influence of the angle of confluence on the flow in a vertebro-basilar junction model. *J Biomech*. 1996;29:281-299

12. Ravensbergen J, Ravensbergen JW, Krijger JK, Hillen B, Hoogstraten HW. Localizing role of hemodynamics in atherosclerosis in several human vertebrobasilar junction geometries. *Arterioscler Thromb Vasc Biol*. 1998;18:708-716

13. Wei W, Yi X, Ruan J, Duan X, Luo H, Lv Z. Influence of collateral circulation on cerebral blood flow and frontal lobe cognitive function in patients with severe internal carotid artery stenosis. *BMC Neurol*. 2019;19:151

14. Lan L, Liu H, Ip V, Soo Y, Abrigo J, Fan F, et al. Regional high wall shear stress associated with stenosis regression in symptomatic intracranial atherosclerotic disease. *Stroke*. 2020;51:3064-3073